UNITED NATIONS UNIVERSITY

UNU-GTP

ORKUSTOFNUN

Meyjarauga hot spring, Hveravellir, Kjölur, Central Iceland

Moneer Fathel Alnethary

# PETROLOGY OF THE HORNFELS CONTACT ZONE AROUND THE HROSSATUNGUR GABBRO IN THE ERODED HAFNARFJALL CENTRAL VOLCANO, W-ICELAND

Report 1
February 2018

UNITED NATIONS UNIVERSITY
UNU-GTP
Geothermal Training Programme

Orkustofnun, Grensasvegur 9,
IS-108 Reykjavik, Iceland

Reports 2018
Number 1

# PETROLOGY OF THE HORNFELS CONTACT ZONE AROUND THE HROSSATUNGUR GABBRO IN THE ERODED HAFNARFJALL CENTRAL VOLCANO, W-ICELAND

**MSc thesis**
School of Engineering and Natural Sciences
Faculty of Earth Sciences
University of Iceland

by

**Moneer Fathel Alnethary**
Ministry of Oil and Minerals
Geological Survey and Mineral Resources Board
Geothermal Energy Project
P.O. Box 297, Al-Tahrir
Sana´a
YEMEN
*moneer_f@hotmail.com; moneer.fathel@yahoo.com*

United Nations University
Geothermal Training Programme
Reykjavík, Iceland
Published in February 2018

ISBN 978-9979-68-467-1 (PRINT)
ISBN 978-9979-68-468-8 (PDF)
ISSN 1670-7427

This MSc thesis has also been published in February 2018 by the
School of Engineering and Natural Sciences, Faculty of Earth Sciences
University of Iceland

# INTRODUCTION

The Geothermal Training Programme of the United Nations University (UNU) has operated in Iceland since 1979 with six-month annual courses for professionals from developing countries. The aim is to assist developing countries with significant geothermal potential to build up groups of specialists that cover most aspects of geothermal exploration and development. During 1979-2017, 670 scientists and engineers from 60 developing countries have completed the six month courses, or similar. They have come from Africa (39%), Asia (35%), Latin America (14%), Europe (11%), and Oceania (1%). There is a steady flow of requests from all over the world for the six-month training and we can only meet a portion of the requests. Most of the trainees are awarded UNU Fellowships financed by the Government of Iceland.

Candidates for the six-month specialized training must have at least a BSc degree and a minimum of one-year practical experience in geothermal work in their home countries prior to the training. Many of our trainees have already completed their MSc or PhD degrees when they come to Iceland, but many excellent students with only BSc degrees have made requests to come again to Iceland for a higher academic degree. From 1999, UNU Fellows have also been given the chance to continue their studies and study for MSc degrees in geothermal science or engineering in co-operation with the University of Iceland. An agreement to this effect was signed with the University of Iceland. A similar agreement was also signed with Reykjavik University in 2013. The six-month studies at the UNU Geothermal Training Programme form a part of the graduate programme.

It is a pleasure to introduce the 57$^{th}$ UNU Fellow to complete the MSc studies under a UNU-GTP Fellowship. Moneer Fathel Alnethary, BSc in Geology from the Geological Survey and Minerals Resources Board (GSMRB) in Yemen, completed the six-month specialized training in *Borehole Geology* at UNU Geothermal Training Programme in October 2010. His research report was entitled: *Borehole geology and alteration mineralogy of well HE-52, Hellisheidi geothermal field, SW-Iceland.* After five years of geological and geothermal energy work in Yemen, he came back to Iceland for MSc studies in *Geothermal Geology*, at the School of Engineering and Natural Sciences, Faculty of Earth Sciences, University of Iceland in November 2015. In January 2018, he defended his MSc thesis presented here, entitled: *Petrology of the hornfels contact zone around the Hrossatungur gabbro in the eroded Hafnarfjall central volcano, W-Iceland*. His studies in Iceland were financed by the Government of Iceland through a UNU-GTP Fellowship from the UNU Geothermal Training Programme. We congratulate Moneer on the achievements and wish him all the best for the future. We thank the School of Engineering and Natural Sciences, Faculty of Earth Sciences, University of Iceland for the co-operation, and his supervisors for the dedication.

Finally, I would like to mention that Moneer's MSc thesis with the figures in colour is available for downloading on our website www.unugtp.is, under publications.

With warmest greetings from Iceland,

Lúdvík S. Georgsson, Director
United Nations University
Geothermal Training Programme

## ACKNOWLEDGEMENTS

I would like to express my gratitude to the United Nations University Geothermal Training Program (UNU-GTP) and to the government of Iceland for funding this project. I would like also to thank Mr. Lúdvík S. Georgsson, director of the United Nations University and Geothermal Training Programme and the deputy director Mr. Ingimar G. Haraldsson for giving me this opportunity. The UNU staff, Ms. Thórhildur Ísberg, Ms. Málfrídur Ómarsdóttir and Mr. Markús A.G. Wilde. Thank you for your technical support and guidance. How could I forget to thank Ms. Rósa Jónsdóttir for finding for me all the papers I needed on the right time. To my fellow UNU MSc and PhD students, I am grateful to you all for the time we spent encouraging each other and sharing common problems.

I would sincerely like to thank my supervisor Dr. Hjalti Franzson for his dedicated time, his very constructive criticism and careful reading of the manuscript. Your countless words of support utterly encouraged and motivated me so much. I am grateful as well to my supervisor Dr. Gudmundur H. Gudfinnsson for providing the facilities for this research at the University of Iceland and for the many insightful discussions during my study period. I am deeply obliged to them and will always be. I would like also to thank my external examiner, Dr. Bjarni Gautason for his constructive criticism of the thesis. I would also acknowledge Jóhann Gunnarsson and Saemundur A. Halldórsson for their assistance during my laboratory work. Warm thanks are also goes to Atli Hjartarson for preparation of the microprobe samples.

I would like to extend my gratitude to the Geological Survey and Minerals Resources Board (GSMRB) in Yemen for allowing me to pursue this study at the University of Iceland. To the Yemen Geothermal Energy Project team in particular to Abdulsalam Al-dukhain, Taha Al-kohlani and Ali Al-sabri, just to mention a few.

My appreciation geos to Dr. Mohamed Mattash for his noble encouragements and endless help. I furthermore thank Dr. Mohammed Al kubati and Dr. Faisal Alhuzaim for their good motivation all the time. It was a great pleasure to work with you and indeed am very thankful. I owe a large debt of gratitude to my colleague Samir Alrefaie for being there for me to support whenever I need assistance. You are indeed an awesome person and I am greatly indebted.

I take this opportunity to express the profound gratitude to my wife Somia for her enduring patience during the most difficult time in Yemen, she managed to stand firm and survive during the time she needs me most. To my children Malak, Mohammed and Noor for their great moral support. Thanks more to my parents for their love, for their continuous spiritual and material support. I feel honored and blessed to have you both in my life. Above all, utmost glory and praise be to Almighty Allah the lord of all mankind and all exists who gave me strength, patience and ability to complete this academic endeavor successfully.

## DEDICATION

*The thesis is dedicated to my beloved country (Yemen)*
*wishing it to recover from crisis soon.*

*In the hopes that this work may sometime in the near future contribute*
*to the development of the geothermal project in Yemen*

## ABSTRACT

This study focusses on a hornfels zone on the southern side of the Hrossatungur gabbro, within the Hafnarfjall-Skardsheidi central volcano, W-Iceland. The intrusion formed by repetitive injections of basaltic cone sheets, which were trapped at a lava-pyroclastite boundary within the Hafnarfjall caldera fillings. During contact metamorphism in response to the intrusion emplacement, a hornfels contact zone was created by a recrystallization process of previously hydrothermally altered basalt. Here, the hydrothermal alteration and chemical composition of minerals is closely studied to evaluate the development during the contact metamorphism event forming the hornfels around the gabbro.

The hornfels mainly contains clinopyroxene compositions ranging widely from augite, salite, ferrosalite to hedenbergite in vesicle fillings, with minor orthopyroxene, while the groundmass clinopyroxene ranges from diopside, augite to salite. The plagioclase composition ranges from andesine, labradorite to bytownite and occasionally to anorthite within the vesicles and veins, while the groundmass plagioclase ranges from labradorite to anorthite. Other minerals found in the hornfels are iron-titanium oxides (magnetite, ilmenite and titano-magnetite), garnet, titanite, minor apatite and hornblende. The orthopyroxene include bronzite ($Fs_{10-30}$), hypersthene ($Fs_{30-50}$) and ferro-hypersthene ($Fs_{50-70}$). Garnet compositional range goes mainly from andradite to about 20% grossular.

Loss-on-ignition measurements reveal that the majority of samples located at the inner hornfels zone experience <1% LOI, while samples that show more extensive LOI are mostly situated at the outer hornfels zone. A comparison of the hornfels LOI with the LOI of Icelandic rocks in different alteration zones indicates that the hornfels rocks should have shown LOI >1% to <10% prior to the gabbro emplacement, which indicates that the water has been driven out of the rock by the replacement of hydrous minerals by non-hydrous minerals.

For comparison, the mineralogy of the hornfels zone surrounding a dyke intrusion in drillhole HE-42 in Hellisheidi geothermal field was studied. There the clino-pyroxene ranges from augite to salite in veins and vesicles, with minor orthopyroxene in the groundmass, the plagioclase composition ranges from labradorite to bytownite and anorthite. The hornfels in the well was more intense than that found around the gabbro observed by more pronounced granoblastic crystallization, less iron rich clinopyroxenes and more calcium rich plagioclases.

The study shows that the formation of the hornfels is due to direct heat conduction, the expulsion of water from the rock and preventing a direct water-magma interaction.

**TABLE OF CONTENTS**

Page

Page



**LIST OF FIGURES**

Page



## LIST OF TABLES



## ABBREVIATIONS

| | |
|---|---|
| a.s.l. | Above sea level |
| b.s.l. | Below sea level |
| BSE | Backscattered electrons |
| cm/y | Centimetre per year |
| EMP | Electron microprobe analysis |
| GEORG | Geothermal research group |
| DRG | Deep root geothermal systems |
| HCV | Hafnarfjall central volcano |
| HTG | Hrossatungur gabbro |
| IES | The Institution of Environment science |
| ICP-OES | Inductively coupled plasma-Optical emission spectrometry |
| ISOR | Iceland GeoSurvey |
| LaB6 | Lanthanum hexaboride cathodes for electron microscopes |
| LOI | Loss on Ignition |
| Ma | Million years |
| MLC | Mixed layer clay |
| mol% | Mol percent |
| nA | Nano ampere |
| PPl | Plane-polarized light |
| ppm | Parts per million |
| REE | Rare earth element |
| SEM | Scanning electron microscope |
| Th | Homogenization temperatures |
| WDS | Wavelength dispersive spectrometer |
| wt% | Weight percent |

# 1 INTRODUCTION

## 1.1 Geological setting

Iceland, located in the North-Atlantic Ocean, lies astride the Mid-Atlantic Ridge, and is underlain by an anomalous mantle plume. The volcanic zones cross the country in a complex manner as seen in Figure 1. Extension, with a half-spreading rate of about 1 cm/y in NE-SW direction, is contained within the rift zones. The rifting occurs to a large extent within specific fissure zones each with a central volcano residing in the central part. Each of these volcanic systems is active for 0.5-1.5 Ma (Franzson, 1979) and then move outside the rift zone and become gradually eroded by the multiple glacial periods in the last 3 Ma or so. Figure 1 shows the location of active and fossil central volcanoes.

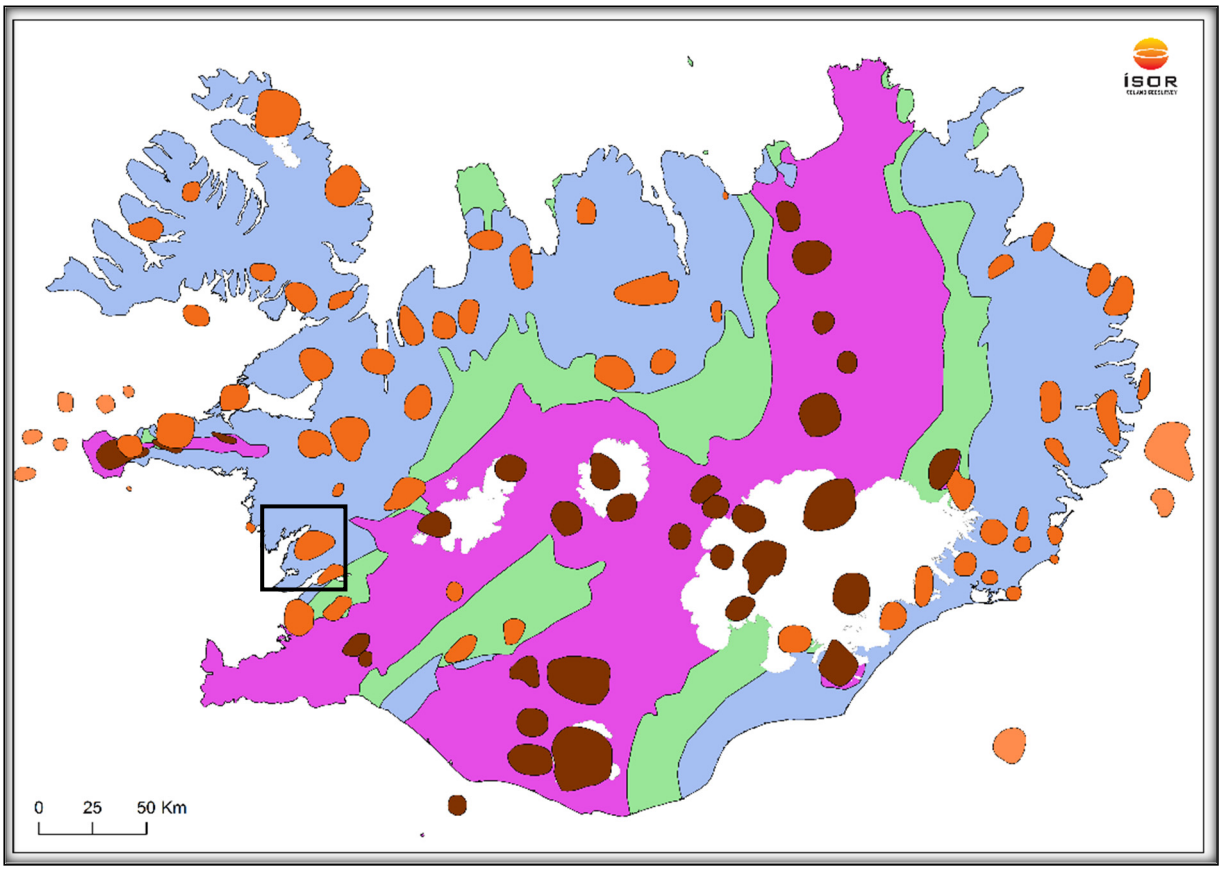


FIGURE 1: Active central volcanoes (dark red) and fossil central volcanoes (orange) across Iceland. The Hafnarfjall-Skardsheidi central volcano is in the area enclosed by the black square (Hjartarson and Saemundsson, 2014)

The central volcano, to which this study relates, is Hafnarfjall-Skardsheidi and is located about 100 km north of Reykjavík. It was active for about 1.5 Ma, or from 4-5.5 Ma ago, and is thus Tertiary in age (Figure 1). The geology of the area was originally mapped by Franzson (1979), who recognized four spatially separate volcanic phases, i.e., the Brekkufjall, Hafnarfjall, Skardsheidi and Heidarhorn phases (Figure 2). Each of these phases produced compositions ranging from basalts to rhyolites. Franzson (1979) identified two calderas, an early one in the Brekkufjall area and a later one in the Hafnarfjall mountain range. Fossil high-temperature systems are widespread in the area, in particular associated with the Hafnarfjall volcanic phase. The central volcano was formed at the initial stages of a new rift zone, which was breaking through an older crust. Tertiary formations in Iceland have been eroded to relatively deep levels by the multiple glaciations since about 3 Ma. In the case of Hafnarfjall-Skardsheidi, the erosion has been estimated to range from a few hundred metres to $\leq$2 km.

## 1.2 Hafnarfjall caldera formation

The location of the Hafnarfjall caldera is shown in Figures 2 and 3, the latter also showing the locations of exposed and postulated larger intrusions associated with the central volcano. The caldera consists of three contemporaneous basin structures. There are two main eruptive units within the caldera, steeply dipping lavas mostly occupying the southern and the northernmost parts and these are succeeded by basaltic to basaltic andesite pyroclastics, which indicate volcanic eruptions within a caldera lake environment. The dominant intrusives found within the caldera are cone sheet swarms, which seem to coalesce at 2-3 km depth, coinciding with the center of two of the basins, which in turn points to the top of deeper magma chambers underlying and related to the caldera basins. The largest of these intrusions is the Hrossatungur Gabbro (HTG) (Figure 3). It is exposed in a semi-circular manner in the southern and western parts of the Hrossatungur basin. Multiple dolerite cone sheets are located in a circular continuation of the gabbro in the east and are assumed to be a part of the same intrusive episode. No intrusions are seen cutting through the gabbro, and all evidence suggests that the gabbro is the last intrusive in this part of the central volcano (Franzson, 1979).

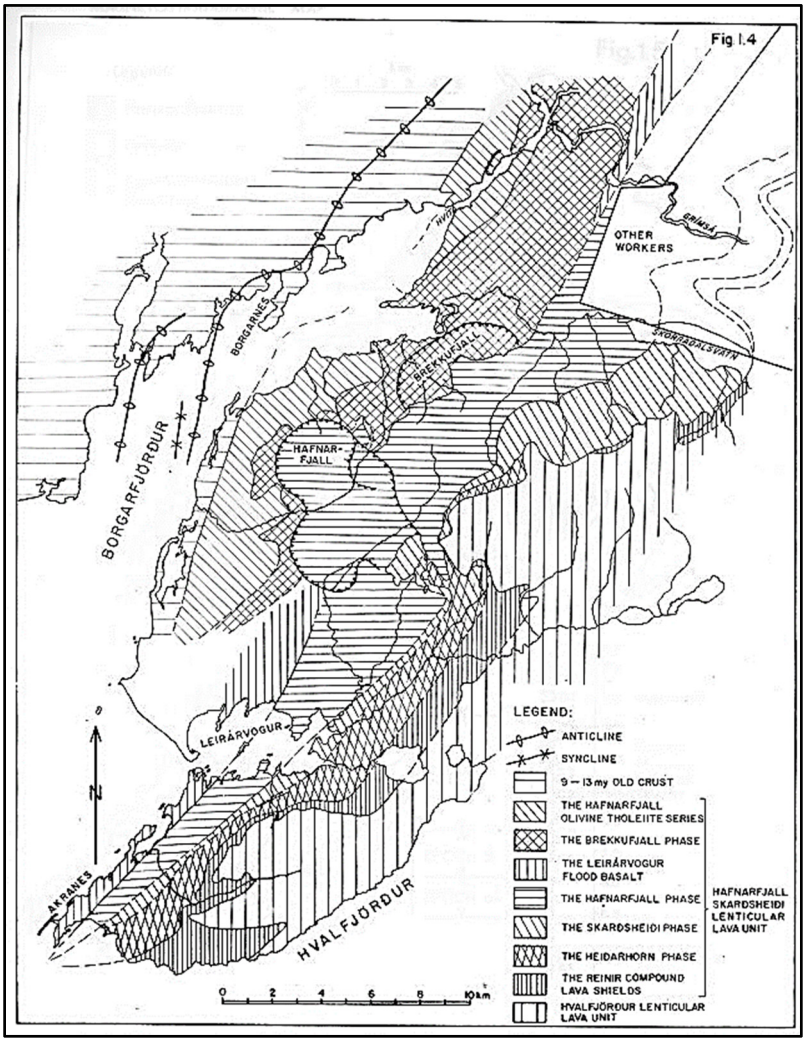


FIGURE 2: A simplified geological map showing the division of volcanic phases in the Hafnarfjall-Skardsheidi central volcano (Franzson, 1979)

## 1.3 Geothermal systems

Hafnarfjall-Skardsheidi is a major and especially large central volcano, active for over 1.5 Ma, which is an anomalously high age compared to other such volcanoes in Iceland. Geothermal activity was thus widespread due to the high intrusive rate in the area. Figure 3 shows the location of large intrusions found within the central volcano and vicinity, each of which is likely to have been a heat source for a localized overlying high-temperature system. High-temperature alteration is present in all these areas, which could be an evidence for the geothermal systems having developed by heat exchange between these heat sources and the surrounding groundwater systems. Franzson (1979) only studied the hydrothermal alteration within the central volcano in a preliminary way. However, later mapping has confirmed that high-temperature alteration is present around these postulated and exposed intrusions. The hydrothermal alteration within the caldera is particularly intense around the caldera margin and lava succession inside the caldera at the northern and southern parts. In these areas, alteration characterizing the epidote-actinolite zone is predominant. Low-temperature alteration is predominantly found within

the pyroclastic caldera fillings which implies the hydrological control of the groundwater system connected to the caldera lake (Franzson, 1979, unpublished data).

### 1.4 GEORG-DRG project

The project titled Deep roots of geothermal systems (DRG), conducted in cooperation with the Geothermal Research Group (GEORG), aims to understand the relationship between water and magma in the roots of volcanoes, in particular how heat is transferred into geothermal systems to maintain their energy, and how to utilize superheated steam from greater depths.

The understanding of geothermal systems in Iceland and worldwide has been expanding in the last decades, concomitant with increasing utilization geothermal energy. One area of limited understanding, though, has been the process of heat exchange between groundwater systems and magma heat sources. Does this occur as direct heat exchange between molten magma and the fluid (the most effective process) or is this exchange more distant from the molten magma? This is difficult to assess for active systems, and very expensive, as deep drill holes are needed. Another way to do this is to study deeply eroded areas where fossil geothermal systems and related magma bodies can be evaluated. To address this issue, GEORG provided scientific grants in 2013, including a grant for the mapping of a deeply eroded gabbro body and the enveloping geothermal system. The chosen location is the Hrossatungur gabbro in the southern part of the Hafnarfjall region. The project, which started in 2013, includes field mapping and sampling, along with petrographic studies, mainly addressing the hydrothermal alteration. The results have so far only been presented in several oral presentations. Below, data pertinent to this study is presented.

### 1.5 Geological and geothermal features of Hrossatungur gabbro and surrounding area

Figure 3 shows the location of Hrossatungur gabbro and its relation to the Hafnarfjall caldera. Figure 4 represents a more detailed map of the gabbro along with sample locations and points of interests. Figure 5 shows the view from the south delineating the gabbro. The gabbro was intruded

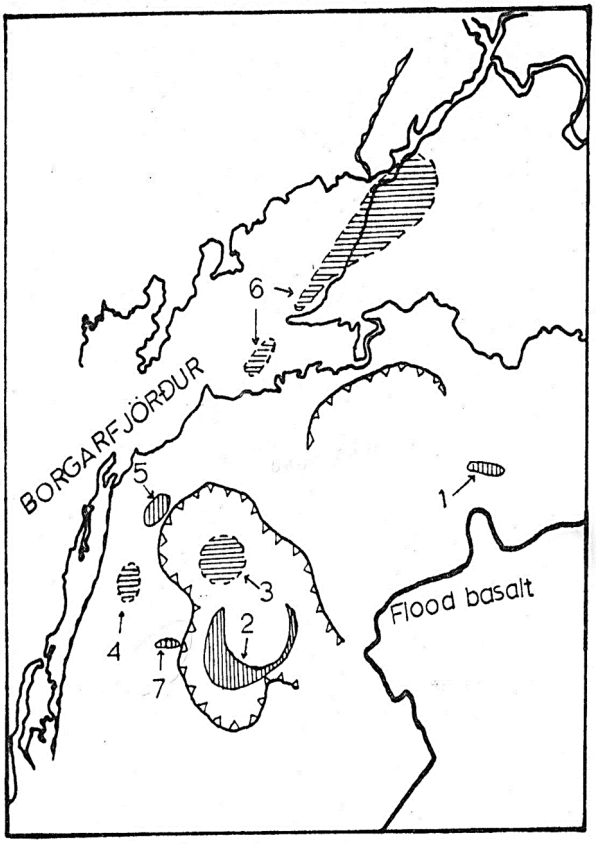


FIGURE 3: Location of larger intrusions in the central volcano. Solid lines show exposed intrusions, while intrusions outlined by broken lines are proposed based on indirect evidence. Intrusion marked 2 is the Hrossatungur gabbro (Franzson, 1979)

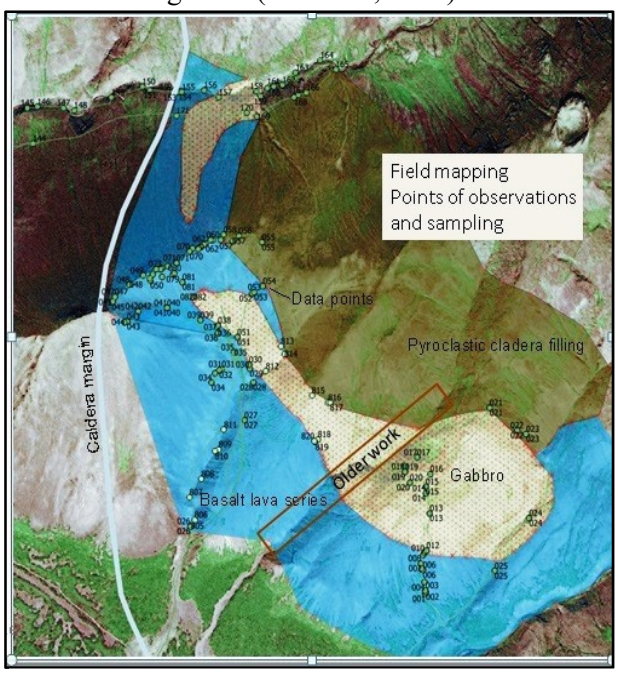


FIGURE 4: Simplified geological map of the Hrossatungur gabbro, with lava series along the south and west contact and pyroclastic caldera filling to the north

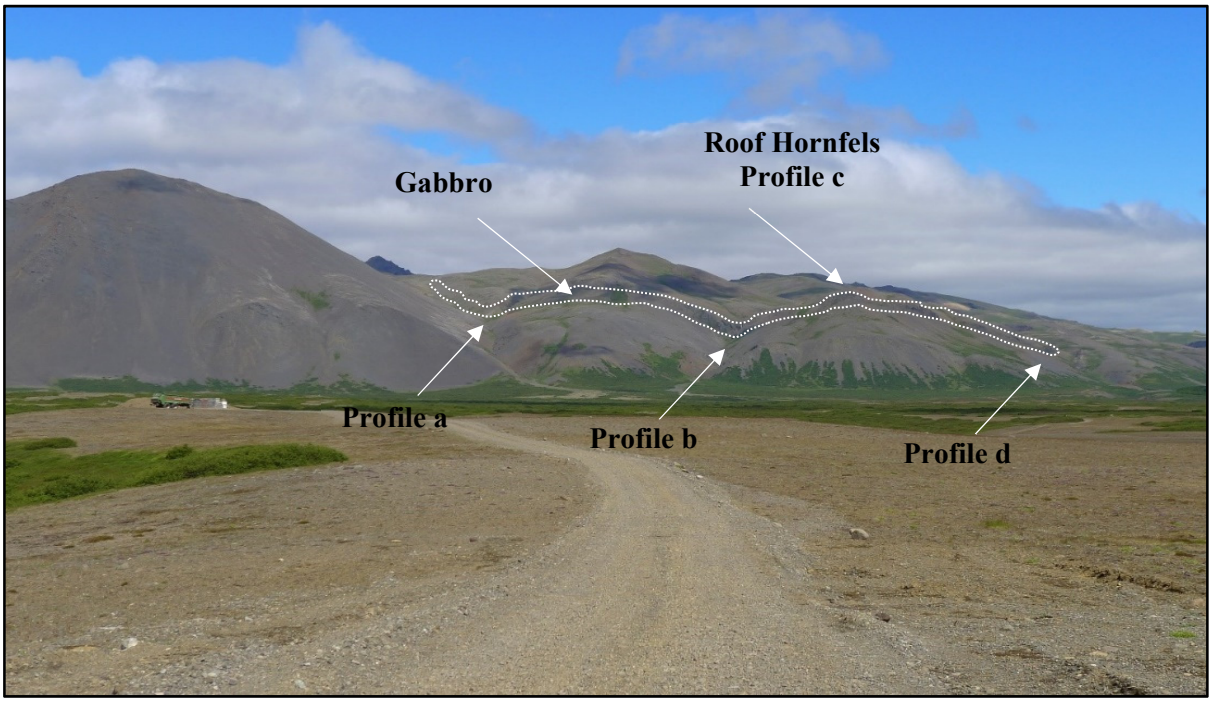


FIGURE 5: A view of the Hrossatungur gabbro from south. The broken line marks the outer boundary of the gabbro. Locations of profiles through the hornfels in this study are marked specifically

into the caldera fillings and appears to follow the boundary between the steeply dipping lava series and the pyroclastic fillings, except in the west where it intrudes only the basalt. It forms a sub-circular body with an indication in the east of ballooning, while it is more elongated in the western part. Geological evidence points to the gabbro being formed during a multiple cone sheet intrusive event where magma was pumped into a magma trap at the formation boundaries. Further evidence also indicates that magma was ejected from the gabbro intrusion as cone sheets (see e.g. Figure 12). The gabbro is probably the last intrusive event within this part of the volcano as no other intrusions are found cutting the gabbro. This, along with the freshness of the gabbro, implies that it was also the last heat source for a geothermal system in this part of the volcano.

One of the features studied within the DRG project was hydrothermal alteration. For this purpose, several samples were taken for petrographic analyses (Franzson, pers. comm.). The results show two main types of hydrothermal conditions. Very intense hydrothermal alteration is found within the basalt succession south of the intrusion, west and above the intrusion to the west. There, the hydrothermal minerals include very common garnet, wollastonite, actinolite, quartz, chlorite and wairakite and minor epidote. Calcite is also widespread but becomes particularly dominant above the roof of the gabbro in the west where it aggressively alters the primary mineralogy. High-degree alteration is found at the caldera fault structure to the south, and it is proposed that it served as a geothermal upflow channel prior to or contemporaneously with the geothermal system associated with the HTG. The postulated two geothermal systems are shown in Figures 6a and b.

A sharp contrast in hydrothermal alteration is between the basalt succession to the south and the one found within the pyroclastic caldera fillings north of the HTG, where the alteration dominantly belongs to the zeolite zone, with scolecite/stilbite dominating in vesicles and vugs. There is an obvious lack of a high-temperature system that might relate to the HTG heat source. The only plausible explanation for this is that the pyroclastic fillings contained a powerful cold groundwater system, which flowed towards the gabbro heat source, and thus prevented geothermal flow into that area (Franzson, unpublished data, and Brett et al., 2016).

Figure 6 shows an overall model with the high-temperature system associated with the caldera fault structure preceding the HTG (a), followed by the gabbro intrusion and its derivative geothermal system

(b). In both cases, the groundwater system within the caldera (controlled by the overlying caldera lake) prevented the flow of geothermal fluids into that domain, as this was the inflow towards the heat source.

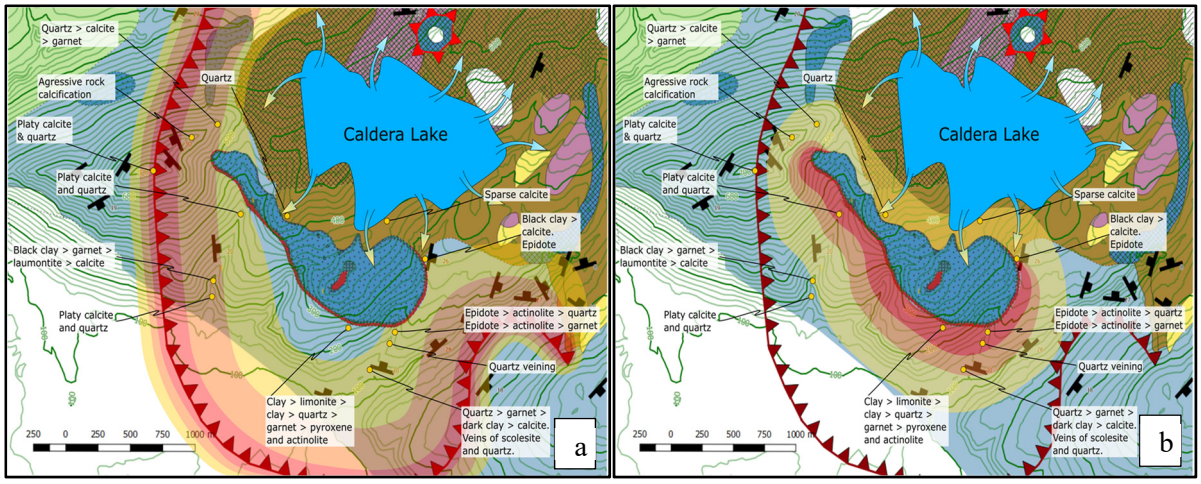


FIGURE 6: Geothermal systems in the study area a) The first geothermal system coinciding with the approximate extent of hydrothermal alteration around the caldera fault. The gabbro would not have intruded until later. b) The later geothermal system coinciding with the approximate extent of hydrothermal alteration around Hrossatungur gabbro (figures from Brett et al, 2016)

Brett et al., (2016) conducted a preliminary study of homogenization temperatures (Th) within the high-temperature alteration area south and west of the HTG, mainly in quartz. Maximum fluid inclusion temperature in water-dominated geothermal systems is confined to the boiling point curve. Higher temperatures may be experienced if vigorous boiling occurs or in dry steam systems. Figure 7 shows histograms of Th versus the altitude of sample locations. A boiling point curve fitted to the Th measurements is very important as it puts definite depth constraints on the geothermal system. Indeed, it provides a potent evaluation of the intrusive depth of the HTG, and indicates that the water table of the "overlying caldera lake" at that time was at approximately 1300 m a.s.l.

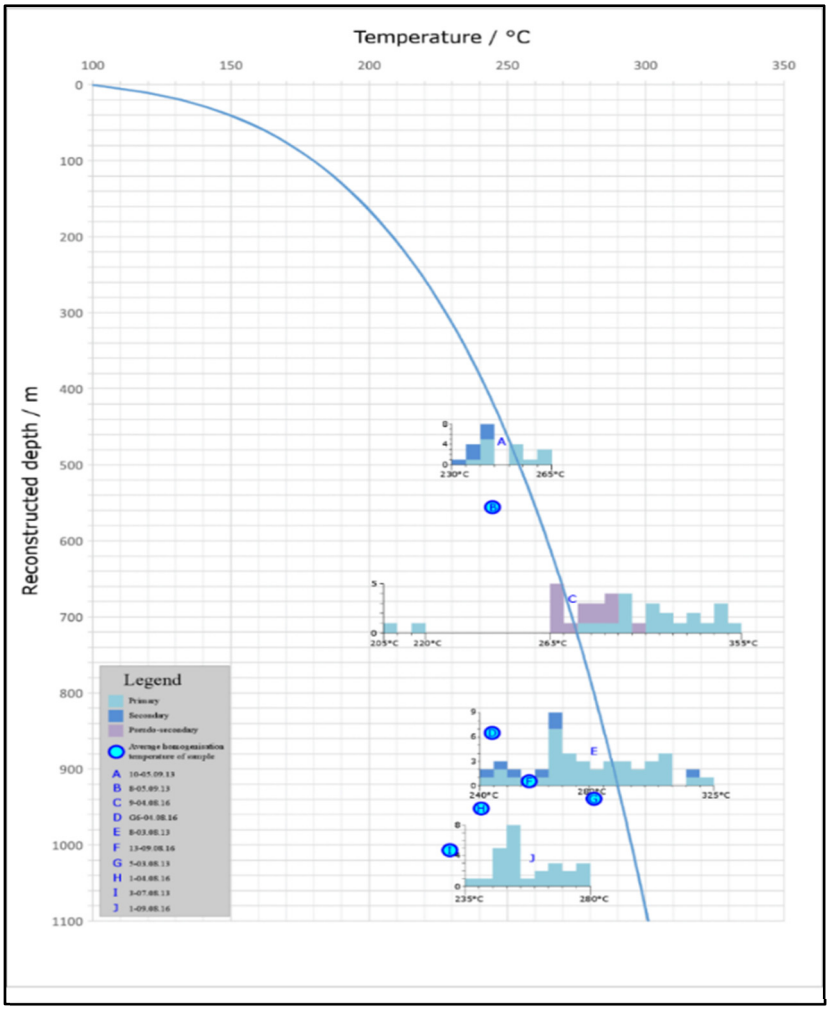


FIGURE 7: Histogram of homogenization temperatures (Th) measurements of fluid inclusions, mainly in quartz, plotted against temperature and relative altitude of samples. Best fit of boiling point curve (Brett et al., 2016)

## 2. DEFINITION AND PREVIOUS STUDIES OF HORNFELS IN ICELAND

Hornfels is a type of granofels that is typically a fine-grained and compact metamorphic rock. It develops at the contact (thermal metamorphism) with a magmatic intrusion. Hornfels is a hard rock that tends to splinter or display conchoidal fracture when broken. The structure of hornfels is distinctive with lack of foliation or preferential plane of fracture. These shallow rocks occur under conditions of low deviatoric stress (Winter, 2014). However, although pressure is not an important factor in the rock formation, these rocks show the tendency for alignment parallel to the direction of least resistance, which gives a characteristic type of micro-structure (Harker, 1964). The hornfels rocks evolves towards granular or granoblastic textures and they occasionally include porphyroblasts. Hornfels rocks were first described and defined by Goldschmidt (1911) for a series of contact-metamorphosed hornfels of palaeozoic age in the Oslo region, southern Norway. He described the relationship between the equilibrium mineral assemblage of the metamorphic rock and its bulk composition. Eskola (1914) studied similar hornfels conditions in the Orijärvi region of southern Finland and confirmed the concept of Goldschmidt by noting the same relationship between the mineral assemblage and chemical composition (Eskola, 1914). On the basis of this predictable relationship, Eskola (1920) developed the concept of metamorphic facies. Five original metamorphic facies were proposed; greenschist, amphibolite, hornfels and eclogite facies. Numerous classification schemes have further been proposed that include other facies and sub-facies (Winter, 2014). Thus, hornfels mineralogy is typically split into the following metamorphic sub-facies: albite-epidote, hornblende, pyroxene, and sanidinite hornfels facies.

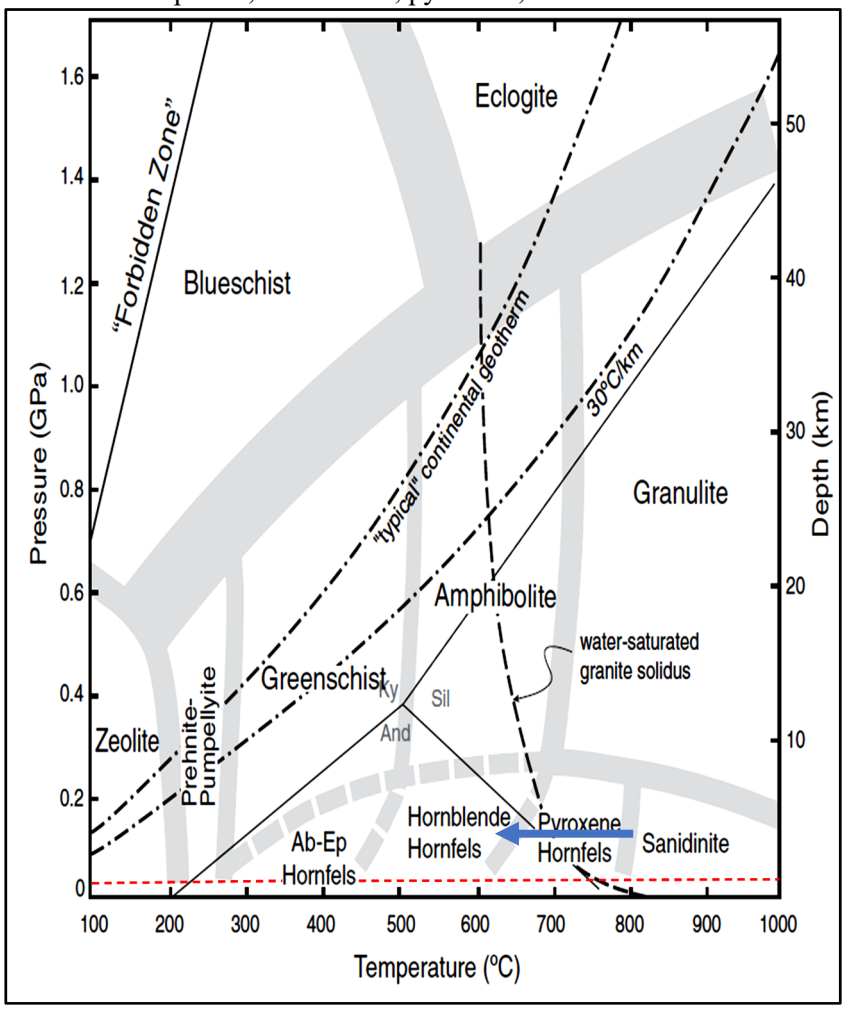


FIGURE 8: Temperature-pressure diagram showing the general limits of various metamorphic facies. Boundaries are approximate and gradational (Winter, 2014). The dotted line at the bottom of the figure indicates the approximate pressure expected around the gabbro during the hornfels event. The arrow shows the location of the pyroxene hornfels at Hrossatungur

The hornfels in the Hrossatungur area was brought about by the emplacement of the gabbro intrusion. As the depth of the hornfels occurrence is approximated as 800-1000 m, it will correspond to the broken line in the lower part of Figure 8. The temperature of the gabbro can be estimated as 1000-1100°C. This should have been the maximum temperature of the hornfels nearest to the gabbro, but the temperature should diminish in a conductive way with distance from the gabbro. Evidence of rocks belonging to sanidinite, pyroxene and hornblende hornfels facies should therefore be searched for in this locality.

Fridleifsson (1983) studied the chemical composition of pyroxene in the hornfels around an exhumed gabbro system in the Geitafell central volcano. He extensively analysed pyroxene and plagioclase compositions in lava hornfels and illustrated their

compositional range in terms of the pyroxene quadrilateral (Wo-En-Fs) and the plagioclase ternary (Ab-An-Or). His study revealed that the compositional variation and transition from the rock into the vesicle/vein centres is augite, salite, ferroaugite, ferrohedenbergite and hedenbergite with Fe-enrichment trend toward the centre of the veins. By this trend in composition, he inferred the cause of the thermal metamorphism as being the gabbro intrusion, whereas primary pyroxene of basaltic rocks are mainly augite with higher Fe content in the groundmass augite. The plagioclase in Geitafell central volcano, as described by Fridleifsson (1983), is characterized by a narrow zone of oligoclase and albite. The study revealed also that the hydrothermal system is created by the interaction of hot intrusive rock and groundwater system. Moreover, heat transfer in the system was dominated by supercritical or superheated fluids, which existed within the hornfels contact zone (Fridleifsson, 1983).

Other studies of hornfels mineralogy have also been conducted in Iceland. Marks et al. (2011) referred to Fe and Mg in Reykjanes as dominant substituted elements in the compositional variation of pyroxene, because they are sensitive to hydrothermal change in the system. They reported the composition of igneous, hydrothermal and granoblastic clinopyroxene in terms of the familiar Wo-En-Fs system ($CaSiO_3$-$MgSiO_3$-$FeSiO_3$). The typical granoblastic clinopyroxene compositions are consistently of less calcic composition (augite) than the hydrothermal clinopyroxene, which is found in quartz-epidote-actinolite veins. The hydrothermal clinopyroxene ranges from salite to ferrosalite. The igneous augite is less calcic and less Fe-rich than both granoblastic and hydrothermal clinopyroxene (Marks, et al., 2011). This hydrothermal calcic plagioclase and recrystallized granoblastic hornfels are associated with the transition from amphibolite facies to pyroxene hornfels facies alteration in RN-17. It shows that high-temperature granoblastic assemblages are found with epidote, actinolite and spinel. The study also showed that granoblastic orthopyroxene is common below a depth of 2150 m.

Helgadóttir et al. (2017) studied samples that were taken from cores drilled into the eastern side of the alteration contact surrounding the Geitafell gabbro body. They discovered that the majority of pyroxene is Mg-rich clinopyroxene, which falls close to a composition between hedenbergite and diopside (salite-ferrosalite), but some compositions are shifted towards the diopside end-member. Microprobe analyses confirmed the existence of alteration minerals that formed at supercritical condition. Helgadóttir et al. (2017) observed a high-temperature mineral assemblage in veins, including secondary clinopyroxene (salite and ferrosalite), actinolite, garnet, titanite, epidote and feldspar, which are part of the contact zone that formed at the time of the cooling a gabbro intrusion in the Geitafell central volcano (Helgadóttir et al., 2017).

Schiffman et al. (2014) studied the granoblastic hornfels which is located above a molten rhyolitic intrusion in well IDDP-1 in Krafla geothermal system. Temperatures assessed as high as 615-954°C were recorded within the pyroxene and oxides within the hornfels. This temperature exceeds the brittle-ductile transition zone for mafic rocks in the oceanic crust at the depth of 2.1 km. Therefore, the conclusion of the study is that, because of the ductile conditions at those temperatures, the hornfels would be incapable of sustaining an open fracture network to allow convection, and thus the heat transfer from the roof of the molten rhyolite would be conductive. Furthermore, the strong thermal gradient extending from the gabbro causes alteration and recrystallization, and drives the water out of the rock, forming a water-phobic environment. Hence, heat mining by direct “water” contact with magma appears not to exist (Schiffman, et al., 2014).

## 3. THE PRESENT STUDY

### 3.1 Objectives

One of the main purposes of the GEORG-DRG project was to evaluate the process of heat exchange between a molten magma body and the surrounding groundwater system. An important factor in this respect is the study of the contact rocks around the heat source in order to find evidence either for the infiltration of the groundwater towards the magma or the outwards conduction of the heat from the magma into the surrounding rocks. Hornfels is defined as a rock that has been altered and partly recrystallized due to heating from a nearby magmatic intrusion, also termed contact alteration. This study focusses on the processes of the formation of hornfels and an evaluation of the role of water and heat in its formation. It is divided into the following parts:

- A review of field relations.
- ICP-OES chemical analyses of about 30 samples from the hornfels zone to evaluate the chemical exchange that may have taken place during the hornfels process and potential contamination from the gabbro.
- Petrographic analyses of about 33 hornfels rock samples
- Loss-on-ignition analyses of about 30 hornfels samples to estimate the water and carbon content within the hornfels zone.
- SEM and partly electron microprobe analyses to identify the mineralogy of the hornfels.
- A comparative study of a hornfels zone found in drillhole HE-42 at Hellisheidi high-temperature system.
- A comparison with other hornfels locations, which have been studied in a similar way.

### 3.2 Field relations

Figure 9 shows a geological map of the HTG and surroundings. A hornfels zone is marked around the intrusion. Its thickness is variable as indicated in the figure. In appearance, the hornfels rock is very dark, very fine grained, hard and flinty (Appendix VII). This character is most pronounced near the margin of the gabbro (dolerite) but gradually changes into a normal intensely hydrothermally altered rock at some distance from the gabbro. This transition is evidenced by the change from the fine grained

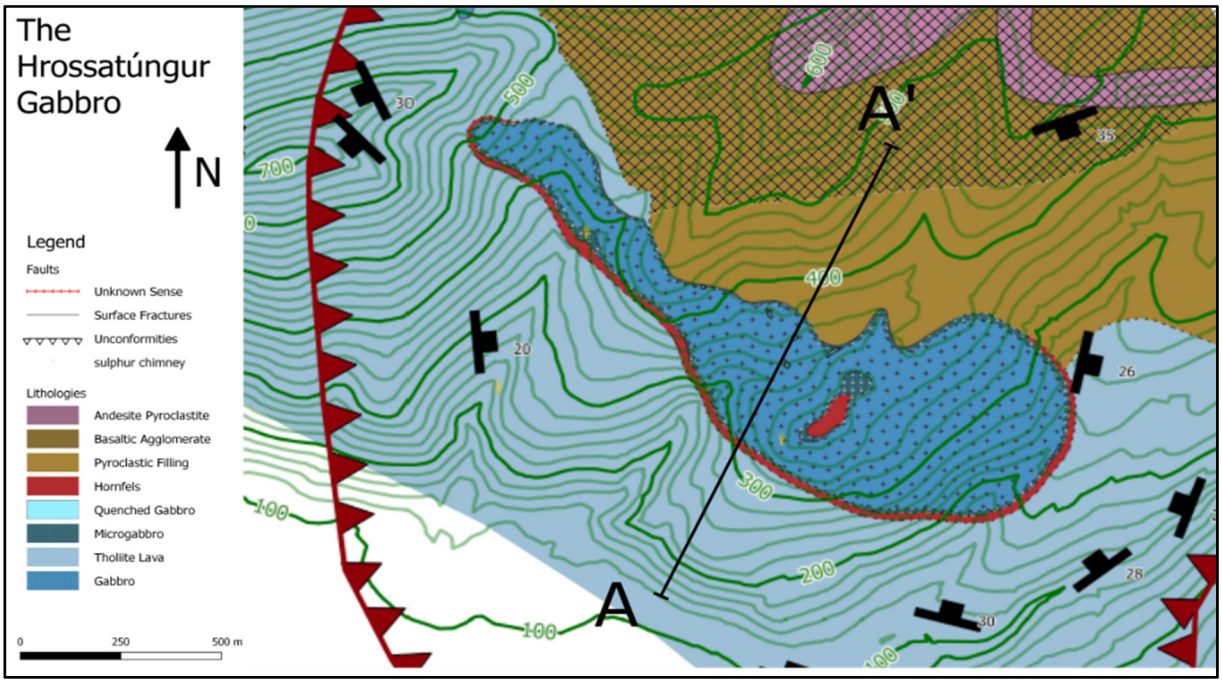


FIGURE 9: Hrossatungur gabbro and the surrounding basalt and pyroclastic caldera filling. The red contact indicates the relative thickness of hornfels around and at the roof of the intrusion

and dark colour of the rock into the more heterogeneous high-temperature alteration. It is also seen by the decreasing hardness away from the gabbro, which shows up as more erodible rocks. Another interesting feature is the similar cooling jointing that crosses the contact from the dolerite to the hornfels, which indicates contemporaneous consolidation of the margin of the gabbro and the hornfels. This conclusively shows partial melting and recrystallization of the hornfels contemporaneously with the margin (dolerite) of HTG. The thickness of the hornfels in the south part, as defined above, ranges from about 20-40 m, while the thickness to the north, where the HTG contacts the pyroclastic caldera fillings, appears to be much less. There, the exposures are more scree-covered, which in turn indicates that the rock never went through hornfels recrystallization/consolidation, as on the southern side. Instead, exposures show pillow-like structures, evidence for magma migration into water-saturated pyroclastics. At one location, clear brecciation has occurred, which has been interpreted as being due to the intrusion of water into the gabbro, causing steam-explosion activity and brecciation of the dolerite/gabbro. The hornfels on the northern side may therefore only be in the range of a few metres. This difference is interesting as it clearly implies that the transfer of heat from the intrusion is drastically less on the northern side, where it contacts with the pyroclastic caldera fillings, than at the southern contact against the basalt. An interesting aspect is that a thin hornfels zone is found in the central part of the gabbro, as shown in Figure 12, which marks the roof of the intrusion. The field relations are mainly derived from earlier unpublished studies from 2016 by Franzson and Brett.

### 3.3 Sampling

Sampling was done specifically for this hornfels research. The sites where most of the numbered samples were collected are shown in Figure 10. The total number of samples is 52. The sampling was threefold; firstly, individual samples from various hornfels locations around the gabbro; secondly, sampling of three specific profiles away from the gabbro (Figures 11, 12 and 13); and thirdly, a few samples from the roof of the intrusion in the eastern part.

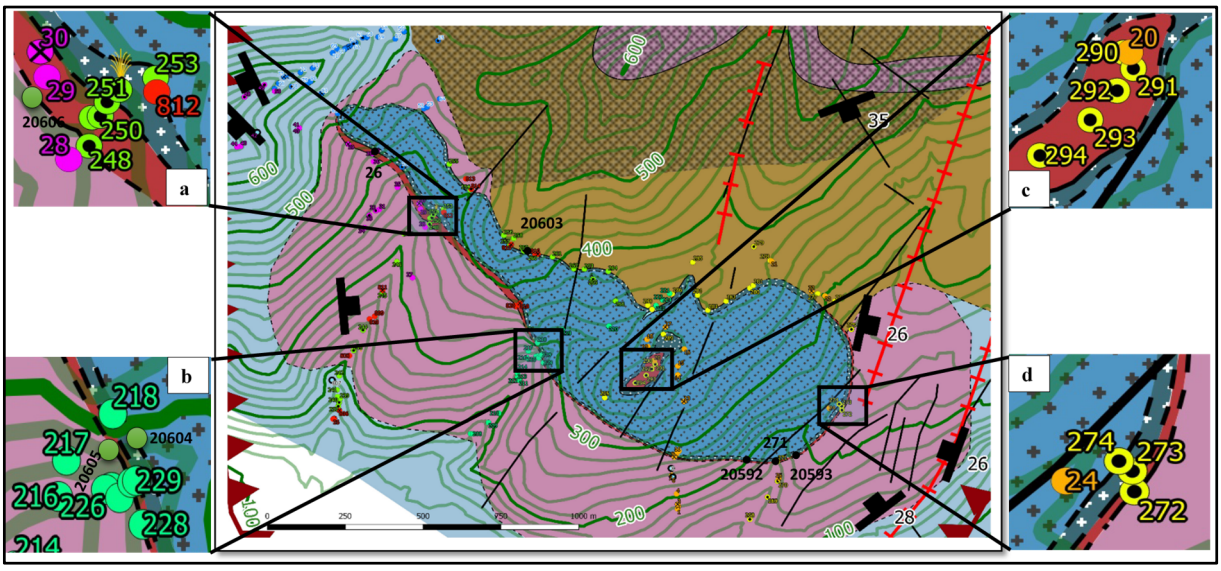


FIGURE 10: Geological map of the Hrossatungur gabbro and surroundings. Small squares enclose the locations of sampling profiles (a), (b), (c) and (d) while A, B, C and D subfigures show the analytical numbers referring of as listed in appendices. The varying colours of the numbers represent different field days. Sample location 272, represents a profile containing four samples (id of the four samples)

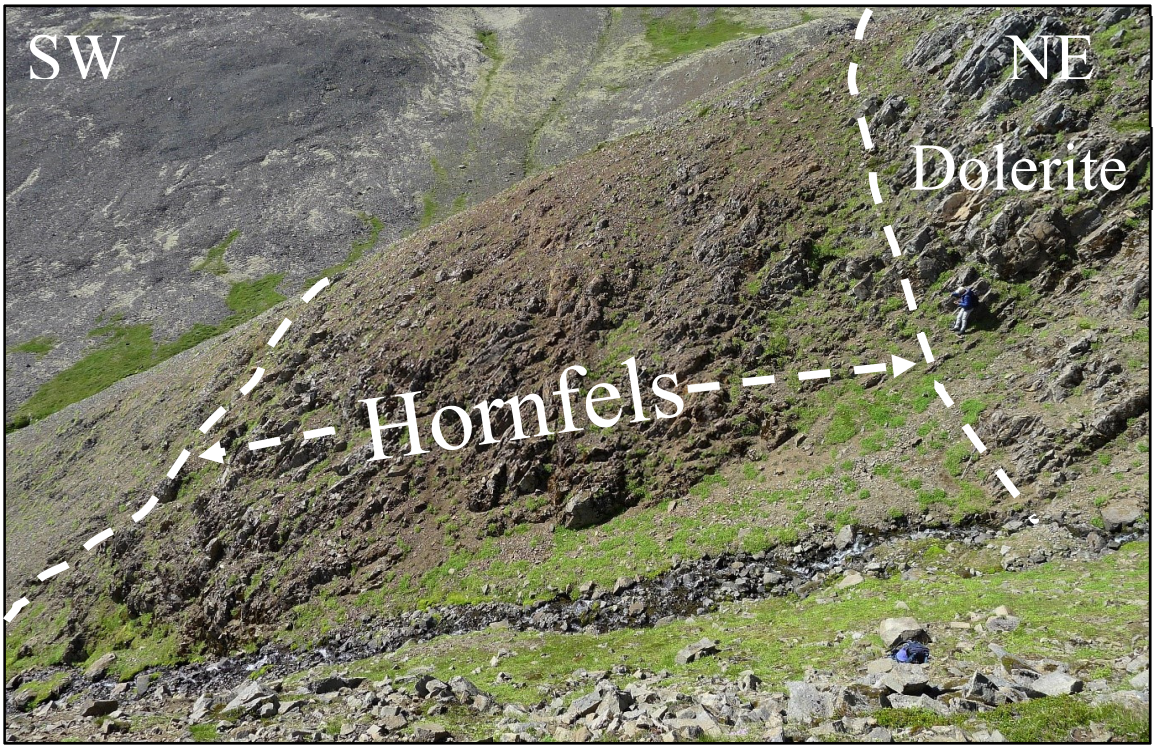


FIGURE 11: Hornfels contact zone in profile a

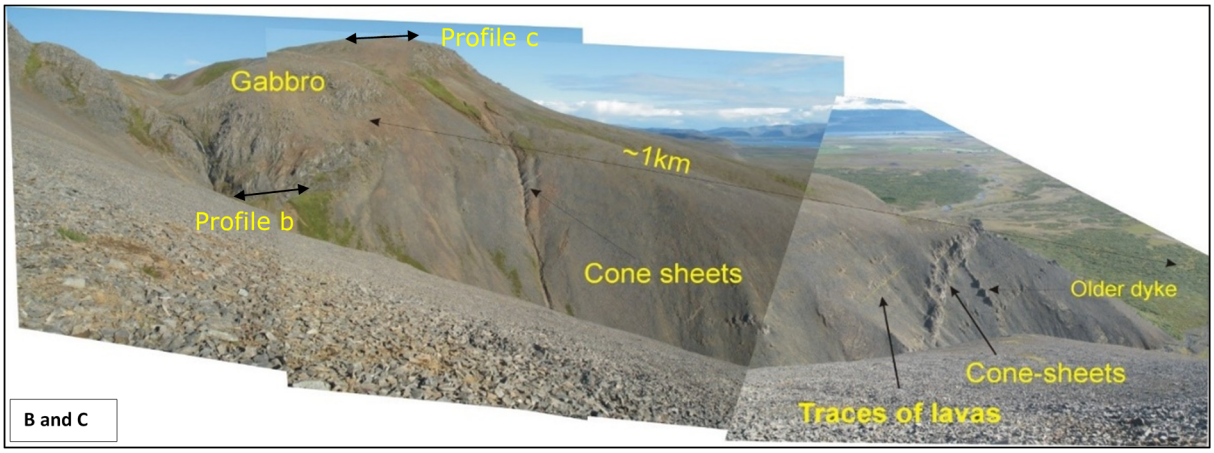


FIGURE 12: The southern margin of the gabbro showing the hornfels zone, profile b, roof hornfels profile c, steeply dipping lavas and cone sheets contemporaneous to the gabbro

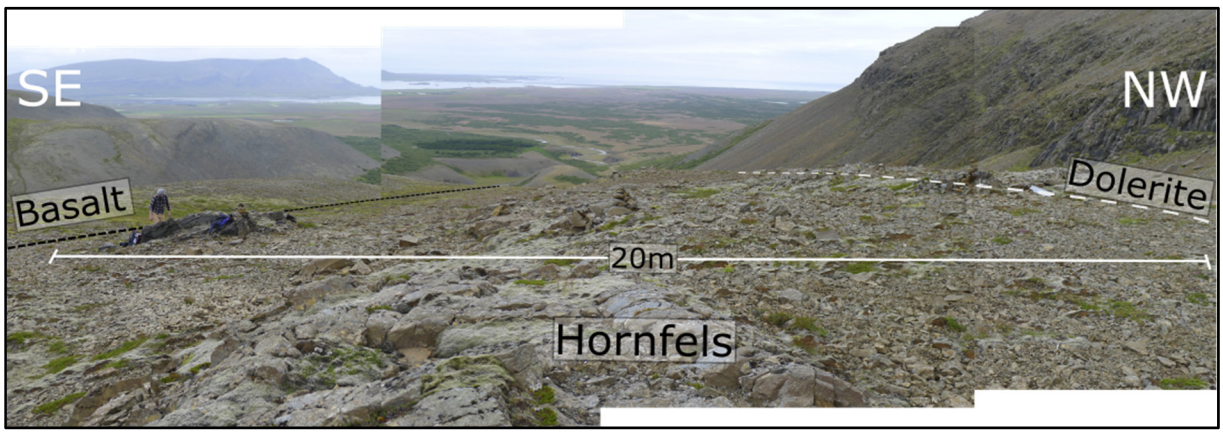


FIGURE 13: Hornfels contact zone, profile d

## 4. ANALYTICAL TECHNIQUES (METHODS)

The collected samples underwent several types of analyses as described below.

### 4.1 Binocular microscope analyses

Binocular microscope is one of the primary analytical techniques carried out with the aim to identify rock characteristics, such as texture, rock type(s), primary minerals, hydrothermal alteration intensity and vein fillings. The analyses were done at Iceland GeoSurvey (ÍSOR) petrography laboratory using an Olympus SX12 binocular microscope. Hornfels samples were collected from different locations around HTG as described earlier. Descriptions of the rock samples collected for this research are in Appendix VII.

### 4.2 Petrographic microscope analyses

The petrographic analytical technique assists in determining the finer details of the primary and hydrothermal alteration mineralogy and paragenetic mineral sequences. This method is used to add more details of the characteristics and features of minerals not distinguishable by the binocular microscope. Samples for thin-section analyses were selected from the hornfels zone around the HTG, mainly within four representative gabbro distance related profiles as inner and outer hornfels zones (a, b, c and d), along with individual samples along the hornfels zone. The locations of the profiles are shown in Figures 9-12. The aim of the study was to map and obtain a better overview of mineral distribution, degree of remineralization and hornfels types. A total of 33 thin-sections were analyzed based on the optical properties of the minerals using a Leitz Wetzlar and an Olympus BX51 petrographic microscopes (magnification range between 4x to 50x) at ÍSOR and at the Institute of Earth Sciences, University of Iceland (IES).

### 4.3 Inductively Couple Plasma-Optical Emission Spectrometry (ICP-OES)

Inductively Coupled Plasma-Optical Emission Spectrometry (ICP-OES) is one of the most powerful tools of optical emission spectrometry for quantitative elemental analysis. The basic principle behind this technique is atomic emission spectroscopy. A sample in the form of a solution is injected into the ICP unit through a narrow torch tube. Argon gas is supplied to the torch coil where it is ionized and plasma generated by an electromagnetic radiation field. This plasma has high electron temperature and density (10000 K) that is used for the excitation of the sample, which emits radiation as it goes back to ground state. The intensity and characteristics of the emitted radiation is measured optically with a detector (Xiandeng et al., 2000). The detector measures wavelengths and the intensity of the light, which is used to determine how much of each metal is present. The information is collected from the data system and compared with standard curves. A total of 30 samples from the hornfels zone around the HTG was analyzed. Most of the samples are homogeneous as they are derived from homogeneous basalt. A few of the samples, however, are hornflesed basalt with injected dioritic to silicic veins derived from late-stage gabbro melts. The samples from the hornfels contact zone around HTG were pre-treated by dissolving them. A Spectro Ciros 500, ICP-OES instrument at IES was used to measure major and trace elements.

### 4.4 Loss-on-ignition analyses (LOI)

The ICP-OES analysis described above does not take account volatiles that may be present in the samples. As this study focusses on the interaction between a molten magma and the surrounding groundwater system, it was deemed necessary to evaluate the amount of volatiles, mostly considered to be water and $CO_2$. This was done with loss-on-ignition test (LOI), which measures the amount of volatiles lost when the sample is ignited. The ruling factors controlling the analyses is the combustion

time and temperature. The ratio of the two aforementioned constituents is not determined directly by this method. This can, however, be assessed by petrographic observations of the samples.

In this study, about 30 samples were selected for LOI analyses in order to determine the water/carbon content in the hornfels. From 0.9 g to 1.6 g of each sample was accurately weighed, heated to 1000°C and weighed again to calculate the LOI ratio. Procedures and sample preparation for LOI analyses are described in detail in Appendix IV. The results are presented and discussed in Chapter 5.

### 4.5 Scanning electron microscopy (SEM)

In a scanning electron microscope (SEM), a narrowly focused beam of electrons (typically ≤1 μm in diameter) is used to probe the surface of a sample. Different detectors are used to measure electrons of different energy that are emitted from a sample and X-rays that are produced from the interaction of beam electrons with the sample. By scanning the beam over the sample, an image of the sample surface can be generated. Relatively low-energy secondary electrons are useful for imaging the surface relief of a sample, whereas emission of higher energy backscatter electrons (BSE) is strongly dependent on the mean atomic number of different parts of a sample. BSE images are therefore especially useful for distinguishing different minerals, as well as rock textures and zonation of minerals.

Each element in a sample emits X-rays of characteristic wavelengths with intensity that is proportional to the concentration of the element in the sample. This can be used for quantitative chemical analyses. Compared to an optical microscope, the scanning electron microscope (SEM) is capable of imaging at much higher magnification and greater focal depth. It is a versatile instrument for examination, capable of yielding multiple types of information about a geological sample, such as microstructural characteristics, crystal structure and chemical composition.

The SEM analyses (Appendix II) were done at IES. The analyses were performed with a Hitachi TM 3000 instrument, which is equipped with a BSE detector for imaging. This SEM also has an energy-dispersive spectrometer with a silicon-drift detector (SDD-EDS) from Bruker that was used for quantitative analyses and elemental mapping.

For chemical analyses of samples and good BSE images, it is important to use well-polished thin sections to avoid any surface topography. Moreover, it is also essential to have good electric conductivity on the surface, and for this purpose, the thin sections in this study were coated with about 25 nm thick carbon layer. Nine specific samples were selected from the southern part of the hornfels for inspection and analyses with the SEM.

### 4.6 Electron microprobe analyses (EMP)

The electron probe micro-analyzer at IES is a JEOL-8230 SuperProbe equipped with a LaB6 thermionic electron emitter. It has five wavelength-dispersive spectrometers (WDS), one with four different analytical crystals and the other four WDS with two different crystals each. This equipment provides the most accurate analyses of the minerals studied. It is, however, more expensive to use, and the main purpose of the EMP study was to confirm the SEM analyses.

For all analyses, the accelerating voltage was 15 keV. The probe current was measured at the Faraday cup prior to each analysis. Apatite and plagioclase were analyzed with 5 nA and 10 nA cup current, respectively, whereas pyroxene, oxides, garnet, amphibole and titanite were all analyzed with 20 nA. All of the minerals were analyzed with a focused beam, except amphibole with a 5 μm beam diameter. The standards used for the EMP analyses are listed in Tables 19a-g (Appendix VI). Most of the standards were provided as a courtesy of the Smithsonian Institution (NMNH and USNM standards). The CITZAF correction program (Armstrong, 1991) was used for all analyses, except for oxides and titanite where ZAF correction was applied.

Five samples (226, 230, 290 and 291) from the hornfels around HTG and from Hellisheidi geothermal field (well HE-42) were selected for analysis. These samples were carefully selected to present inner and outermost hornfels zone around HTG and compare with a hornfels zone around a dyke within the high-temperature geothermal system at Hellisheidi. The elements analyzed were Si, Mg, Fe, Ca, Na, Al, K, Mn and Ti. The structural formula has been recalculated on the basis of 24 oxygen, while Fe is calculated as ferrous iron in all analyses. The chemical composition of the representative minerals obtained in wt% and full results are shown in Appendix III.

## 5. RESULTS

### 5.1 Whole-rock chemistry

The rocks around HTG originated as eruptives, which subsequently were buried, and suffered after that variable but progressive hydrothermal alteration within the geothermal system(s), which is bound to have changed the rock compositions (e.g. Franzson, et al., 2008). The hornfels is the last major alteration phase of the rock. This involves both heating up and partially remelting of the rock. Further to that, one may speculate whether there have been some metasomatic reactions reaching outwards from the gabbro. The chemical analyses are an attempt to evaluate what changes took place during these episodes. For this purpose, a total of 30 samples from the hornfels zone around HTG were analyzed for whole-rock composition (major and trace element concentration). The major oxides include $SiO_2$, $Al_2O_3$, FeO (total), MgO, CaO, $Na_2O$, $K_2O$, MnO, $TiO_2$ and $P_2O_5$. Trace elements include Ba, Cu, Ni, Zn, Zr, Co, Cr, La, Sc, Sr, V and Y, as shown in Table 1. A detailed description of the procedures and sample preparation for ICP-OES analyses is presented in Appendix I.

$SiO_2$ is always the most abundant oxide and exhibits a wide variation in concentration. It was proposed by Harker (1909) that $SiO_2$ content increases steadily with magmatic evolution and that it could be used in variation diagrams to indicate the extent of differentiation (Harker, 1909). $SiO_2$ in the hornfels samples show a wide range in concentration, or from 30-75% by weight. Petrographic analyses of samples 248, 225, 231, 272c, 20604, 250, 229 and 273, which had elevated silicic contents, are affected by veining of andesitic to silicic material. The heterogeneity of the hornfels compositions indicates the shift in the original composition toward dacitic composition. For instance, sample 248 (basalt hornfels + magmatic), 225 (hornfels + magmatic diorite), 231 (quartz abundant in groundmass), 272c (quartz veining occurred after the hornfelsing process), 20604 (hornfels + diorite and silicic veining), 250 (quartz veins and intermediate rock composition), 229 (hornfels + diorite veining), and 273 (hornfels + silicic veins). These instances of veining explain the high silica content that has been added to the hornfels rocks during the metamorphism process. The veins originated as late stage melts, ejected from the gabbro and into the hornfels. The veins are fresh magmatic material, and the sample compositions cannot therefore be adequately interpreted in the context of the hornfels process. These veins do not show any cooling against the hornfels, which indicates similar temperatures as prevailing in the hornfels. The samples that contain dioritic to silicic magmatic veins are marked specifically on the diagrams.

Harker variation diagrams have been prepared to display the chemical data obtained from the ICP-OES analyses. These simple X-Y diagrams depict major elements content (Figure 14) and trace element concentration (as ppm) (Figure 15) versus $SiO_2$ content (wt%). The analyses have also been done in order to evaluate the chemical evolutionary trend of the system (Franzson, 1979). These samples, plotted together with the hornfels samples in Figures 14 and 15 were taken from relatively fresh rocks that have experienced minimum hydrothermal alteration, and are used here to establish the difference between the primary chemical trend and the hornfels, and in that way unravel the possible chemical enrichment or depletion that has taken place. This is evaluated below. In any comparison of chemical analyses, a consideration has to be made of whether the major elements are calculated in terms of percentage where the total is always 100% (Winter, 2014), because in that case, if one or more constituents are not included, it will proportionally increase the percentage of all the other constituents.

#### 5.1.1 Major elements

Major elements are plotted against $SiO_2$ in Figure 14. These are grouped, as mentioned above, into two parts; on the one hand, primary rock compositions (X and field encircled as shown in Figures 14 and 15) (Franzson, 1979); and, on the other, the compositions of the hornfels samples. If a sample falls within the primary compositional field, one may not be able to interpret whether enrichment or depletion has taken place or not. However, if an analysis falls outside the primary field, a change is likely to have taken place, but it may not be clear which of the oxides (elements) plotted has been added or removed. Therefore, the interpretation of the chemical change may have to rely more on the overall shift of oxide/elemental abundance of the hornfels samples rather than individual analyses.

TABLE 1: Major and trace elements of the hornfels contact zone around Hrossatungur gabbro based on ICP-OES analysis. See Figure 10 for location of the samples

| ICP No. | 1 | 2 | 3 | 4 | 5 | 6 | 7 | 8 | 9 | 10 | 11 | 12 | 13 | 14 | 15 |
|---|---|---|---|---|---|---|---|---|---|---|---|---|---|---|---|
| **Sample No.** | **225** | **226** | **227** | **228** | **229** | **230** | **231** | **248** | **250** | **251** | **252** | **271** | **272A** | **272B** | **272C** |
| **Major elements in wt%** | | | | | | | | | | | | | | | |
| **SiO2** | 59.56 | 46.61 | 48.71 | 48.71 | 53.71 | 50.35 | 55.57 | 75.47 | 53.82 | 49.37 | 42.73 | 45.31 | 47.99 | 49.36 | 55.17 |
| **Al2O3** | 13.16 | 16.91 | 13.81 | 15.11 | 13.72 | 13.59 | 12.34 | 11.37 | 14.75 | 14.84 | 22.87 | 18.02 | 16.75 | 16.53 | 14.71 |
| **FeO** | 14.39 | 14.71 | 13.09 | 14.82 | 12.75 | 14.97 | 12.33 | 2.78 | 14.03 | 14.40 | 21.92 | 17.60 | 17.18 | 18.17 | 14.81 |
| **MnO** | 0.13 | 0.21 | 0.23 | 0.31 | 0.20 | 0.27 | 0.21 | 0.03 | 0.38 | 0.36 | 0.15 | 0.39 | 0.31 | 0.26 | 0.20 |
| **MgO** | 2.71 | 9.51 | 6.08 | 3.13 | 3.64 | 3.47 | 2.78 | 0.39 | 3.18 | 2.86 | 1.65 | 2.90 | 2.88 | 3.89 | 1.70 |
| **CaO** | 4.00 | 6.49 | 11.47 | 9.29 | 7.87 | 10.08 | 7.28 | 0.72 | 4.55 | 9.37 | 3.38 | 9.96 | 8.17 | 4.61 | 4.72 |
| **Na2O** | 2.31 | 2.70 | 2.96 | 2.90 | 3.22 | 2.78 | 3.59 | 0.85 | 4.67 | 4.12 | 0.72 | 0.41 | 1.24 | 1.08 | 3.39 |
| **K2O** | 0.63 | 0.19 | 0.25 | 0.83 | 1.03 | 0.26 | 1.97 | 7.81 | 0.16 | 0.11 | 0.66 | 0.10 | 0.43 | 1.21 | 0.09 |
| **TiO2** | 2.78 | 2.27 | 2.91 | 3.80 | 3.11 | 3.46 | 2.68 | 0.23 | 3.02 | 3.09 | 4.65 | 4.42 | 4.26 | 4.29 | 3.59 |
| **P2O5** | 0.19 | 0.20 | 0.34 | 0.95 | 0.59 | 0.62 | 1.04 | 0.02 | 1.29 | 1.34 | 0.98 | 0.72 | 0.63 | 0.42 | 1.49 |
| **Trace elements in (ppm)** | | | | | | | | | | | | | | | |
| **Ba** | 147.65 | 123.29 | 92.93 | 154.11 | 253.54 | 140.92 | 349.30 | 1833.87 | 50.23 | 43.58 | 134.48 | 41.39 | 152.66 | 237.53 | 28.92 |
| **Co** | 66.59 | 78.57 | 65.12 | 58.97 | 52.82 | 63.54 | 57.37 | 3.94 | 45.04 | 44.94 | 104.03 | 89.34 | 77.77 | 82.51 | 49.87 |
| **Cr** | 25.49 | 300.37 | 16.98 | 3.92 | 5.94 | 4.94 | 8.53 | 4.18 | 4.64 | 4.12 | 88.30 | 30.46 | 27.14 | 38.76 | 8.15 |
| **Cu** | 180.81 | 125.94 | 98.69 | 45.09 | 24.87 | 53.20 | 43.93 | 67.13 | 37.69 | 43.16 | 565.49 | 113.72 | 114.45 | 220.17 | 58.60 |
| **La** | 21.03 | 12.45 | 22.66 | 42.44 | 43.45 | 35.16 | 70.50 | 80.86 | 52.64 | 55.91 | 36.15 | 48.30 | 39.57 | 36.00 | 54.26 |
| **Ni** | 48.03 | 250.63 | 60.36 | 25.76 | 2.47 | 6.07 | 10.82 | 15.78 | 16.50 | 10.88 | 85.34 | 42.35 | 52.07 | 75.76 | 89.68 |
| **Sc** | 38.99 | 45.89 | 43.28 | 36.07 | 30.59 | 35.37 | 36.22 | 2.05 | 33.67 | 35.12 | 71.88 | 51.18 | 46.56 | 45.61 | 35.77 |
| **Sr** | 150.35 | 211.33 | 262.45 | 222.79 | 297.61 | 237.12 | 352.32 | 210.57 | 273.29 | 286.74 | 98.29 | 138.27 | 156.35 | 123.83 | 136.36 |
| **V** | 361.02 | 386.04 | 395.62 | 232.05 | 229.75 | 294.70 | 181.86 | 25.68 | 121.81 | 131.82 | 910.10 | 463.97 | 459.98 | 472.77 | 142.41 |
| **Y** | 36.16 | 26.33 | 34.93 | 81.18 | 64.08 | 66.23 | 107.20 | 115.00 | 104.45 | 108.01 | 64.70 | 74.74 | 60.98 | 55.26 | 106.81 |
| **Zn** | 129.13 | 157.45 | 105.04 | 166.31 | 119.53 | 174.96 | 174.45 | 76.31 | 177.92 | 183.57 | 277.03 | 224.49 | 187.95 | 180.30 | 116.89 |
| **Zr** | 224.78 | 173.74 | 196.36 | 368.44 | 415.28 | 294.30 | 636.25 | 634.77 | 485.80 | 488.11 | 376.48 | 415.41 | 334.69 | 286.94 | 475.92 |

| ICP No. | 16 | 17 | 18 | 19 | 20 | 21 | 22 | 23 | 24 | 25 | 26 | 27 | 28 | 29 | 30 |
|---|---|---|---|---|---|---|---|---|---|---|---|---|---|---|---|
| **Sample No.** | **272D** | **273** | **274** | **292** | **293** | **20592** | **20603** | **20604** | **20604** | **20606** | **20608** | **20622** | **25** | **26** | **27-gabbro** |
| **Major elements in wt%** | | | | | | | | | | | | | | | |
| **SiO2** | 50.75 | 52.54 | 51.11 | 48.98 | 48.51 | 49.83 | 47.07 | 49.05 | 54.22 | 50.63 | 48.33 | 48.71 | 44.31 | 30.83 | 48.76 |
| **Al2O3** | 16.23 | 15.41 | 13.86 | 20.45 | 17.96 | 19.03 | 13.73 | 16.25 | 14.34 | 15.49 | 13.39 | 13.50 | 15.24 | 23.65 | 18.74 |
| **FeO** | 13.19 | 12.29 | 12.93 | 14.62 | 16.25 | 11.35 | 16.34 | 15.71 | 13.94 | 15.53 | 14.84 | 15.10 | 15.03 | 29.56 | 8.17 |
| **MnO** | 0.16 | 0.19 | 0.23 | 0.27 | 0.40 | 0.22 | 0.28 | 0.20 | 0.18 | 0.27 | 0.20 | 0.27 | 0.26 | 0.22 | 0.14 |
| **MgO** | 5.46 | 5.41 | 4.52 | 2.64 | 3.35 | 3.77 | 3.79 | 4.50 | 3.92 | 2.50 | 6.61 | 5.41 | 7.11 | 2.05 | 5.56 |
| **CaO** | 9.26 | 8.69 | 9.61 | 5.69 | 6.39 | 6.76 | 12.72 | 7.41 | 6.86 | 6.71 | 11.03 | 10.44 | 12.30 | 2.53 | 14.31 |
| **Na2O** | 1.91 | 2.19 | 3.34 | 2.24 | 1.79 | 4.39 | 2.13 | 3.03 | 2.84 | 4.41 | 2.08 | 2.47 | 1.85 | 1.13 | 2.35 |
| **K2O** | 0.25 | 0.48 | 0.82 | 1.70 | 0.75 | 0.20 | 0.11 | 0.27 | 0.30 | 0.16 | 0.05 | 0.16 | 0.14 | 2.83 | 0.26 |
| **TiO2** | 2.42 | 2.35 | 2.88 | 3.04 | 3.84 | 3.76 | 3.25 | 2.98 | 2.84 | 2.89 | 3.02 | 3.37 | 3.24 | 6.10 | 1.47 |
| **P2O5** | 0.25 | 0.28 | 0.54 | 0.17 | 0.57 | 0.50 | 0.44 | 0.43 | 0.41 | 1.26 | 0.31 | 0.43 | 0.36 | 0.80 | 0.12 |
| **Trace elements in (ppm)** | | | | | | | | | | | | | | | |
| **Ba** | 92.94 | 172.03 | 176.05 | 341.57 | 181.00 | 123.14 | 92.45 | 103.39 | 113.51 | 29.89 | 52.21 | 77.22 | 93.25 | 692.93 | 69.61 |
| **Co** | 61.84 | 60.14 | 57.51 | 70.67 | 80.41 | 63.42 | 75.59 | 60.92 | 54.14 | 39.06 | 68.64 | 70.19 | 73.82 | 142.03 | 47.28 |
| **Cr** | 94.06 | 91.92 | 14.33 | 109.59 | 37.66 | 72.42 | 27.53 | 16.01 | 14.13 | 5.98 | 40.74 | 26.49 | 46.30 | 50.89 | 90.56 |
| **Cu** | 106.02 | 181.50 | 103.09 | 199.00 | 107.25 | 182.53 | 100.08 | 118.19 | 141.68 | 23.62 | 97.77 | 87.23 | 197.70 | 201.91 | 171.02 |
| **La** | 16.50 | 17.17 | 31.27 | 19.89 | 38.14 | 28.76 | 28.46 | 40.57 | 39.74 | 55.75 | 19.82 | 24.99 | 25.06 | 49.35 | 11.17 |
| **Ni** | 96.24 | 92.43 | 18.18 | 62.46 | 31.62 | 65.46 | 40.31 | 36.37 | 19.87 | 2.84 | 59.49 | 31.80 | 66.22 | 129.34 | 207.96 |
| **Sc** | 42.40 | 41.87 | 35.05 | 50.75 | 48.08 | 56.10 | 41.61 | 38.32 | 35.14 | 34.71 | 41.07 | 41.32 | 47.17 | 78.73 | 34.55 |
| **Sr** | 198.70 | 244.52 | 274.21 | 179.76 | 189.08 | 429.53 | 244.34 | 250.19 | 253.33 | 190.77 | 192.46 | 223.23 | 227.50 | 109.28 | 315.70 |
| **V** | 285.08 | 313.33 | 322.38 | 457.99 | 476.11 | 422.74 | 419.36 | 380.41 | 357.86 | 133.10 | 416.43 | 467.76 | 454.10 | 875.10 | 245.84 |
| **Y** | 22.95 | 26.08 | 51.07 | 37.96 | 76.12 | 50.74 | 46.48 | 70.75 | 63.98 | 109.78 | 32.80 | 44.66 | 35.59 | 90.87 | 14.01 |
| **Zn** | 109.26 | 108.75 | 122.30 | 160.79 | 198.81 | 112.84 | 141.09 | 170.69 | 147.00 | 194.83 | 151.14 | 143.06 | 141.25 | 324.51 | 81.20 |
| **Zr** | 153.42 | 146.91 | 284.49 | 163.18 | 305.17 | 302.02 | 215.75 | 422.01 | 403.32 | 557.70 | 164.71 | 219.09 | 194.29 | 402.08 | 99.61 |

Four of the samples show $SiO_2$ content less than 45%, which indicates depletion. One of them has only 30%, a sample taken from a zone of strong sulphidisation superimposed on the hornfels process. Six samples have 52-56% $SiO_2$, which may indicate enrichment as described above. $Al_2O_3$ appears to show general enrichment, while CaO shows a sign of depletion, as does MgO. FeO seems, in general, to stay within the primary field, but a few samples appear to be enriched. $Na_2O$ has tendency to be depleted, while $K_2O$ shows more diverse compositional tendencies, as do MnO and $P_2O_5$. $TiO_2$ falls largely within the primary compositional field.

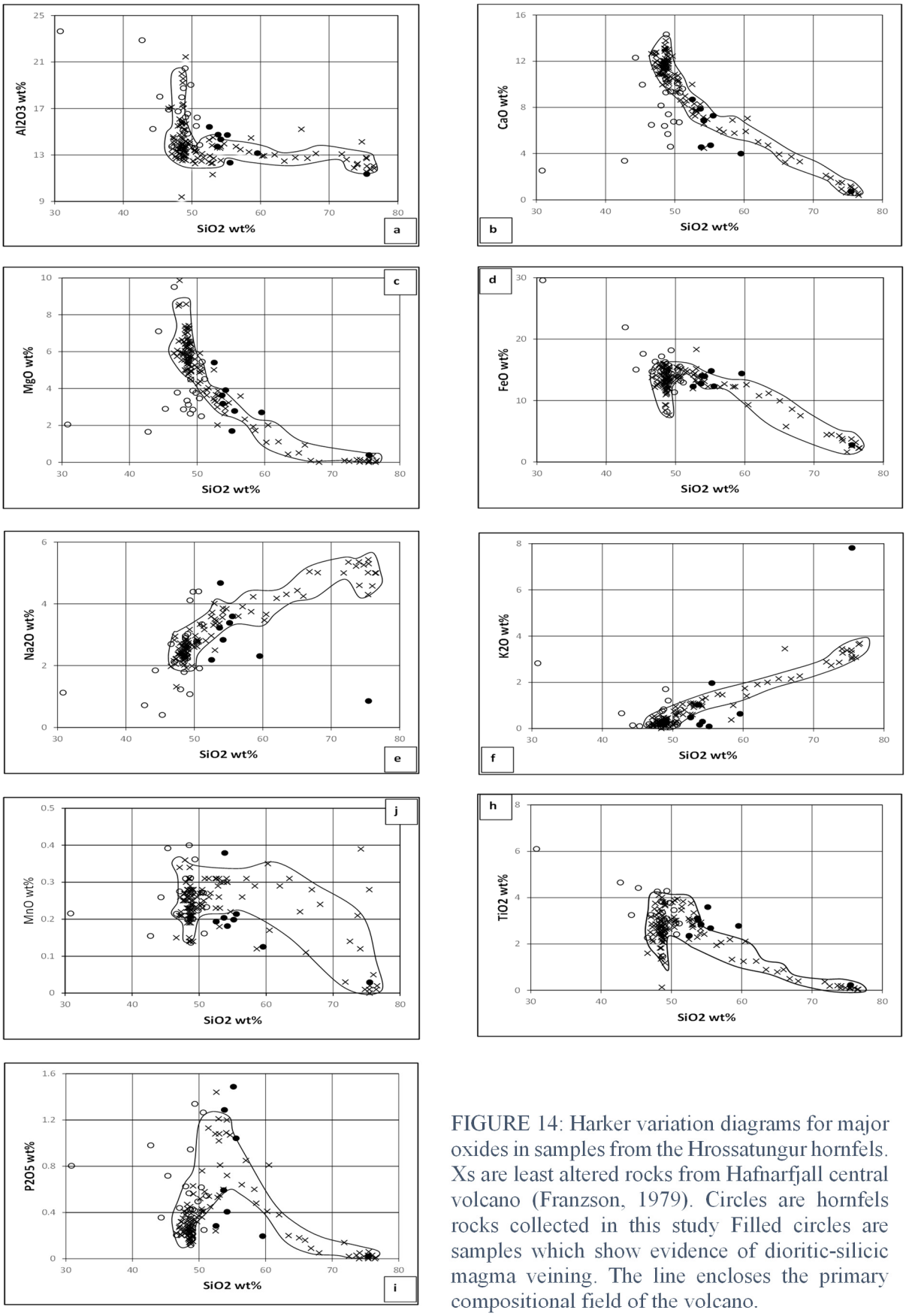


FIGURE 14: Harker variation diagrams for major oxides in samples from the Hrossatungur hornfels. Xs are least altered rocks from Hafnarfjall central volcano (Franzson, 1979). Circles are hornfels rocks collected in this study Filled circles are samples which show evidence of dioritic-silicic magma veining. The line encloses the primary compositional field of the volcano.

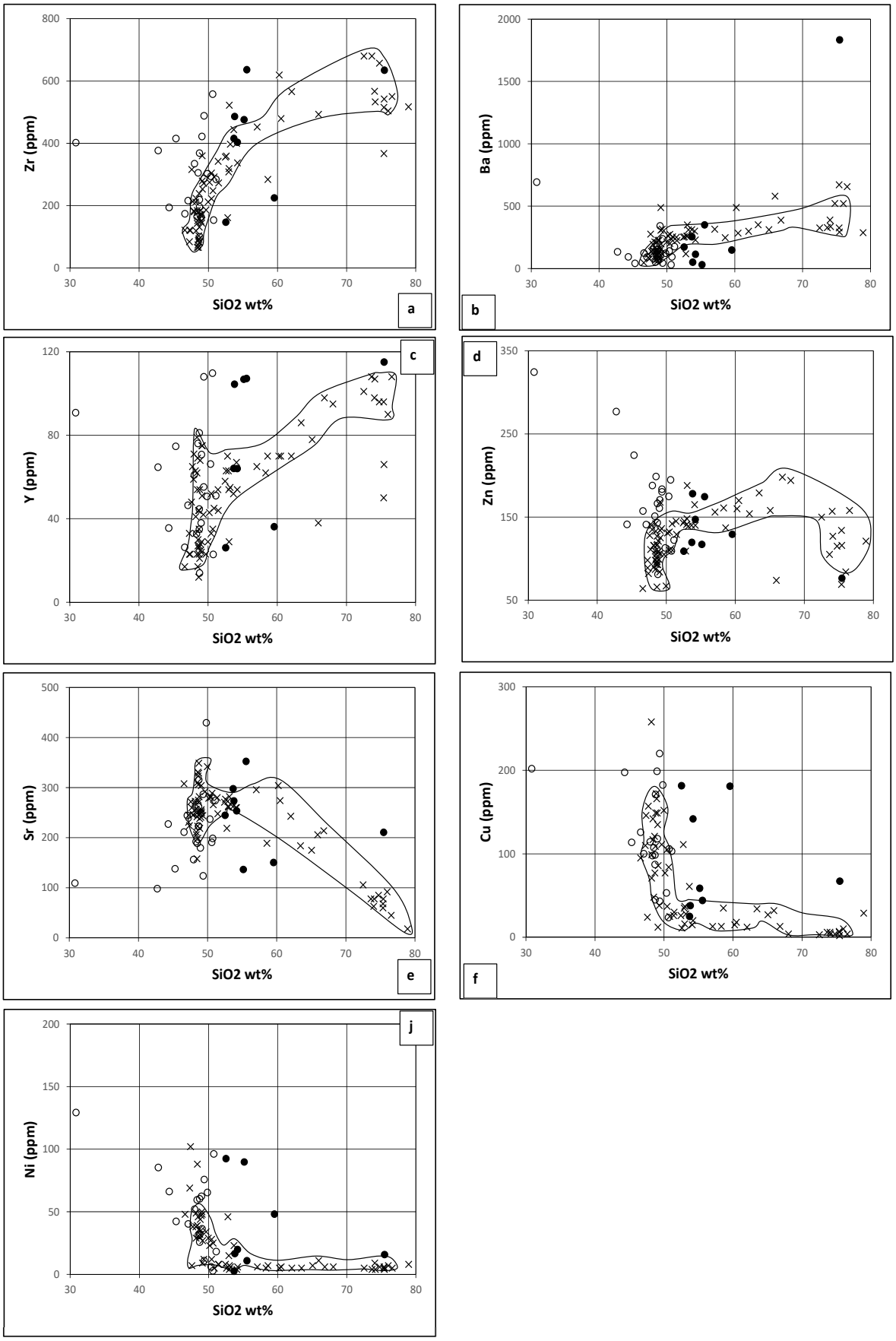


FIGURE 15: Harker variation diagrams for trace elements in samples from the Hrossatungur hornfels. Xs are least altered rocks from Hafnarfjall central volcano (Franzson, 1979). Circles are hornfels rocks collected in this study Filled circles are samples which show evidence of dioritic-silicic magma veining. The line encloses the primary compositional field of the volcano

### 5.1.2 Trace elements

Trace elements plotted against $SiO_2$ in the hornfels rocks show, as do the major elements, greater compositional diversity compared to the fresh rock equivalents, and only general observations can be made regarding compositional changes. Zr, Zn, Cu and Ni appear to show an overall increase, while Ba and Sr may show signs of depletion. These trace element trends are described in detail below.

Barium concentration increases with $SiO_2$ concentration during magmatic differentiation. It was pointed out by Deer (1965) that Ba and Sr often replace Ca in titanite. Sample 248 is enriched in La due to the silicic vein enrichment. Samples 272 and 231 are located at the inner contact and have higher La compared to 225 and 226 located at the outer margin. Strontium concentration increases with SiO2 and ranges from 98-429 ppm. Samples 251, 229, and 274 at the inner hornfels zone have higher Sr than samples 248, 226 and 225 (outer margin). Yttrium concentration is enriched in some samples and depleted in others. Apatite tends to have relatively high concentration of Y. Zirconium concentration increases with SiO2 and samples 248 and 231 from the outermost hornfels zone have higher Zr contents due to the high sulphide contents, while samples 292 and 226 (inner margin) have the lowest Zr contents.

Barium, Sc, V, Cr and Co show depletion. V tends to substitute for Ti in titanite (Deer, 1965). Samples 292, 272, 273 and 252 show higher amount of Cr, while samples 225 and 248 have the lowest amounts. It is notable that the Ni concentration ranges by two orders of magnitude. Nickel is a strongly siderophile element and is depleted in the silicate portion of the Earth. It is much concentrated in the core, but behaves similar to Mg in silicates and is concentrated in early forming mafic minerals (White, 2013).

### 5.1.3 Comparison between Zr and major or trace elements

The degree of chemical exchange can commonly be evaluated by plotting element concentrations of both samples affected and unaffected by hydrothermal alteration versus immobile elements like Zr (Franzson, et al., 2008). This method allows us to test the alteration trends of the hornfels samples around Hrossatungur gabbro compared to the least altered samples collected from the Hafnarfjall central volcano. Figures 16 and 17 show major elements and trace elements, respectively, plotted against Zr. The diagrams show a division of the hornfels samples into two groups, where the filled circles indicate samples (petrographic analysis) that contain dioritic-silicic magma veins and thus apparent silica enrichment. As it is known that Zr is an immobile element, samples falling outside the primary compositional field would imply mobility of that particular oxide or trace element. $SiO_2$ largely follows the primary trend with Zr, but there seems to be an overall shift of the hornfels sample group towards depletion. This is in particular the case for highly sulphidised rocks. $Al_2O_3$, on the other hand, shows in general enrichment, also in particular in the sulphide-rich samples. FeO and MgO seem to fall nicely within the primary trend, while $Na_2O$ only partly follows the trend with slight shift towards depletion. Other major elements do not show clear deviation from the primary compositional trend.

Trace elements plotted against Zr, on the other hand, show a clearer picture. Zinc, Cu and Ni seem to show an overall slight shift towards enrichment, but Ba, and possibly Sr show depletion. Copper, Ni and Zn enrichment might be connected to sulphide-rich volatiles released from the gabbro.

## 5.2 Loss-on-ignition (LOI) analyses

The LOI method is used to estimate water and carbonate content in rocks. Igneous rocks generally contain only small amount of primary water. For example, tholeiitic basalts on the seafloor usually contain about 0.25% primary water and Hawaiian basalts about 0.5% (Moore, 1970). When hydrothermal alteration starts, primary minerals break down to form hydrous varieties, which then increases the water content of the rocks. Prior to the intrusion of HTG, the surrounding rocks had gone through hydrothermal alteration to a different degree, relatively high alteration south of the intrusion, but only to the smectite-zeolite stage within the pyroclastic caldera fillings north of the gabbro intrusion. For this study, 30 samples were collected within the hornfels contact zone, same as the ones that were chemically analyzed (Appendix IV). The purpose of the LOI analyses was to evaluate the volatile content of the hornfels zone.

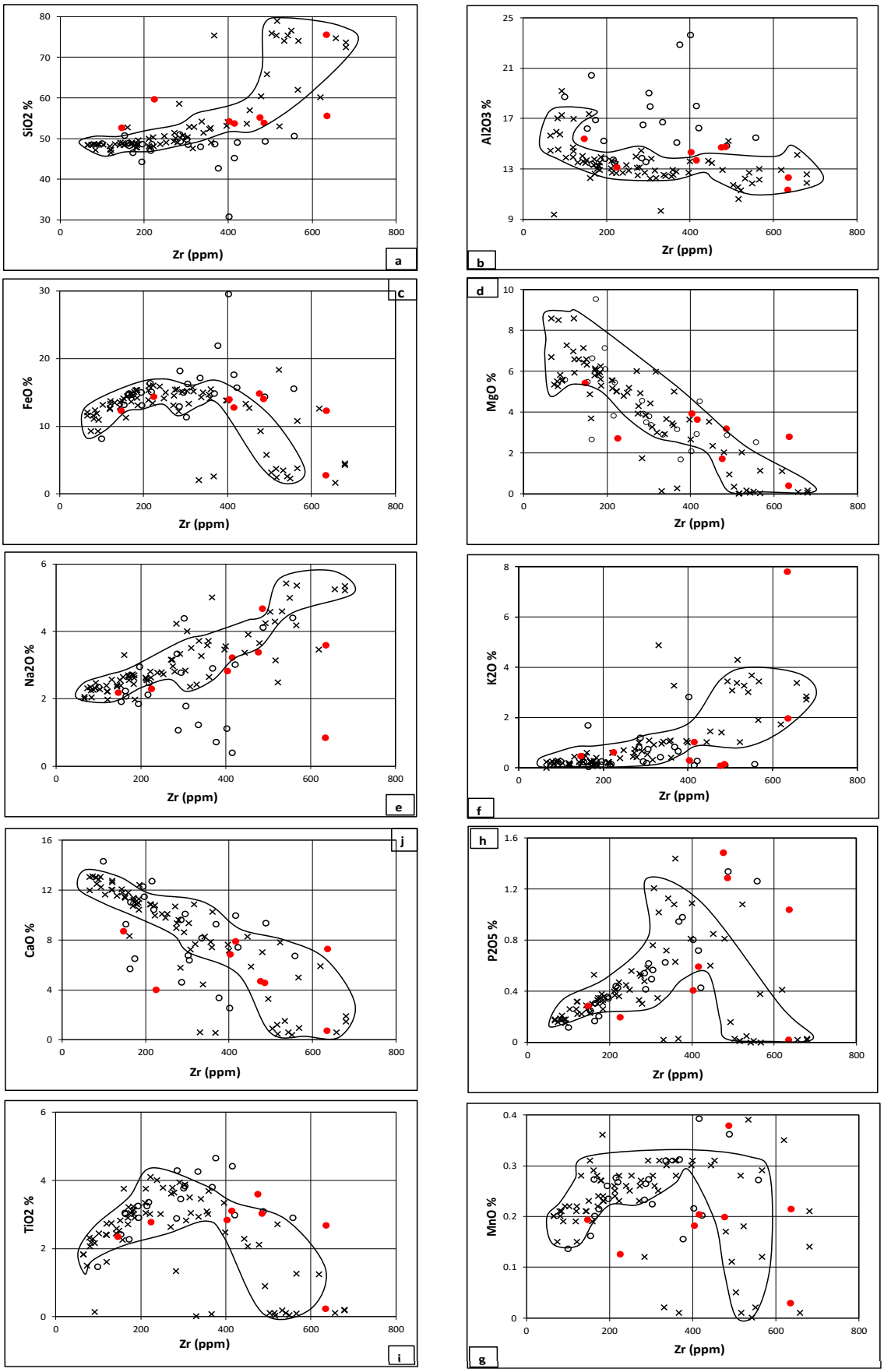


FIGURE 16: Major elements plotted against Zr. Xs are least altered rocks from Hafnarfjall central volcano (Franzson, 1979). Circles are hornfels rocks collected in this study. Filled circles are samples which show evidence of dioritic-silicic magma veining. The line encloses the primary compositional field of the volcano

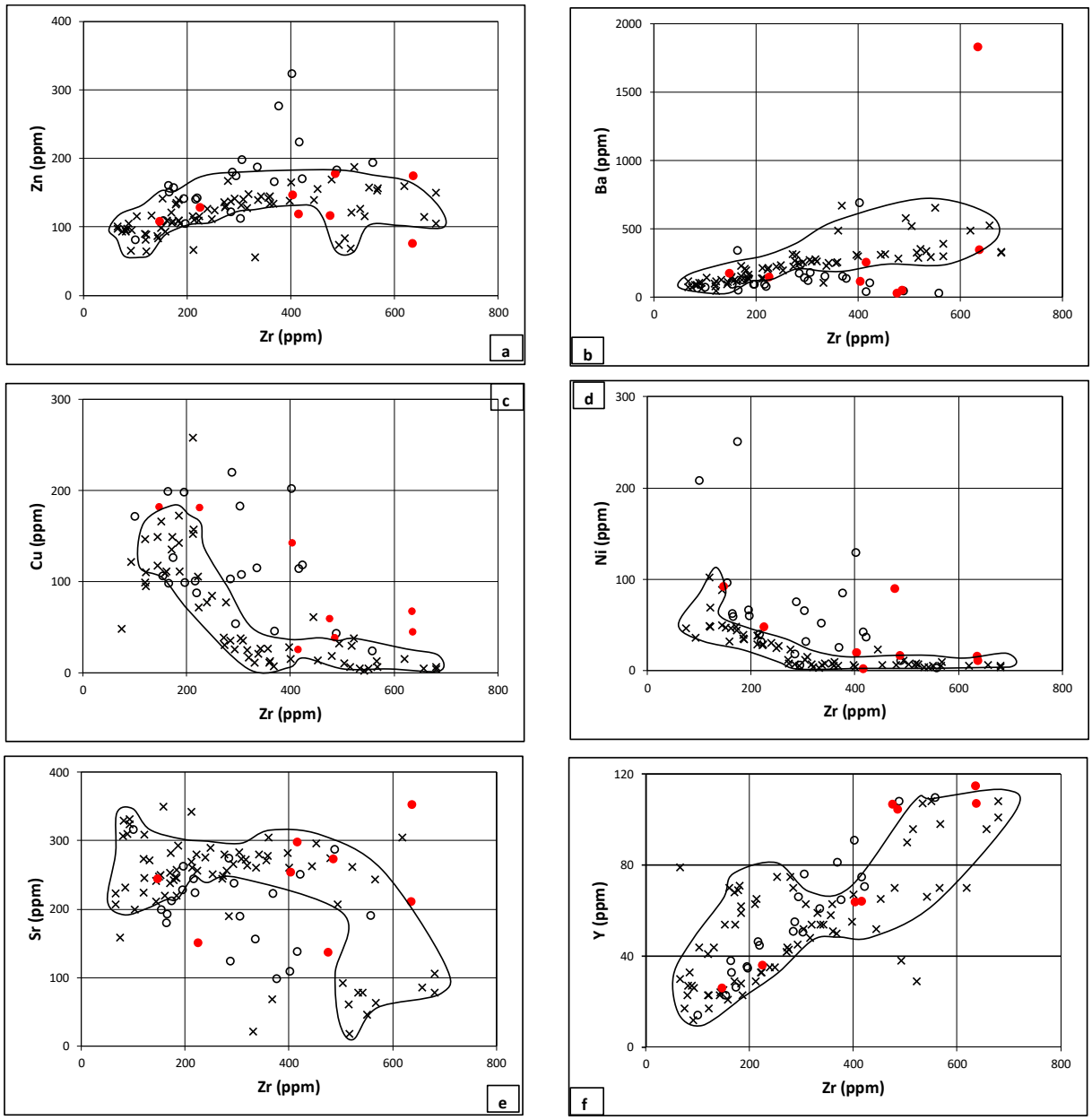


FIGURE 17: Trace elements plotted against Zr. Xs are least altered rocks from Hafnarfjall central volcano (Franzson, 1979). Circles are hornfels rocks collected in this study. Filled circles are samples which show evidence of dioritic-silicic magma veining. The line encloses the primary compositional field of the volcano

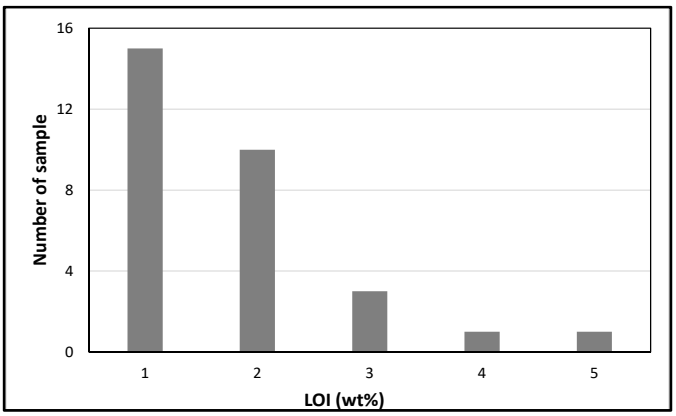


FIGURE 18: A histogram showing the range of LOI in the hornfels samples around Hrossatungur gabbro

Figure 18 is a histogram showing the range of LOI of the samples. The majority of the samples experience <1% LOI. The samples that show higher values are mostly from the outer hornfels zone, in particular samples 250 and 272. Figure 19 shows a comparison of LOI values of Icelandic rocks in different alteration zones with the values from the hornfels (Franzson, et al., 2001). These show clearly that the hornfelsed rocks, which should have had LOI contents >1 to <10% prior to the gabbro emplacement, have had water driven out by the replacement of hydrous minerals by non-

hydrous minerals. The petrographic evidence is ample as the hornfels contains dominantly plagioclase, pyroxene and oxides. Minor carbonates are present in the hornfels, indicating that the LOI present water and carbonate. Only minor amount of garnets and amphiboles are observed which may contain the water, largely found in the former vesicle and vein fillings of the rocks.

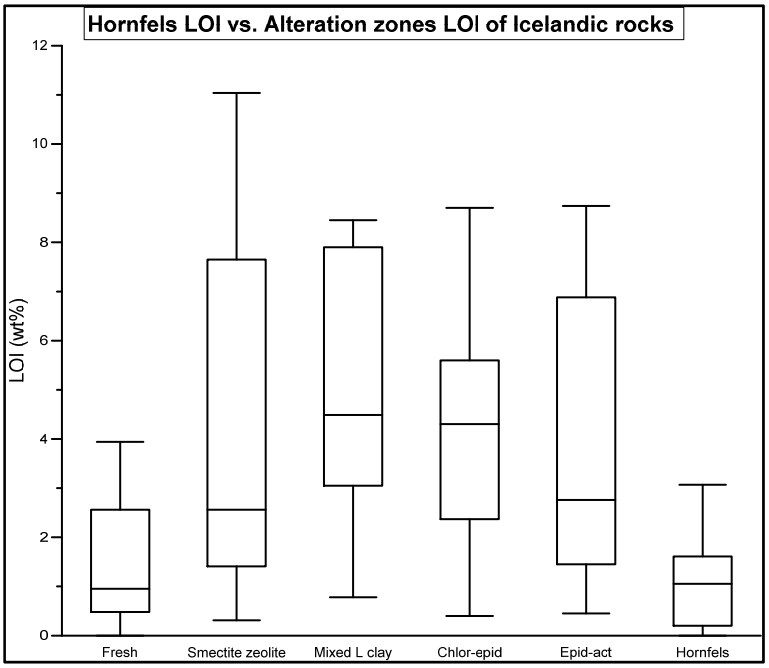


FIGURE 19: Comparison between loss on ignition (wt%) of different alteration zones in Icelandic rocks (Franzson, et al., 2001) and LOI of the hornfels around Hrossatungur gabbro. Solid line in the boxes indicates a median value. Horizontal lines in the boxes represent 25, 50 (median) and 75% of value

### 5.3 Petrography and mineralogy of the hornfels around Hrossatungur gabbro

The Hrossatungur gabbro intrusion in the Hafnarfjall caldera formation was emplaced at the boundary between the lava-dominated high-temperature system to the south and the low-temperature system belonging to the pyroclastic caldera fillings in the north (Franzson, et al., 2008). The exposed hornfels contact zone around the southern part of Hrossatungur gabbro is shown in Figure 9. The contact zone is loosely divided into two zones; an inner and an outer zone. The inner one is the hornfels nearest to the gabbro margin, while the outer one is located up to 20 m further out from the gabbro.

When viewing the hornfels petrography, one has to consider the protolith. In this case, the hornfels protolith comprises various basaltic lava flows, which were partially altered. That includes vesicles and fractures in the rocks being partially or fully filled with alteration minerals, which may have included clays, silica, zeolites and perhaps higher temperature minerals, like epidote, prehnite and amphibole. Volatile content may also have varied in different parts. When the rocks then went through the hornfels stage, all this heterogeneity played a part in the variable mineralogy occurring in the rock. Although the hornfels represents a partly recrystallized rock, vesicle and vein fillings are easily recognized in hand specimens and certainly in the microscope, which strongly indicates recrystallization *in situ*. Two observations are notable in this respect; the vesicle and vein fillings most often show larger crystals than the surrounding groundmass; and we often find a clear reaction zone around the vesicles/veins (e.g., see Figure 20), often represented by the disappearance of oxides and an increase in the amount of pyroxene. The groundmass is very fine grained, and apparently made of pyroxene, plagioclase and then charged with opaque oxides. It is debatable whether the groundmass represents a possible pseudomorphed primary crystallinity or not. In a few

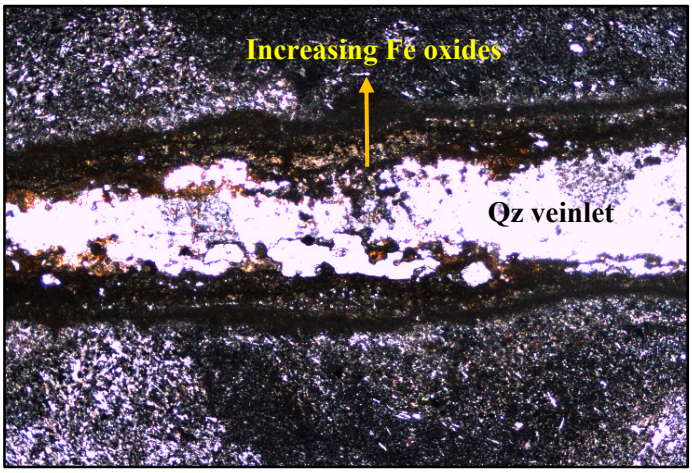


FIGURE 20: Quartz veinlet and Fe oxides increased towards the rim and groundmass (sample 291). Thin section viewed in plane polarized light

locations, the rock possibly shows granoblastic texture of oxides, pyroxene and plagioclase, which is well known in hornfels rocks.

### 5.3.1 Inner contact zone

The fine-grained hornfels in the inner contact zone is characterized by a heterogeneous texture and high degree of recrystallization, and is in places granoblastic, due to the high heat from the cooling gabbro. Vesicle fillings contain abundant opaque minerals in the center, changing to pyroxene nearer to the margins. This pyroxene occasionally shows zoning towards more pleochroic varieties and rare amphibole is present. This indicates that Fe released from magnetite increased the growth of pyroxene. The chemical transfer also included Mg and Ti, which participated in the growth of garnet and titanite in the inner contact zone as a product of thermal metamorphism. The andesine composition of plagioclase is further discussed in the section on SEM/EMP analyses. However, apatite, which is an example of a primary mineral of igneous crystallization, is found in a magmatic veins cross-cutting the hornfels. Three samples 252, 25 and 26 have very high sulphide content and were taken from within sulphide "chimneys", which superimposed and succeeded the hornfels. The analyses of the sulphides are further discussed in the section on SEM analyses below.

Interesting mineral zoning is seen within a vesicle fillings in sample 226 (Figures 21 and 33 (see later)). There, the pyroxene is transparent in the centre, as observed in a petrographic microscope, but contained within a more pleochroic outer margin, and then changing to fibrous amphibole in the outermost part. These mineralogical changes are discussed in more detail in Chapter 5. Felsic veins are found in the hornfels. They provide information about the temperature of the hornfels, against which they show no indication of cooling, which indicates magmatic temperatures of >800°C.

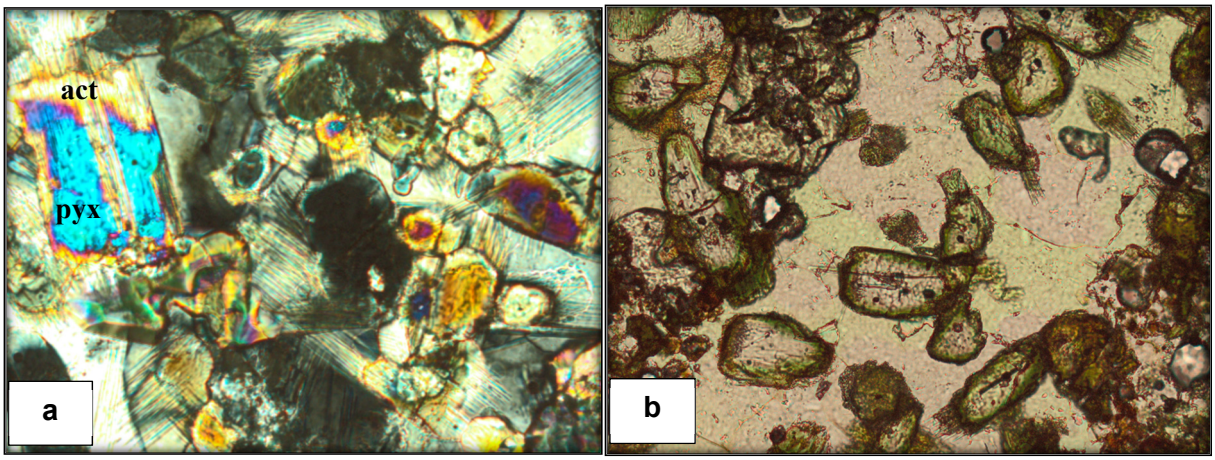


FIGURE 21: (a) Pyroxene grading into actinolite/hornblende (thread-like). Some pyroxene remain as high relief areas in the hornblende cores and along cleavages at the rims in sample 226. Thin section viewed with crossed polarizers. (b) Compositional zoning in pyroxene (sample 226) with pronounced colour variation visible in plane-polarized light; the rims are higher in iron than the cores grading into amphibole

### 5.3.2 Outer contact zone

The apparent petrographic difference between the inner and outer hornfels zones is the generally finer crystallinity of the rock in the latter. There, the rock appears to be more charged with opaques and have less pronounced reaction rims around the vesicles. The crystallinity increases within the vesicles in the inner zone. Similarly, we see in the inner zone more of pyroxene than opaques along with plagioclase. The granodiorite veining is assumed to be more dominant in the inner contact of the hornfels zone. Garnet and titanite are relatively common within the vesicles and minor amphibole. Calcite is occasionally seen in the vesicles.

### 5.4 Mineral analyses with SEM and EMP

The main objective of using the SEM was to evaluate the chemical composition and compositional range of several minerals in the hornfels, in particular pyroxene, plagioclase and oxides. As this method may not provide adequately accurate quantitative analyses in all cases, a selection of the thin sections was also analyzed using the microprobe in order to ascertain the reliability of the former. The rocks are dominantly very fine grained and impossible to pinpoint the same grains to compare the analyses of the two instruments. Pyroxene, plagioclase and oxides were the main phases analyzed, but other minerals were also of interest. Of importance was to observe variations in mineral compositions in the groundmass and compare with compositions of minerals found within vesicles and veins.

The samples chosen for these analyses were basically selected from profiles a, b, c and d (Figure 10), covering the inner part to outermost margin of the hornfels zone. The samples chosen for SEM and EMP analyses are listed in Appendix VII. Further to this, a sample of a hornfels rock located at the margin of a dyke at about 1500 m depth in well HE-42 at Hellisheidi geothermal field (described in Chapter 6) was analyzed in a similar way.

### 5.5 Chemical variation of pyroxene in the hornfels

#### 5.5.1 Inner border of the hornfels contact zone

*Sample 290* was analyzed with both SEM and EMP. The sample comes from the roof hornfels adjacent to the gabbro in profile c (Figures 10 and 22). Clino-pyroxene composition in the vesicles fillings in sample 290 ranges from salite, augite, ferrosalite to ferro-augite, while the orthopyroxene composition observed is hypersthene. Clinopyroxene in the groundmass of sample 290 has salite to ferrosalite composition. The EMP analyses in general show similar compositions and reveal similar compositional range, except that analyses are fewer and orthopyroxene was not encountered. Clinopyroxene composition in sample 230 (inner hornfels zone) from profile b (Figure 10 and 22), determined with SEM, reveals the range from salite to augite and EMP showed similar compositions. SEM analyses furthermore identified Mg-rich orthopyroxene.

*Sample 291* is collected from the hornfels at the top of the HTG in profile c as shown in Figures 10 and 22 and analyzed with SEM and EMP. The centre and the margin of the vesicles imply salite composition, while the groundmass appears to fall within the augite compositional range. No analyses were made of orthopyroxene.

*Sample 251* is from the inner margin of hornfels in profile a in Figure 10 and 23. It was only analyzed by SEM and shows that augite and salite reside in vesicle centers, with minor augite found in groundmass.

*Sample 271* is from the inner margin of the contact zone and was only analyzed with SEM. Orthopyroxene is found in the centre and margin of vesicles. The orthopyroxene of the vesicle center ranges from hypersthene to ferrohypersthene composition.

Sample 274 was taken from the hornfels inner margin in profile d (Figures 10 and 23). The clinopyroxene composition is augite with a groundmass composition extending to diopside. The orthopyroxene composition is magnesian bronzite with less than 1 wt% CaO content, as classified in Figure 25.

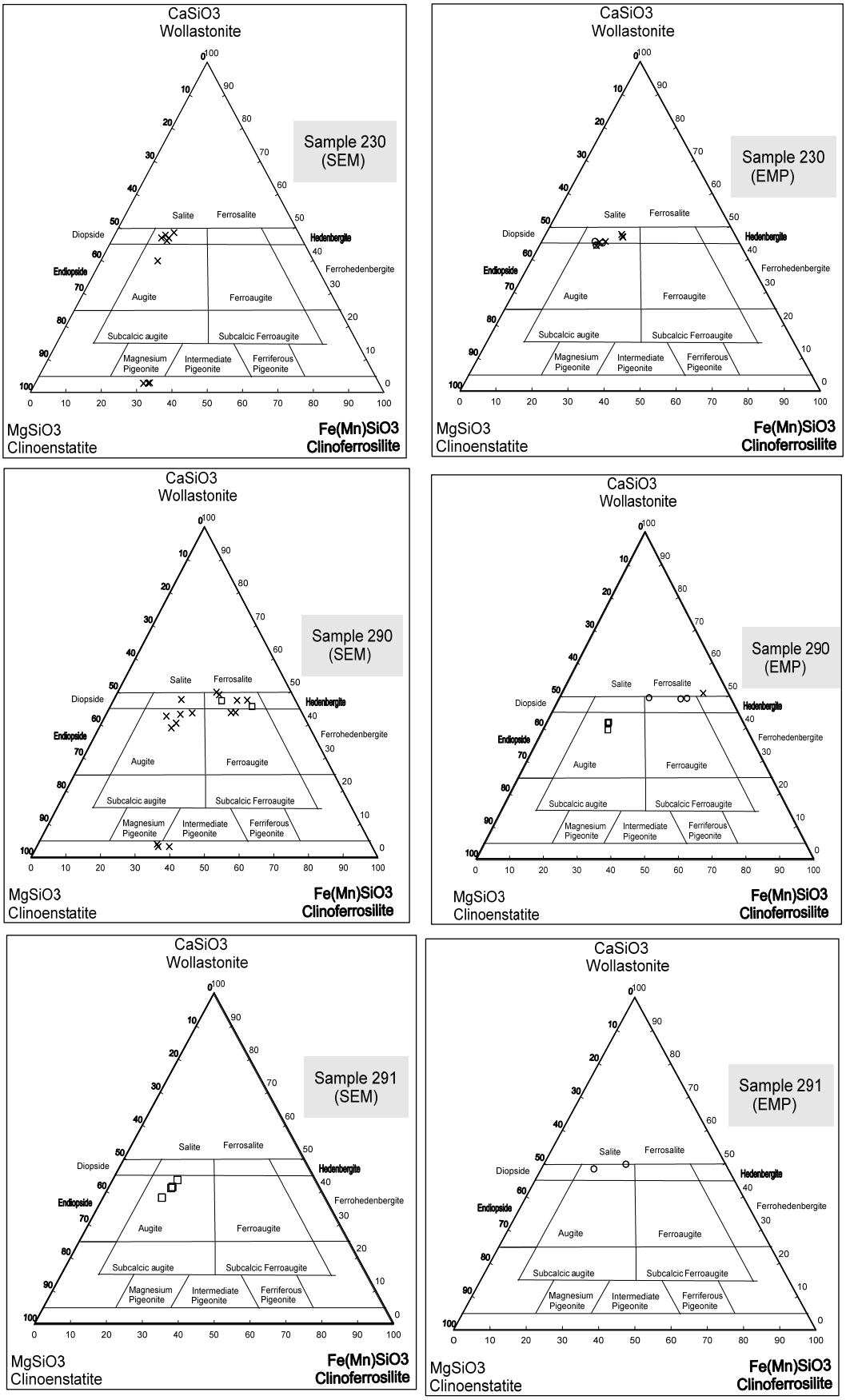


FIGURE 22: Pyroxene composition in the inner hornfels contact zone determinated by both SEM and EMP in term of Ca-Mg-Fe element, data from Appendices II and III. Xs are pyroxene composition at the vesicle centre. Circles are the composition at the margin while squares are at groundmass

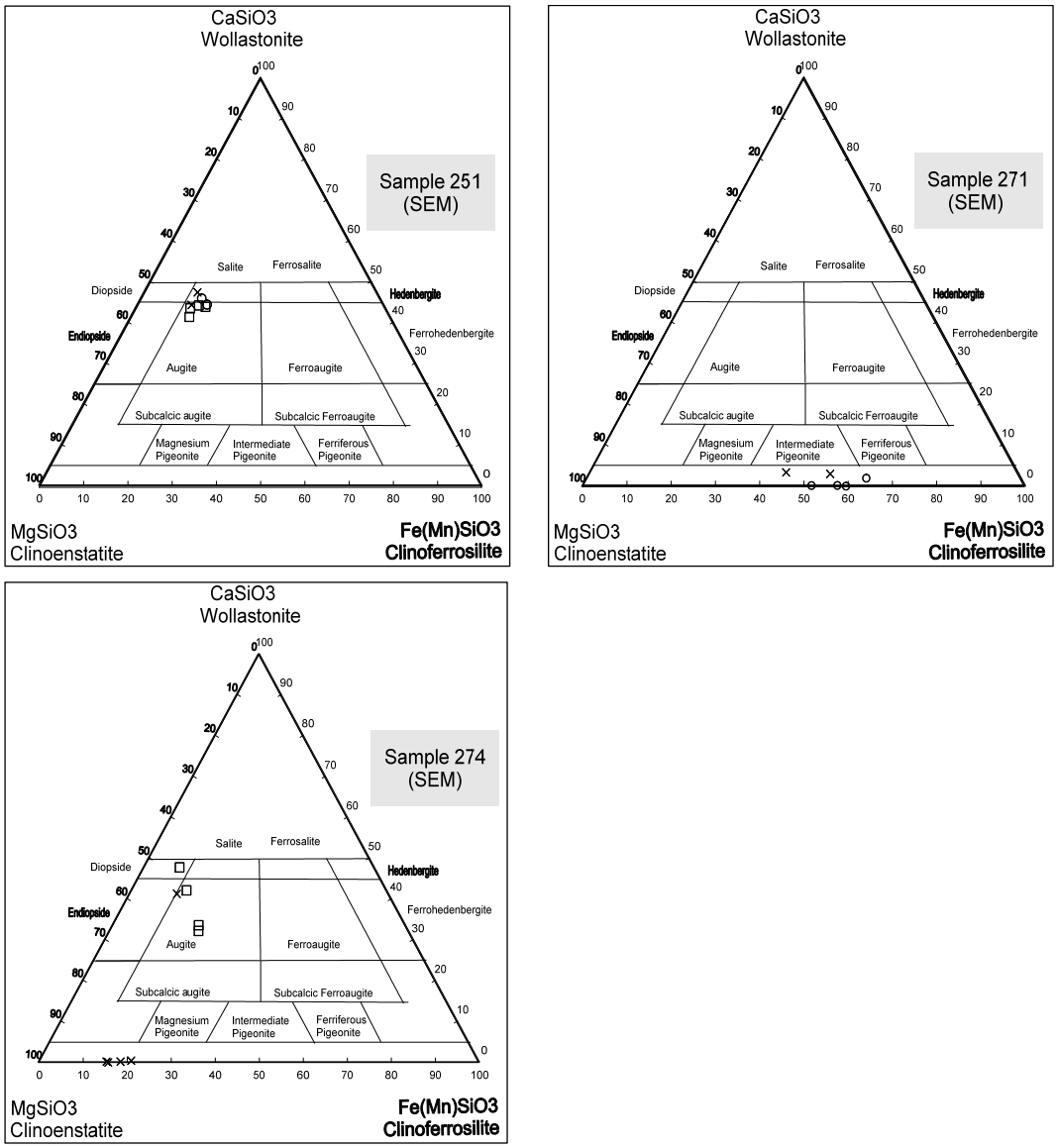


FIGURE 23: Pyroxene composition in terms of the Wo-En-Fs components in the inner hornfels contact zone determined by SEM. Data from Appendix II. X denote pyroxene composition at vesicle centre. Circles are the composition at the margin while squares are at groundmass

### 5.5.2 Outer border of the hornfels contact zone

SEM analyses of sample 226 from profile b (located at the outer hornfels margin) show clinopyroxene composition at the boundary of salite-augite in the center of vesicles (Figure 24). The EMP reveals augite to salite composition at the centers of vesicles and salite to ferrosalite to hedenbergite at the margins. The groundmass shows salite to augite composition. Thus, the variation in clinopyroxene composition from vesicle centers to rock wall is augite, salite, ferrosalite and hedenbergite, and is shown in Figure 24. This means that there is Fe enrichment in the composition of clinopyroxene at the outer hornfels margin. No orthopyroxene (Figure 25) was found in the outer zone, except in one sample 248, which may indicate that orthopyroxene tends to form at the higher temperature range of the hornfels. This sample (248) is from the hornfels taken about 10-40 cm from a cone sheet at the outer hornfels contact zone, and was analyzed only by SEM. The only orthopyroxene analyzed is within the compositional range of hypersthene.

While six samples were analyzed within the inner zone, only two were analyzed in the outer one, which makes a comparison difficult. However, there seems to be a difference between the groundmass pyroxene and vesicle fillings. The groundmass clino-pyroxene is dominantly in the salite-augite range,

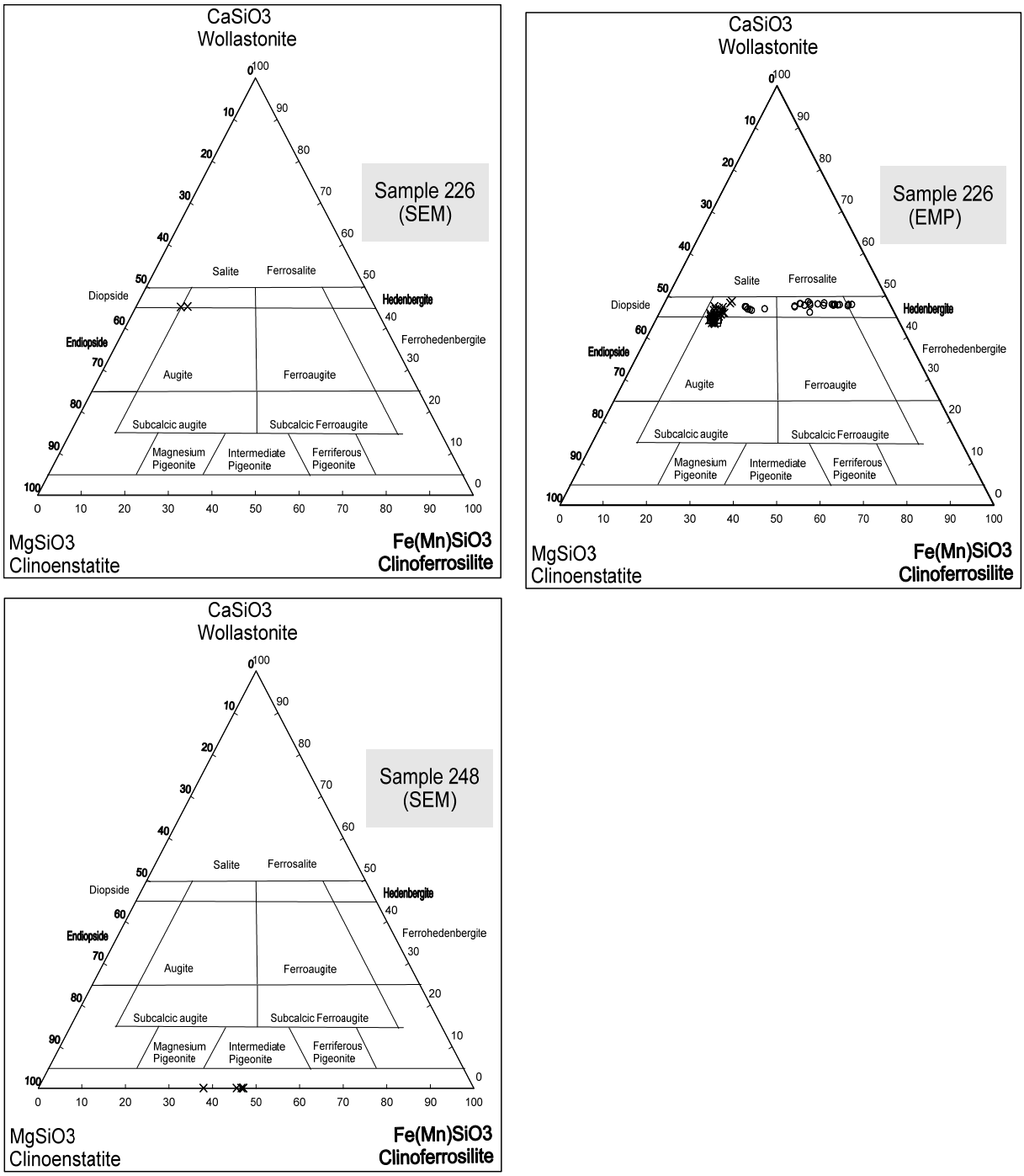


FIGURE 24: Pyroxene composition in the outer hornfels zone determined by both SEM/EMP. Data from Appendices II and III. Xs denote pyroxene composition at vesicle centres. Circles are the compositions at the margin, while squares at the groundmass

but the compositional range is wider reaching to much more iron rich varieties, namely to hypersthene in the vesicle fillings.

### 5.6 Chemical composition of plagioclase within the hornfels

Plagioclase was analyzed with SEM and EMP in a similar way as pyroxene, and classified into three different categories depending on the origin, i.e., from the groundmass, vesicle margins and from near the center of the vesicles at the inner and outer margin of the hornfels contact zone.

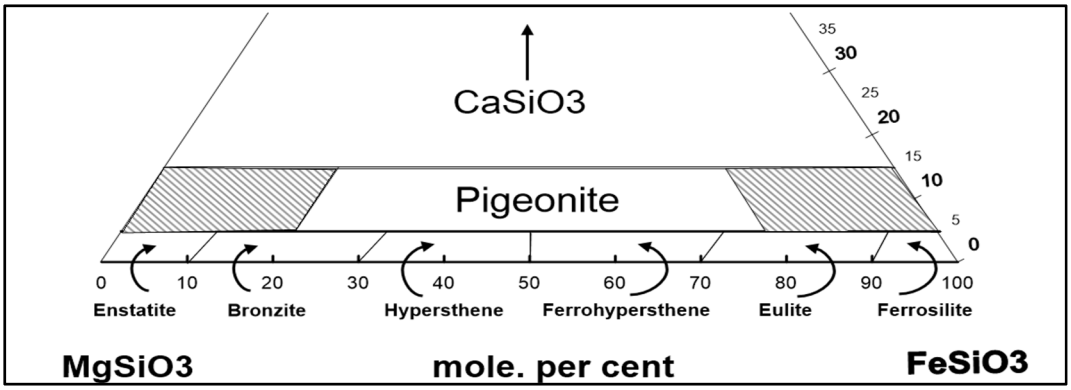


FIGURE 25: Classification diagram for orthopyroxene (Deer and Zussman, 1997)

### 5.6.1 Inner boundary of hornfels zone

*Sample 230* (profile b) was both analyzed with SEM and EMP (Figure 26). Both show mainly labradorite composition, though extending slightly into andesine in the SEM analyses.

*Sample 290* (roof hornfels, profile c) also shows the labradorite as the dominant composition but extending slightly towards andesine in the SEM analyses and bytownite in the EMP analyses.

*Sample 291* (roof hornfels, profile c) has plagioclase compositions within the labradorite range and is similar in both SEM and EMP analyses, slightly more anorthite-rich in the latter.

*Sample 251* (profile a) was analyzed by SEM and shows the range from andesine to labradorite both within vesicles and groundmass.

*Sample 271* (from the southern corner of the gabbro as shown in Figure 27 has plagioclase with compositions within the anorthite field, both in the groundmass and vesicle fillings.

*Sample 274* (profile d) analyzed by SEM shows vesicle compositions of andesine and one analysis of groundmass within the labradorite field.

### 5.6.2 Outer boundary of hornfels zone

Sample 226 (profile b) was analyzed both with SEM and EMP (Figure 28). The former gave largely labradorite composition for plagioclase, extending into the andesine field, while the EMP showed labradorite to bytownite compositions. The groundmass plagioclase appears to be more anorthite-rich. Sample 248 (profile a), which was only analyzed by SEM, has anomalous plagioclase composition, which is within the oligoclase range. A possible reason for this Na enrichment is that this sample contains silicic magmatic veins, which may have increased the Na content of the plagioclase.

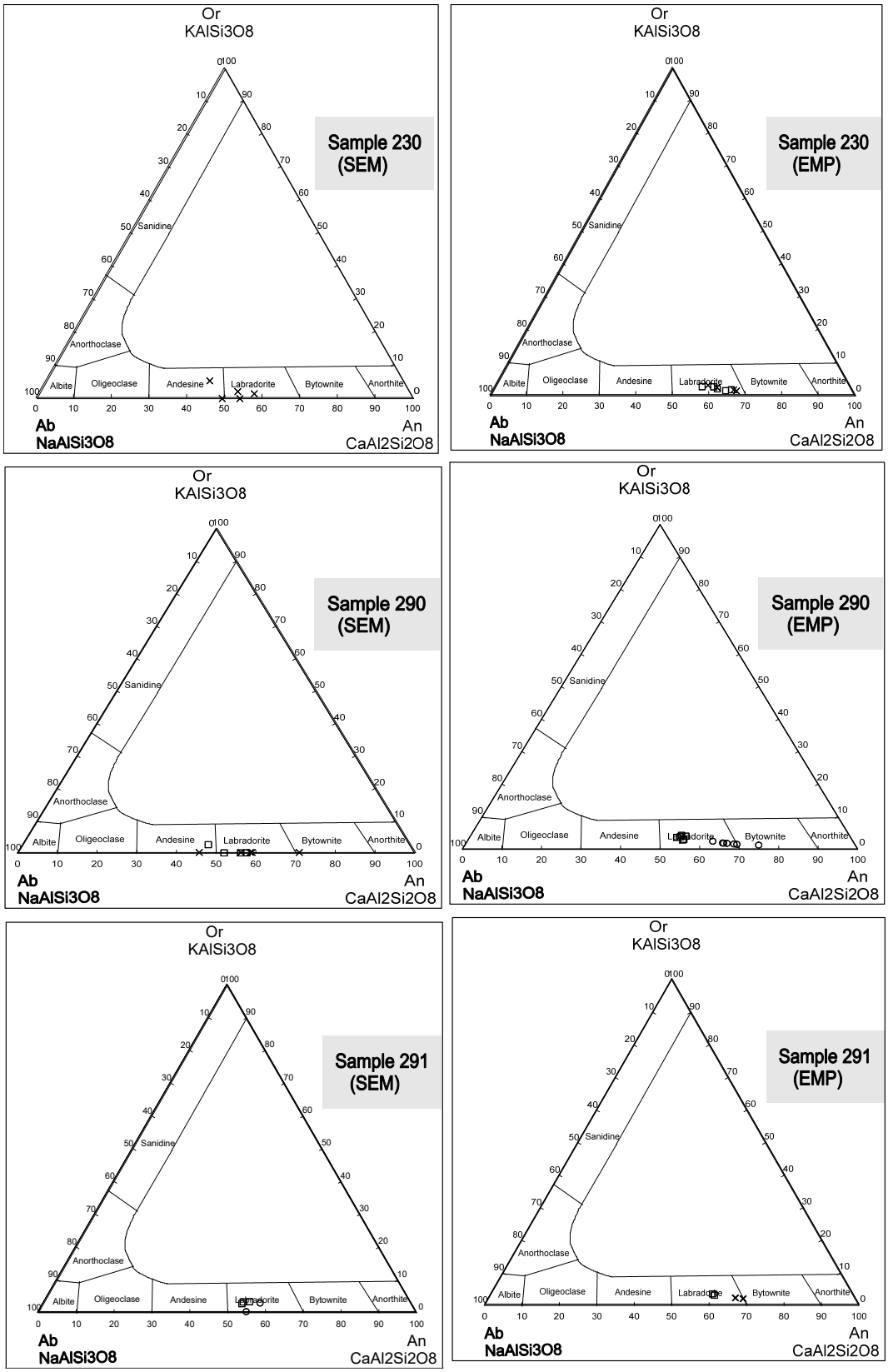


FIGURE 26: Plagioclase composition in the inner hornfels zone determinate by both SEM/EMP, data from Appendix II and III. Xs are plagioclase composition in the vesicle centre. Circles are the composition at the margin while squares are at the groundmass

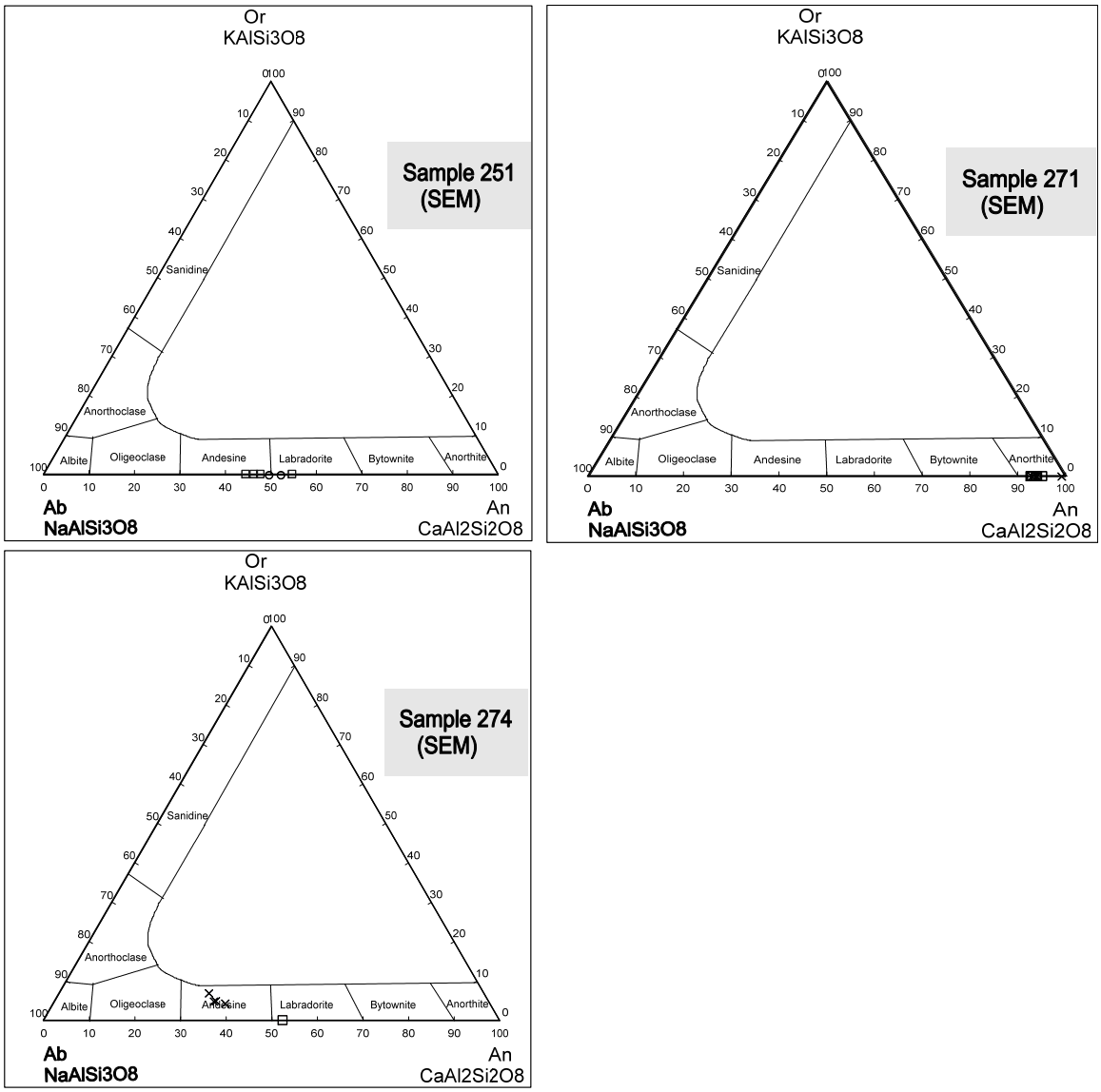


FIGURE 27: Plagioclase composition in the inner hornfels contact zone determinate by only SEM in term of An-Ab-Or element, data from Appendix II. Xs are plagioclase composition at the vesicle centre. Circles are the composition at the margin while squares are at the groundmass

## 5.7 Mineral phases in the hornfels zone around Hrossatungur gabbro

### 5.7.1 Main mineral phases

The texture of the hornfels zone around Hrossatungur gabbro is mainly fine grained with coarser parts showing granoblastic texture. Pyroxene, plagioclase, Fe-Ti oxides and quartz represent the majority of the coarser grain size.

**Pyroxene ($(Ca, Na, Fe^{+2}, Mg)(Si, Al)_2 O_6$)** is one of the main phases in fresh basalt. These are mainly of salite and augite compositions but only rarely orthopyroxene. It is tentatively assumed that the alteration of the basalt around the gabbro was not intense enough to alter the primary pyroxene prior to the hornfels alteration. The pyroxene formed in the hornfels phase shows similar composition as one expects to find in fresh basalt, which indicates that the chemical change is rather limited, and they may possibly have kept their original primary crystal shape. Pyroxene, however, is not expected to have formed within the vesicles and veins and is thus obviously formed during the hornfels phase.

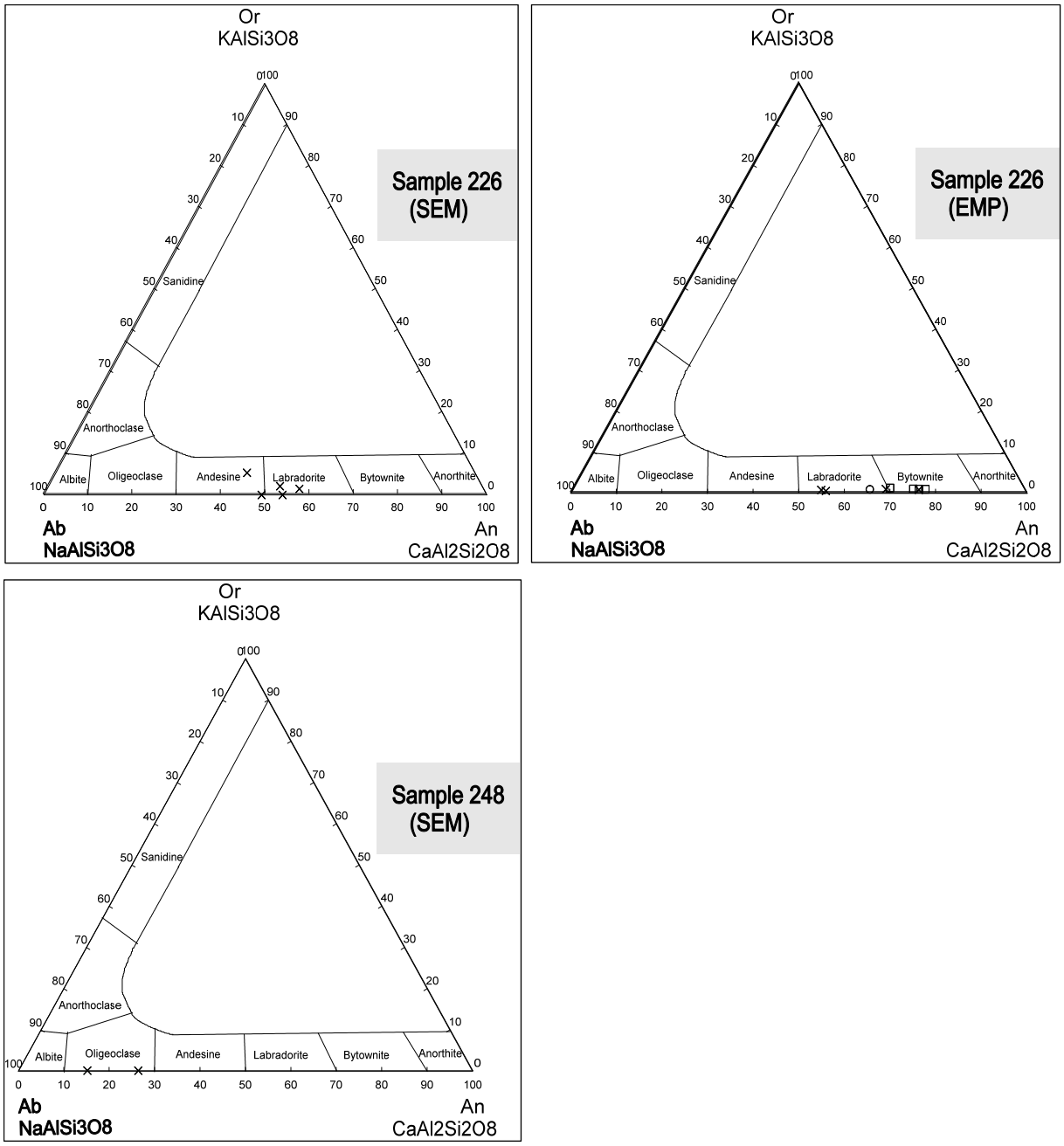


FIGURE 28: Plagioclase composition in the outer hornfels contact zone determined with SEM/EMP in terms of An-Ab-Or component. Data from Appendices II and III. Xs are plagioclase composition at vesicle centres, circles are the composition at the margin, while squares represent the groundmass

The pyroxenes in the groundmass were dominantly salite to augite compositions while the vesicle and veins ones extend more into the ferrosalite to hypersthene fields and show even tendencies to be zoned towards more iron-rich compositions at the rims, and in places even zoning towards hornblende and actinolite, suggesting slight hydrous conditions as shown in Figure 29.

The pyroxene in the vesicles is usually larger than the pyroxene in the groundmass. A difference between the inner and outer hornfels zone is not obvious, partly because of less analyses of the latter. Orthopyroxene may be more commonly found in the inner zone than the outer one (see Figure 29). There seems to be a reaction relationship between the abundance of oxide and pyroxene. In places, there is a distinct reaction rim around the voids, where there is a disappearance of the oxides and increase in

the amount of pyroxene. Oxides may though re-appear near the center of the vesicles, with simultaneous disappearance of the pyroxene.

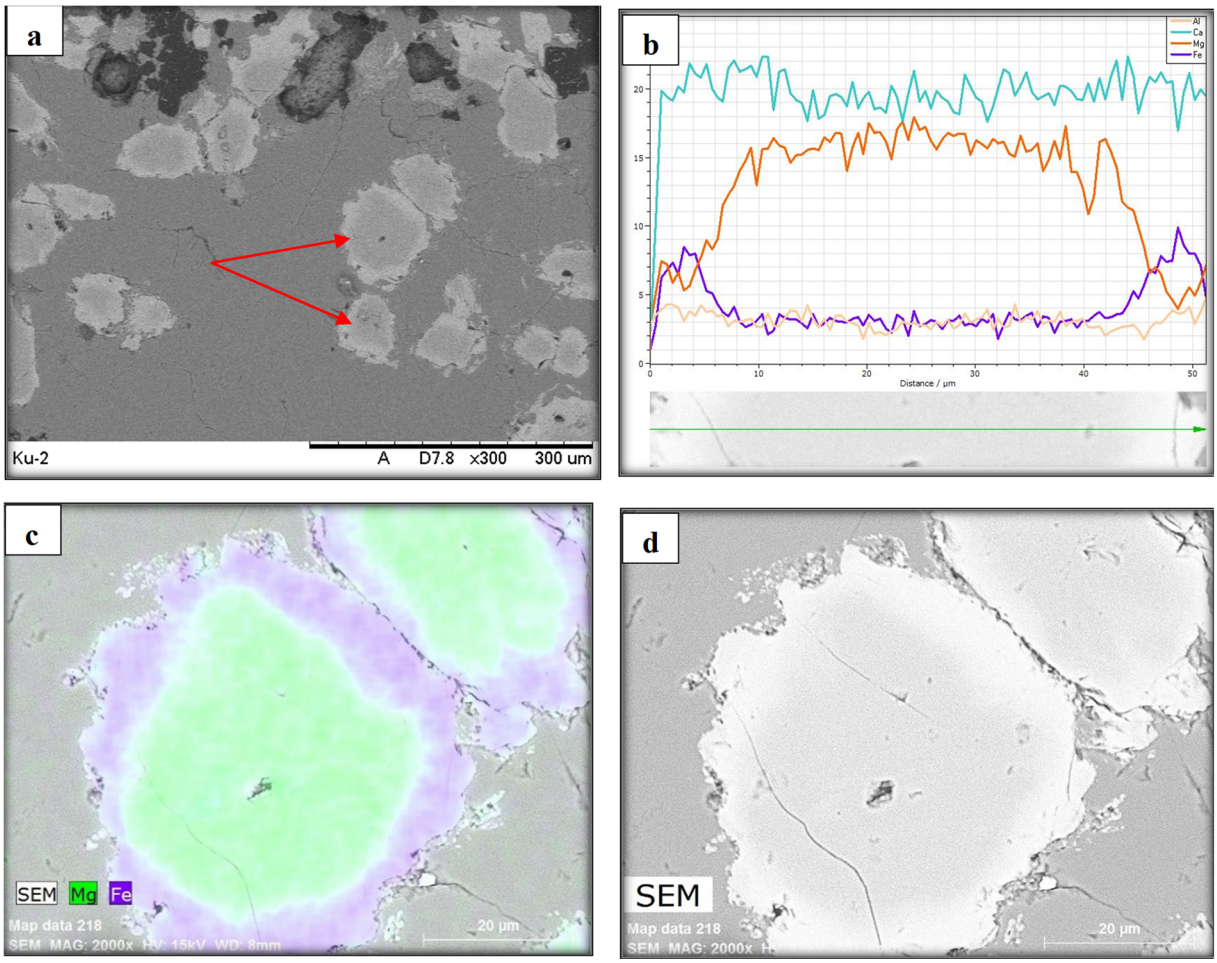


FIGURE 29: BSE micrographs of the hornfels around the Hrossatungur gabbro showing compositional zoning in pyroxene (sample 226). Zoning in different grains of pyroxene within a vesicle filling (b) A profile across a vesicle centre towards the margin showing the distribution of Mg, Fe, Al and Ca. The scale bar is 20 µm. (c) SEM elemental map showing the distribution of Mg and Fe within a vesicle centre. Scale bar 20 µm. (d) Pyroxene showing strong compositional variation, dark to light grey colour, with thick a reaction rim overgrown by zonation

Plagioclase ($NaAlSi_3O_8$ - $CaAl_2Si_2O_8$) is, like pyroxene, one of the main mineral phases in basalt in which its dominant compositional range is from labradorite to bytownite as seen in Figure 26. This is quite similar to the compositional range found in the hornfels and the HTG. Hydrothermal alteration of the plagioclase within the chlorite epidote zone is mostly towards albite composition (Franzson, et al., 2008). Whether such alteration took place prior to the hornfelsing is not known. The compositional range of plagioclase in the hornfels is to a large extent the same as that of the primary plagioclase, so the primary plagioclase may mostly have been in a relatively stable environment and only have changed composition to a minor extent. An interesting occurrence of plagioclase phenocrysts in the roof hornfels appears to be primary (Figure 30), which could indicate compositional change without changing the primary crystal shape. The chemical composition of plagioclase varies from oligoclase (minor) - andesine - labradorite - bytownite towards anorthite. Figure 27 shows that andesine is less abundant (sample 274 and 251) while labradorite and bytownite is more abundant (samples 290, 291, 226 and HE-42). The anorthite composition is less common and mainly represented by sample 271 and samples from well HE-42 (see Chapter 6). Anorthite seems to be more commonly found nearest to the gabbro, which infers higher heat of formation.

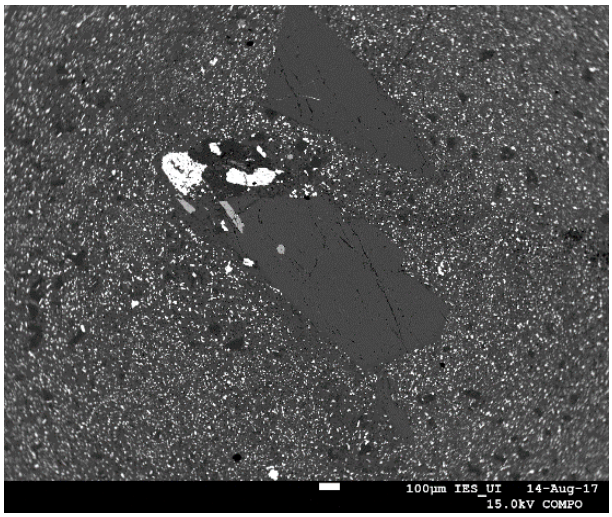


FIGURE 30: BSE micrographs of plagioclase phenocrysts showing an apparent primary composition (sample 291)

*Fe-Ti oxides (magnetite, $Fe^{+2}\ Fe^{+3}{}_2O_4$, ilmenite $FeTiO_2$ and titanomagnatite $Fe^{+2}\ (Fe^{+}3,\ Ti)_2\ O_4$,)* Oxides are the third major primary component in primary basalt and is a mixture of magnetite and ilmenite. Magnetite usually forms cubic crystals, while ilmenite tends to be more elongated. The abundance is quite varied within the basalt range and is dependent on the iron content of the rock. Oxides become abundant in contact alteration and so it is in the hornfels. They are often most abundant within the groundmass, but may disappear in the reaction zone around vesicles and reappear in the central part of the voids, there in general larger in size. They seem to be reacting with the clinopyroxene. The oxides were analyzed in the same way as pyroxene and plagioclases, and the results are shown in Figure 31 (SEM) and Figure 32 (EMP), where the main components, $TiO_2$ and FeO, are plotted. Most of the analyses show a sum of 90-100% of those components. Both analytical methods show a bimodal distribution indicating the dominance of magnetite and ilmenite. Both minerals are equally found in the groundmass

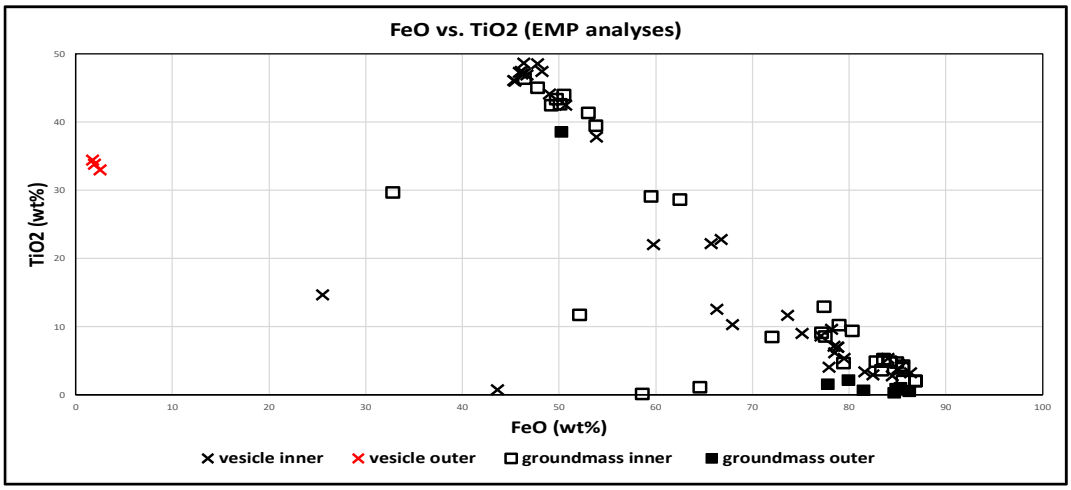


FIGURE 31: FeO vs. $TiO_2$ classification for oxides of the HTG and Hellisheidi hornfels samples (SEM analyses). Data from Appendix III

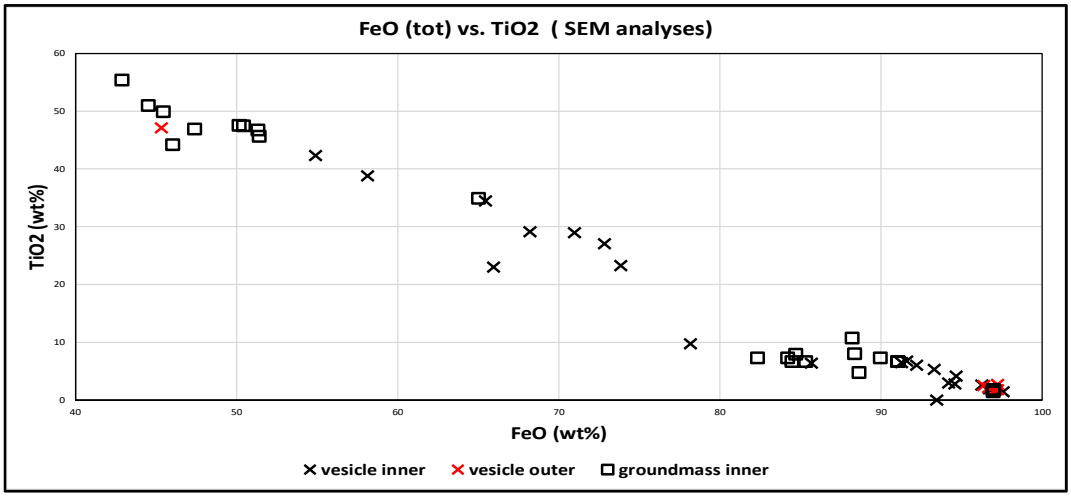


FIGURE 32: FeO vs. $TiO_2$ classification for oxides of the HTG and Hellisheidi hornfels samples (EMP analyses). Data from Appendix II

and void fillings, though magnetite seems to be a little more common within the vesicles. A number of analyses fall between the magnetite and ilmenite and are probably titanomagnetite. The EMP analyses show a few compositions off the tieline between magnetite and ilmenite with total < 90% and thus an addition of other elements. Three of them are from the well HE-42 hornfels (see Chapter 6) and the low iron oxide is from sample 248. Other elements, like $Al_2O_3$ (0.1-6.4%), MnO (0.4-5.3%) and MgO (0.03-4.66%), are commonly found in the oxides.

### 5.7.2 Other mineral phases

Titanite (sphene) (Ca Ti ($SiO_4$) (O, OH, F)) is not found as a primary magmatic mineral in basaltic rocks in Iceland, but may be an accessory mineral in intermediate and felsic plutonic rocks. During hydrothermal alteration, oxides are observed to break down and form titanites. Titanites are, however, not seen as specific deposition within voids of hydrothermally altered rocks. Titanites are commonly found within void fillings in the hornfels (Figures 33).

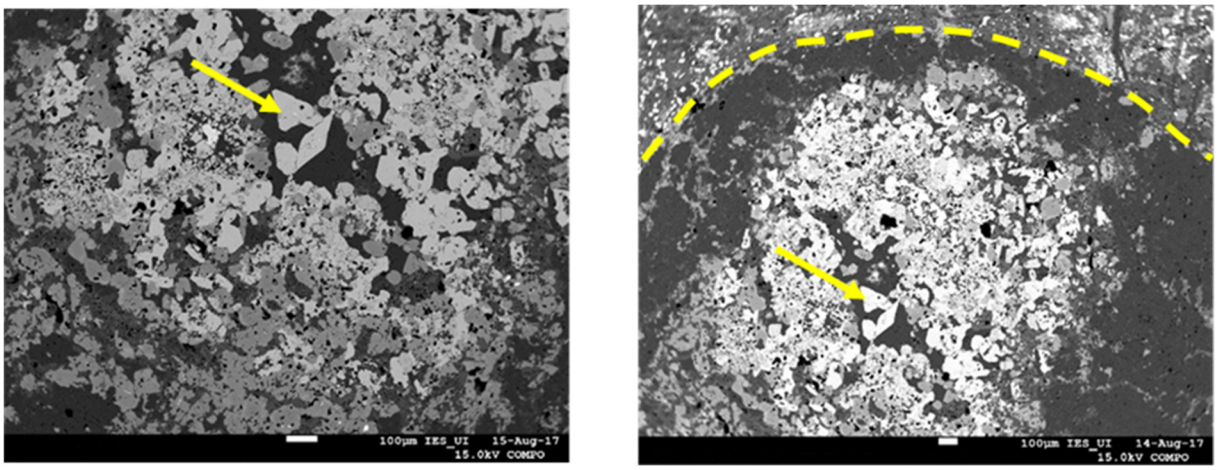


FIGURE 33: BSE micrographs of the hornfels around the Hrossatungur gabbro showing the diamond shaped section of titanite in the centre of the vesicle filling (sample 226). The scale bar is 100 µm

It is euhedral and has a diamond shape. The texture is defined by the lamellar twins and the obvious cleavages. It is distinguished by very high relief and extreme birefringence under the plane-polarized light.

Basically, the titanite is correlated with iron content (Deer, 1965). The FeO content of the titanite in the hornfels zone around HTG ranges between 0.4-25% while Ti ranges from < 1-36%. Titanite was studied by the SEM/EMP and was found to be very common in the inner and outer zone of the hornfels around HTG, like in samples 230, 251 and 271 (inner zone) and samples 226 and 248 (outer zone). It was also found in HE-42 well in Hellisheidi geothermal field (see Chapter 6). One may speculate that the titanite formed during the magnetite-ilmenite-clinopyroxene recrystallization with the separation of $TiO_2$ leading to titanite deposition.

*Apatite ($Ca_5$ $(PO_4)_3$ (OH, F, Cl))* is the commonest P-bearing mineral found in metamorphic rocks. Apatite is often found as primary mineral in evolved rocks. It is easily observed (petrographically) in the late melts of the Hrossatungur gabbro and is particularly notable in the dioritic and silicic veins cutting the hornfels. The hornfels apatite was found by SEM/EMP analyses in samples 226, 271, 274, 290, 251 and HE-42. The high concentrations of $P_2O_5$ in these samples obtained by SEM/EMP are in good agreement with the results of the ICP-OES analyses. Many of the EMP analyses in the hornfels rocks have totals lower than 100%, which renders them as probable occurrence as shown, in Table 16, Appendix III. These analyses are though satisfactory in the hornfels in well HE-42 (Appendix III in Table 15). Other elements such as Zr (6-7.58%), FeO (0.1-0.28%) and MgO (0.1-0.18%) are common in this apatite chemical composition. The SEM and EMP analyses show that apatite was more abundant in the vesicle fillings in the inner zone of the hornfels around the HTG, like in sample (271, 274, 290

and 251). Apatite is also common in samples of well HE-42 at Hellisheidi geothermal field. The apatite is normally associated with hornblende and garnet in the HTG hornfels zone.

*Amphibole ($Na\ Ca_2\ (Mg, Fe, Al)_5\ (Al, Si)_8\ O_{22}\ (OH)_2$)*
Amphibole group of minerals is both formed in plutonic rocks as hornblende, as well as developed by metamorphism contact and alteration of ferromagnesian minerals into hornblende (Deer, 1965). Amphibole, in particular actinolite, is commonly found in the epidote-actinolite zone where temperatures exceed 270°C (Franzson, et al., 2008). There they are found both as alteration product of pyroxene and as void deposition. Hornblende is relatively rare in drilled high-temperature systems, but seems to occur at higher temperatures. Hornblende hornfels succeeds the pyroxene hornfels (c.f. Figure 8) away from the gabbro and one could interpret the existence of the mineral as an indication of the transition towards that facies. The commonest type of amphibole in the hornfels contact zone around HTG is actinolite, both observed in veins and groundmass. It is identified petrographically in this study and distinguished by the two perfect cleavages intersecting at 120 degree. A fibrous structure, indicating actinolite cleavage and rough cross fractures, is common as well (Figure 34). Radial cleavage (sample 226) indicted high alteration degree. The composition of amphibole in the HTG hornfels zone is characterised by $Al_2O_3$ <2%, FeO < 21%, CaO < 16% and MgO <12% with minor MnO < 0.8%, $Na_2O$ <0.3% and $K_2O$ <0.2%, found in the vesicle fillings as well as in the groundmass. Figure 35 shows a division of the amphibole into two groups where low- and high-Al types are observed. Hornblende is relatively rare in HTG hornfels because the rocks belong to the pyroxene hornfels facies (Figure 8). This type of amphibole composition (actinolite) is different from the hornblende composition in Hellisheidi geothermal field (see Chapter 6).

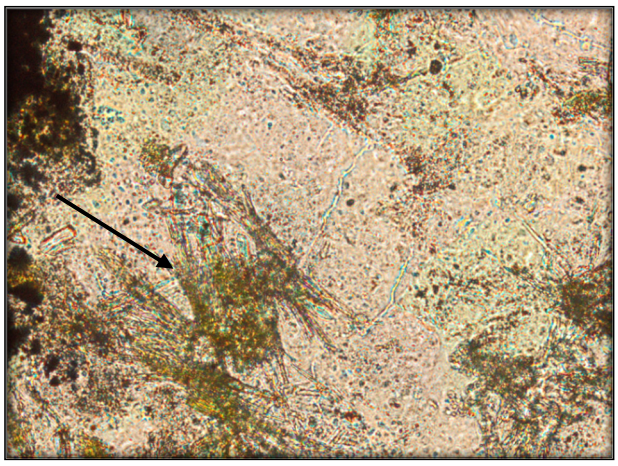

FIGURE 34: Actinolite crystal (sample 294) with green brown colour that shows the interaction of two cleavages at 60° and 120°. Thin section viewed with crossed polarisers

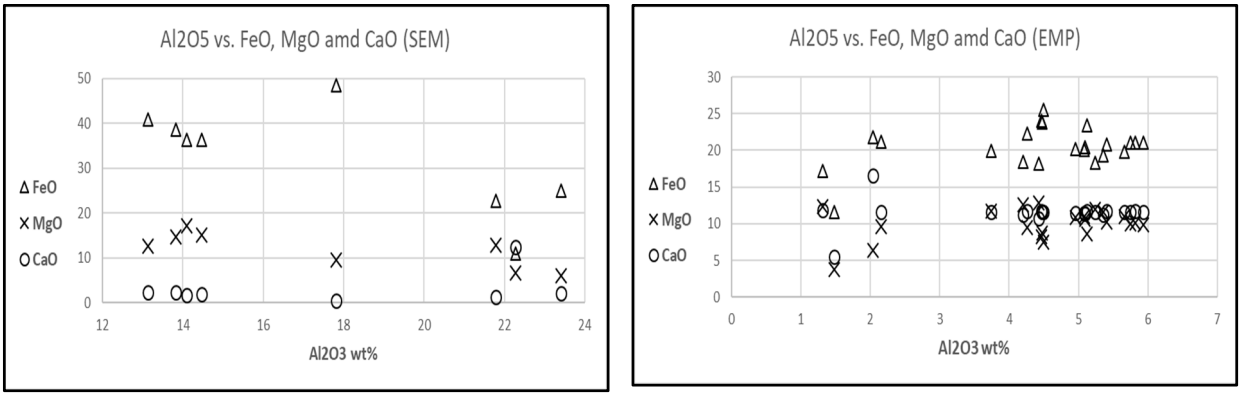


FIGURE 35: Classification of amphibole in the HTG hornfels zone and Hellisheidi using both SEM/EMP

*Garnet ($X_3Y_2(SiO_4)_3$; X occupied by Ca, Mg, Fe and Mn, while Y by Al, $Fe^{+3}$ and Cr)* is particularly characteristic of metamorphic rocks but also found in some igneous rocks and as detrital grains in sediments. Garnet is seen in the HTG hornfels through petrographic microscope observation in vesicle fillings more than in the groundmass. The garnet is yellowish in colour and forms anhedral to euhedral crystals. The electron microprobe analyses confirmed the occurrence of garnet.

The end-member composition of the garnet (Figure 36) is calculated from the result of EMP analyses as shown in Figure 36. The composition was around 65-97 mol%, andradite which is the dominant composition of the garnets in the hornfels around HTG. The grossular component ranges to about 17 mol% and almandine component to about 7 mol% (see Appendix V). Garnet is used in geothermal systems as an index mineral, indicating temperature above 280ºC. This garnet is normally andradite with <35 mol% grossular and <5 mol% pyralspite components (Brid, et al., 1984). Hedenbergite and garnet were the ideal secondary minerals for confirming the occurrence of supercritical fluids or superheated steam at the time of the cooling of the gabbro body associated with the Geitafell geothermal system (Helgadóttir, et al., 2017).

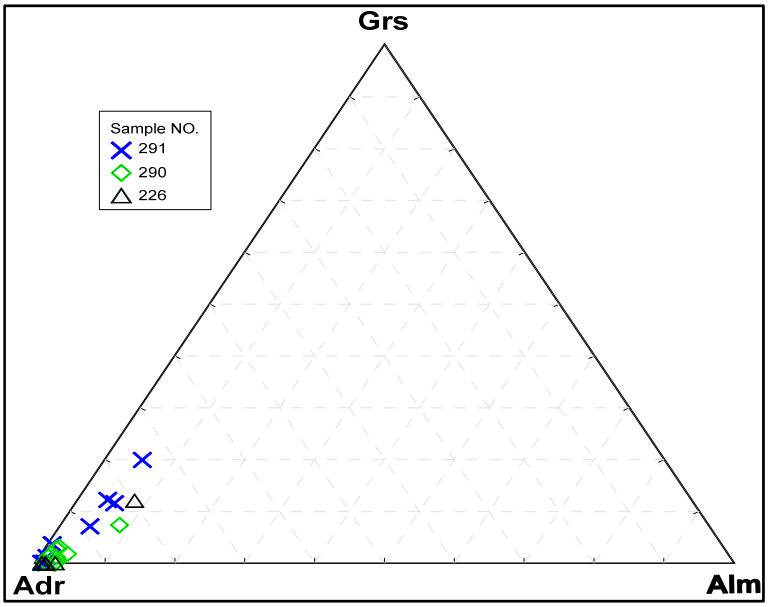


FIGURE 36: Triplot showing the distribution of garnet end-members. Adr-Andradite, Alm-Almandine, Grs-Grossular

Sigurjónsson (2016) studied the garnet composition related to quartz veins in Hafnarfjall by petrographic and SEM analyses. The garnet is mainly found within vesicles and veins. Many of the samples were taken further away from the hornfels zone in his study. The study indicated that the garnet had an alternating zoning of andradite- and grossular-rich bands with dominantly andradite-rich cores, which is different from the andradite-only garnet of the HTG hornfels (Sigurjónsson, 2016).

*Quartz ($SiO_2$)* occurs as an essential constituent of many igneous and metamorphic rocks. It is found as primary mineral and as deposits fillings amygdales in the hornfels contact zone in the study area. It is distinguished under the microscopy by its lack of colour and cleavage. The quartz-rich veins may influence the chemical compositions analyzed by the ICP-MS.

*Sulphides ($FeS_2$)* include strong basic and inorganic anions of sulphur with the chemical formula $S^{2-}$. Sulphide minerals were petrographically observed in reflected light showing strong yellow colour. Sulfides are present in subordinate amounts in most of the hornfels and are also quite frequent in the alteration zones further away from the gabbro. Specific patches of sulphides are observed within the hornfels, which are considered to represent late volatile degassing of the gabbro. Figures 37, 38 and 39 show diagrams where 9 elements are plotted against sulphur by SEM. Iron and sulphur are the dominant elements, which renders them within the pyrite compositional range. They, however, contain 5-11.7% Pb, and other elements include <0.24% As, <0.25% Ti, <0.33% Sb, <0.38% Cu, <0.51% Zn, <0.29% Au and <0.11% Ag. The analytical results of individual grains are quite similar. Therefore, the type sulphide in the hornfels zone around HTG is pyrite, while only two samples analyzed in well HE-42 at Hellisheidi geothermal field show lower totals as they contain 28-29% Cu and considered as Cu-sulphides.

Gunnarsdóttir (2012) reported the formation and composition of the typical sulphides in geothermal fields (well HE-42 in Hellisheidi). The study shows that the hydrothermal sulphides started to form when sulphide-bearing fluid reacted with igneous Fe-bearing phases. The hydrothermal sulphide types most commonly found in the cuttings samples were pyrite, pyrrhotite and Cu-sulphides (Gunnarsdóttir, 2012), whereas the sulphide type in the hornfels zone around HTG is mainly pyrite, which contains <11% Pb as a major element, and As, Ti, Sb, Cu, Zn, Au and Ag as trace elements.

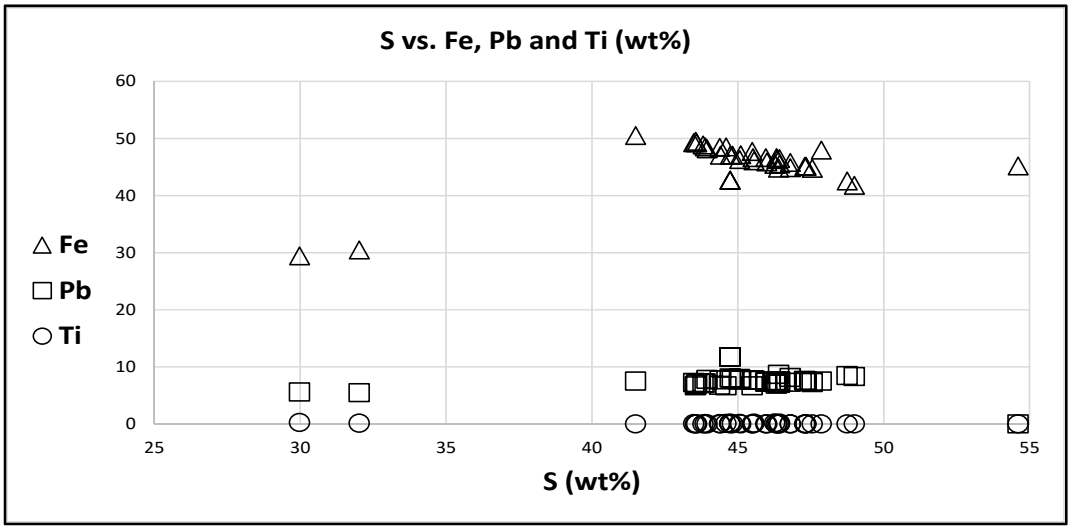


FIGURE 37: Variation of sulphide composition in HTG hornfels contact zone.
(S vs. Fe, Pb and Ti)

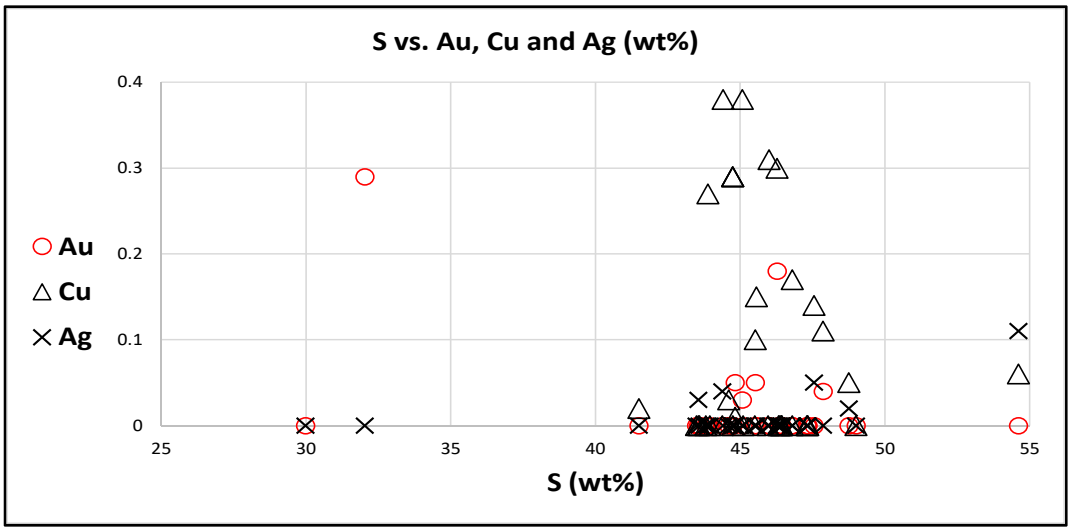


FIGURE 38: Variation of sulphide composition in HTG hornfels contact zone.
(S vs. Au, Cu and Ag)

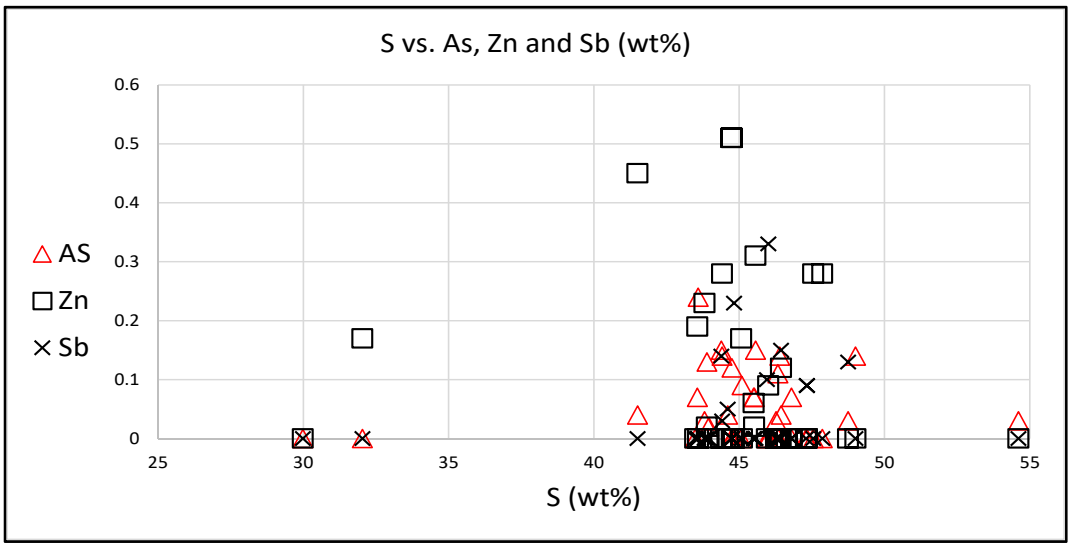


FIGURE 39: Variation of sulphide composition in HTG hornfels contact zone.
(S vs. As, Zn and Sb)

## 6. WELL HE-42 IN HELLISHEIDI GEOTHERMAL FIELD

Well HE-42 is a vertical 3340 m deep well drilled at Hellisheidi high-temperature field in 2010. The cuttings analyses showed a stratigraphy consisting of lavas and hyaloclastites, which were intersected by basaltic intrusions. From about 1400 to over 1700 m depth, the well was drilled through a mixture of a fine to medium grained intrusion and a surrounding zone of hornfels (Gunnarsdóttir, 2012). An interpretation of this is shown in Figure 40 where the drillhole is shown penetrating along the dyke and the contact metamorphic aureole. A sample was taken from the well to compare this kind of alteration in an active high-temperature system with that in a fossil system. The purpose of including this hornfels is to relate with the HTG and show the similarities between a fossil geothermal environment and an active one. The intensity of the hornfelsic recrystallization in well HE-42 is particularly high, even compared with the inner hornfels at HTG, often showing granoblastic character. The thermal effect from a normal dyke injected into a stratigraphic sequence is not sufficient to produce such a strong hornfels recrystallization. However, this could have been produced if the dyke was a "long term" magmatic feeder to a volcanic eruption above, creating a more pronounced thermal anomaly, and leading to the formation of the hornfels zone around the dyke. The rock was originally vesicular basalt, probably altered within the chlorite to epidote-actinolite zone prior to becoming hornfelsed.

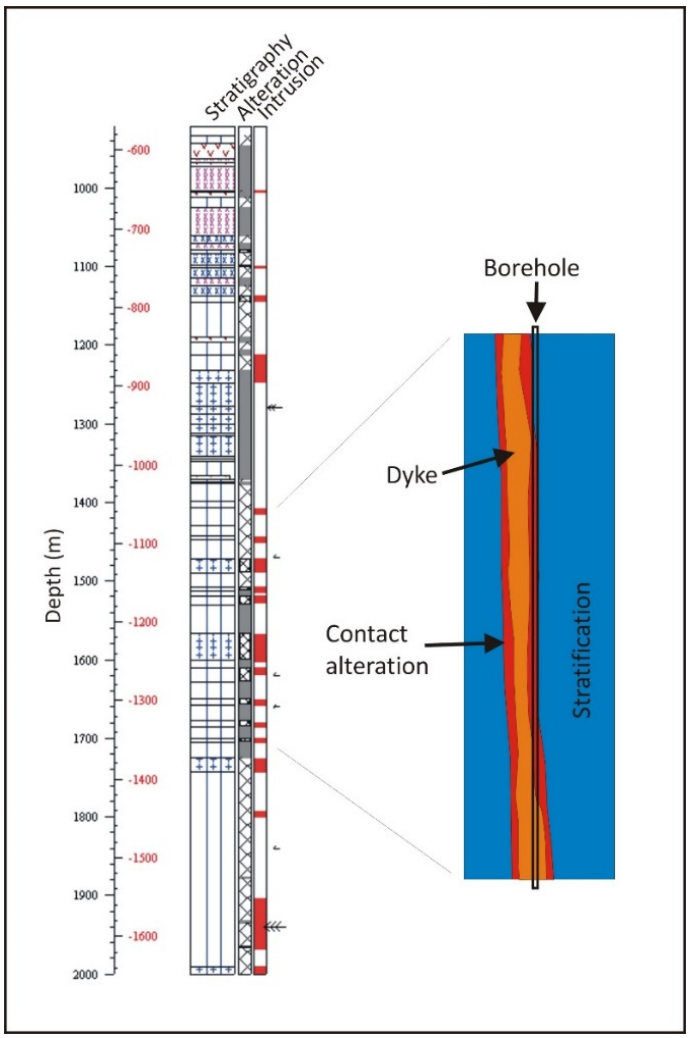


FIGURE 40: A stratigraphic succession of well HE-42 from 900 to 2000 m. Interpretation of the relation between the borehole, intrusion, contact alteration and the surrounding strata is shown to the right

A handpicked sample was taken from the cuttings samples at about 1500 m depth for a petrographic section, which was analyzed using the SEM and EMP. The sample is very fine grained with some heterogeneous variation in crystallinity. This is seen as very fine grained groundmass but slightly larger crystals within the vesicle fillings. Granoblastic crystallinity is more commonly observed within the vesicles, and indeed appears to be more dominant than found in the HTG hornfels. Occasional younger veining is observed, mainly occupied by amphibole. The analytical results are shown in Figure 41 (a to d). Similar reaction zoning around vesicles as in the HTG hornfels is seen, where there is a reduction of oxides near the rim and a simultaneous increase of pyroxene. Both SEM and EMP show compositional range of salite and augite, and the SEM shows additionally magnesian to intermediate orthopyroxene in the groundmass (Figures 41 a and b). Compared to the groundmass, there seems to be a slight Fe enrichment in the vesicle fillings according to the EMP analyses. Plagioclase was also analyzed, as shown in Figure 41c and d. Both analytical methods show that plagioclase in the vesicle fillings has more anorthite-rich composition compared to the groundmass one. Overall, the composition of the plagioclase ranges from bytownite to nearly pure anorthite.

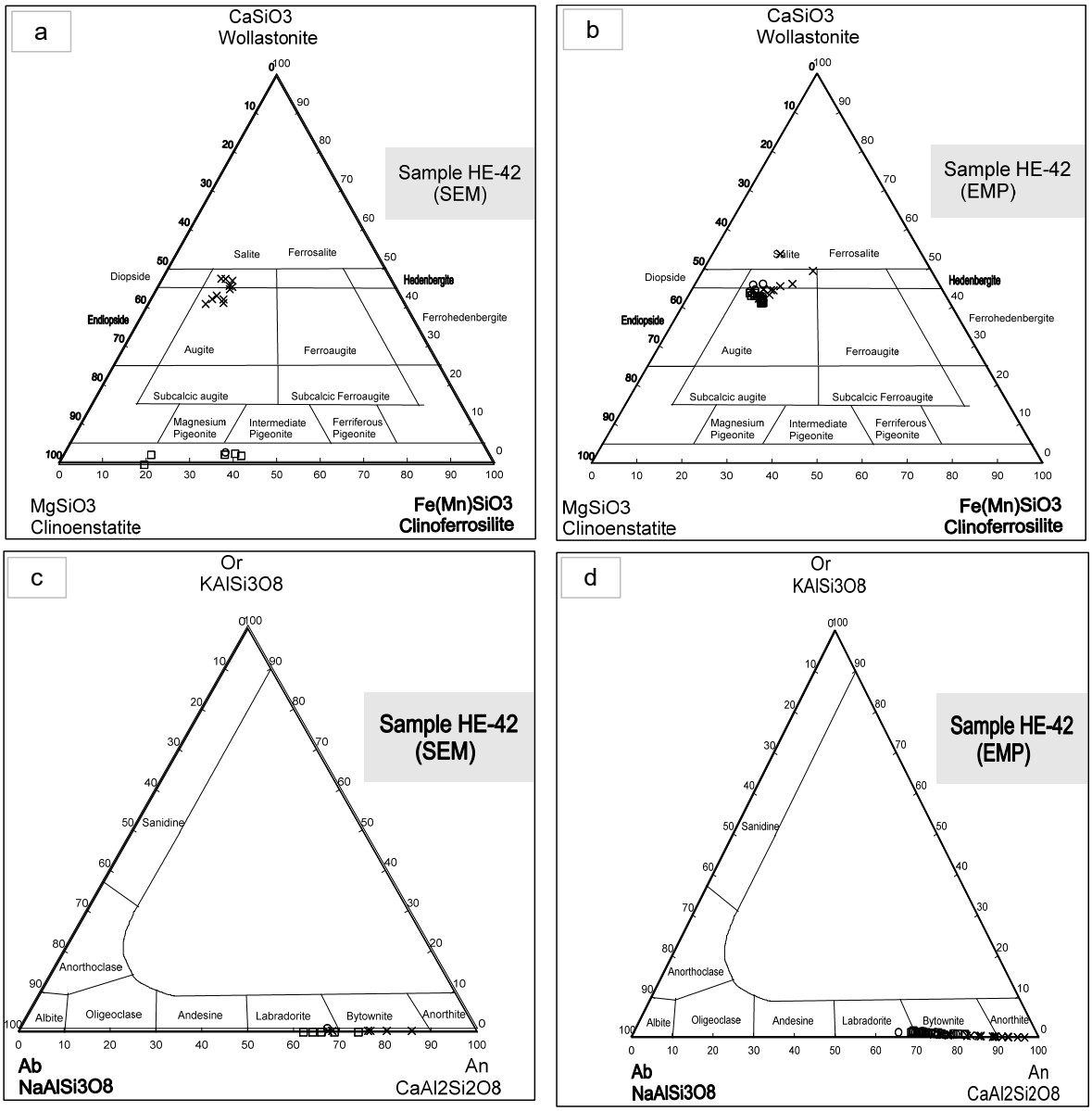


FIGURE 41: Pyroxene and plagioclase compositions in the hornfels zone in well HE-42 (Hellisheidi) determinate by SEM/EMP in term of Ca-Mg-Fe and Ab-An-Or components, data from appendix II and III. Xs are compositions at the vesicle centre. Circles are the composition at the margin while squares are within the groundmass

The mineral assemblage in the hornfels in well HE-42 is clinopyroxene, plagioclase and oxides. Granoblastic texture is even more pronounced than found in the HTG hornfels, indicating more mature recrystallization. Figure 41a and b show the SEM/EMP analysis of pyroxene, which shows a range confined to salite-augite. SEM analyses showed also Mg-rich groundmass orthopyroxene, ranging from bronzite to hypersthene, as shown in Figure 25. Plagioclase shows a range from Ca-rich labradorite to anorthite composition. The plagioclase compositions seem to be more Ca-rich in the voids than groundmass. Amphibole was analyzed in Hellisheidi by both SEM/EMP, and has a high-aluminium hornblende (Tschermakite) composition, as shown in Figure 35. This composition is chemically described by Al <24%, Fe < 48%, Ca < 12% and Mg <13% with minor Mn <0.5% and Na <0.7%, which are found both in vesicle fillings and in the groundmass. Amphibole veining is observed and is obviously succeeding the hornfels, an indication of lowering temperature and the access of fluids into the hornfels. The presence of apatite, titanite, sulphides and amphiboles was noted, all found in the vesicles and groundmass, but no garnet was observed. The oxide composition in well HE-42 is mainly magnetite, minor titanomagnetite and ilmenite, which are observed in the vesicle fillings and in the groundmass, which is comparable to HTG hornfels.

## 7. DISCUSSION

It is difficult to determine how intimate the interaction is between a water reservoir and a magmatic intrusion in active geothermal systems due to the depth at which this occurs, and also how expensive such a study is in deep boreholes. This can be assessed, however, in deeply eroded fossil high-temperature systems. Hafnarfjall central volcano in West Iceland with the Hrossatungur Gabbro heat source is one of these areas. A previous study has shown that the gabbro was emplaced relatively shallow, or from about 700-1500 m below the original surface of the volcano. The high-temperature system surrounding the gabbro shows temperatures of <350°C if it follows the boiling point curve (Brett, et al., 2016). There is strong evidence indicating that the gabbro is the last intrusive phase in the area, and one can thus associate all the hydrothermal imprints to that intrusion as being the heat source for the surrounding geothermal system.

The main research question in this study was what the hornfels tells us about the magma-water interaction.

In the field, one encounters a hard, flinty, very fine-grained dark rock, which in places shows jointing common with the dolerite contact, indicating contemporaneous consolidation. Filled vesicles can easily be observed. The thickness, which is recognized by the aforementioned characteristics of the rock, is quite variable, but appears to be on the order of about 20-40 m on the southern side of the gabbro, that is where it lies against the basalt succession. Exposures on the northern side are covered largely by scree, which is indicative of softer rocks and may indicate the lack of hornfels. The thickness is estimated to be a few metres at the most. The focus of this study is on the southern side.

The methodology used is a mixture of geochemistry, petrography and SEM/EMP mineral analyses and it was hoped that this combination would unravel the water-rock processes near the boundary of the gabbro.

The results of the LOI analyses are very informative, in particular in comparison with LOI in other alteration zones. It shows that LOI increases towards the chlorite-epidote zone, but diminishes and reaches a minimum at the hornfels stage. This decrease is mainly due to the alteration minerals become less hydrous, and when reaching the proper hornfels, the mineralogy is dominantly composed of water-free minerals like pyroxene, plagioclase and oxides. Only minor garnet and amphibole are present. This minor amount of LOI is likely to be caused by remaining water and/or CO2 in the rock since prior to the hornfels alteration. This indicates that thermal conduction around the gabbro has dried up the rock and prevented the access of water/steam to the molten magma and associated heat-mining from the magma.

The chemical analyses of the hornfels rock show that the overall compositional range is in many ways similar to the fresh-rock equivalent of the volcano. However, there seems to be an apparent overall depletion of $Na_2O$. $SiO_2$ content shows a wide range, which can to some extent be explained by dioritic to felsic veining from residual magmatic fluids injected from the gabbro, but also quartz veining and possibly even an andesitic protolith. A few samples show anomalously low values. These samples were taken from locations with a high sulphide content in the rock, which are superimposed on the hornfels. These suggest local late-stage sulphide volatile penetration of the hornfels, probably due to rock dissolution and formation of permeability within a very acidic environment. These samples also show elevated Fe and Al content. Furthermore, there appears to be an overall enrichment of Zn, Ni and Cu in the hornfels samples, probably due to the diffusion of sulphide vapour from the magma into the hornfels.

As noted earlier, the hornfels rock is very fine grained, although the grain size varies to some extent, with the groundmass usually being finer grained than minerals in vesicles and veins. The main minerals analyzed were pyroxene, plagioclase and oxides. The compositional range of pyroxene is dominantly salite-augite-ferrosalite, but may slightly extend into the diopside and hedenbergite fields as seen in Figure 42. Although compositions do vary from one sample to another, there seems to be a tendency for the composition of pyroxene analyzed within veins and vesicle to extend more into the ferrosalite field compared to the groundmass. Secondly, the pyroxene in the hornfels nearest to the gabbro, where

recrystallization is most pronounced, is more dominantly within the salite-augite field, while the composition of pyroxene further away from the contact falls more in the ferrosalite field. Furthermore, orthopyroxene is found in four samples. It is mostly Mg-rich, but one grain belongs to the ferro-hypersthene field (Figure 42). All grains of orthopyroxene are found within vesicle fillings. Zoned pyroxene is found within the vesicle/vein domain with Fe enrichment towards the rim. Oxides are observed in some places in central parts of vesicles, suggesting abundance of Fe in this re-crystallization sequence.

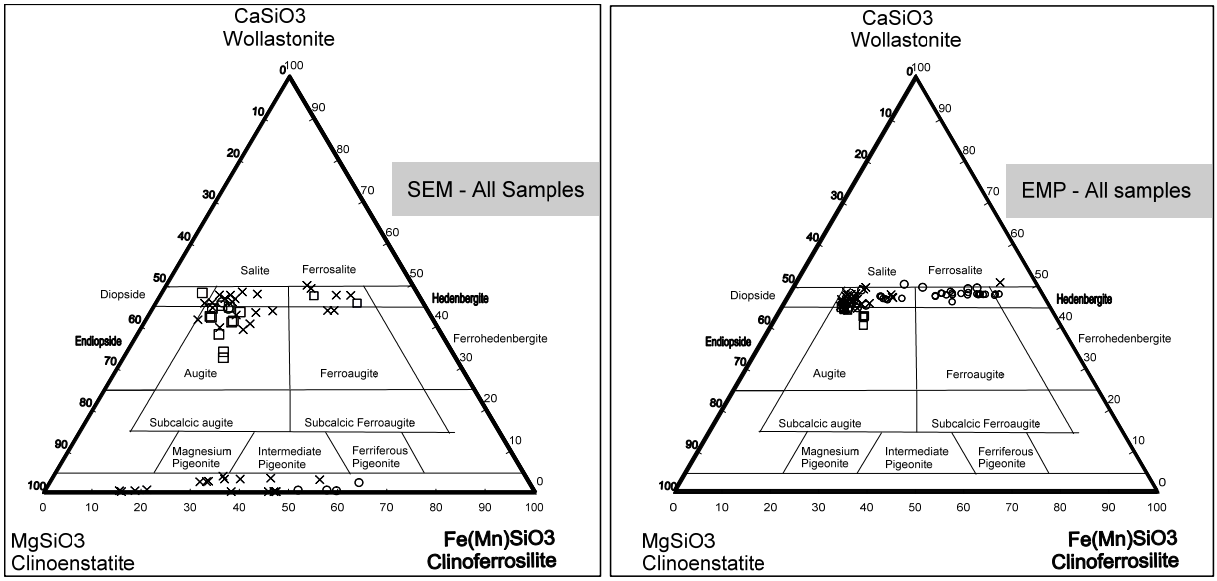


FIGURE 42: Compositional range of pyroxenes in the HTG hornfels.
See text for further explanation

Plagioclase shows a wide range of composition, but is dominantly found to be labradorite, but extends into the andesine field (Figure 43). Only one sample has oligoclase composition, but that sample has a high proportion of silicic veins, which could imply $Na_2O$ contamination of the feldspar. One sample (271), which was taken at the hornfels/gabbro boundary (located separately out of the profiles), shows an anorthite composition. A comparison with the results of the analyses of plagioclase in the hornfels from well HE-42 is highly informative. In well HE-42, the crystallinity of the hornfels is more pronounced than in the hornfels near the gabbro boundary in Hafnarfjall and with very explicit

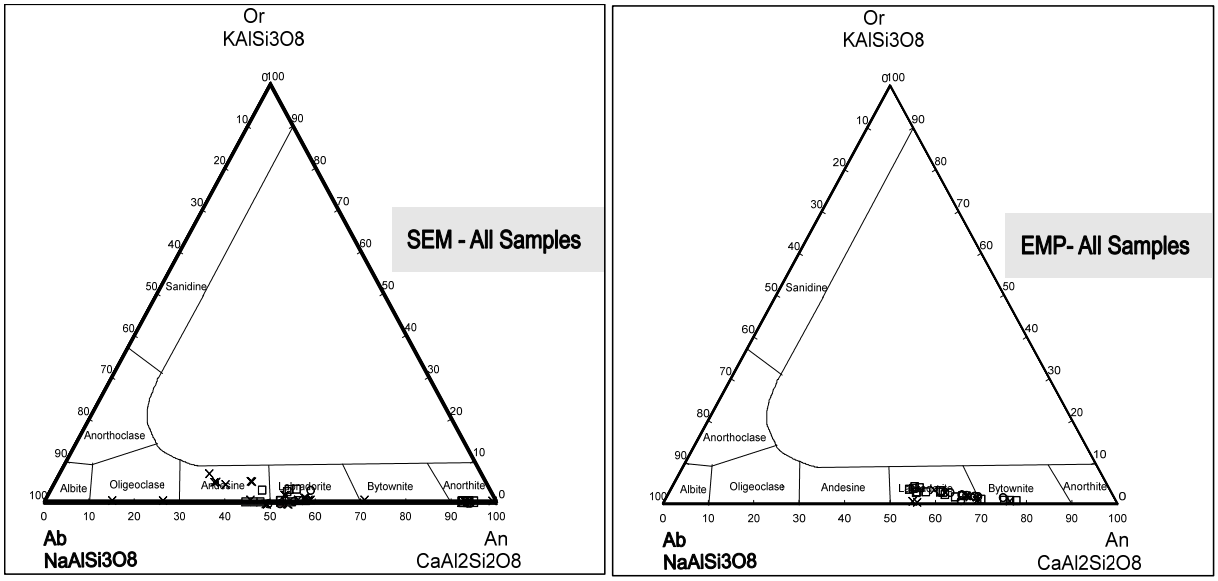


FIGURE 43: Compositional range of plagioclase in the HTG hornfels.
See text for further explanation

granoblastic crystallization. In HE-42, pyroxene is in general more confined within the salite-augite field and plagioclase is more Ca-rich labradorite and extends to nearly pure anorthite. Within vesicles and veins, there is a tendency for the pyroxene to be more Fe-rich (in particular in the EMP analyses), and also for the plagioclase to be more anorthitic.

It is interesting to compare the mineralogy and geochemistry. In this regard, one can see that whole rock samples of the hornfels and least altered rock equivalents from the Hafnarfjall-Skardsheidi central volcano have comparable compositions. This is perhaps not surprising as the hornfels is a recrystallized rock with similar plagioclase and pyroxene compositions, although the pyroxene may shift a little towards Fe enrichment and the plagioclase towards the Ca end. Oxides are also similar to the primary ones.

The oxides dominant in the HTG hornfels are magnetite and ilmenite, which are equally found in groundmass and void fillings, although magnetite seems to be more common within vesicles. Titano-magnetite is also observed in vesicle fillings. Apatite found in the hornfels, both around HTG and in well HE-42, represents the first known occurrence of it as an alteration mineral in Iceland. The occasional garnet and titanite are mostly found in vesicles and veins. A comparison of the present study with the study of Sigurjónsson (2016) shows that andradite compositions are more dominant in the hornfels, while getting more enriched in the grossular component further away from the gabbro.

Sulphide compositions in the HTG hornfels contact zone are characterized by high amounts of Fe and S and up to 11% Pb, which means that they are within the pyrite compositional range. Other elements in minor amounts are As, Ti, Sb, Cu, Zn, Au and Ag. This chemical composition is somewhat different from compositions typical for sulphides in geothermal fields (well HE-42 in Hellisheidi), which are classified as pyrite (common), pyrrhotite and Cu-sulphides. Hence, the main sulphide composition type in HTG is pyrite, while in well HE-42 at Hellisheidi geothermal field show richer Cu-sulfides.

The outer limit of the hornfels was assessed in the field to some degree by the apparent change from fine, dark grained rock to the more normally appearing altered rocks. In some of the samples taken at the outer margin, amphibole (actinolite, hornblende) becomes more abundant. That would suggest the transition from pyroxene hornfels to hornblende hornfels, which also is seen by the abundant garnet in vesicles and veins. Figure 8, which is metamorphic facies pressure-temperature diagram, shows the stability field of hornblende hornfels and how pyroxene hornfels succeeds the former as temperature increases. The temperature of the transition is just above 600°C. The silicic magmatic veins cutting through the hornfels do not show any marginal cooling against the hornfels, which may imply similar temperatures of the hornfels. This would mean temperature in the range of 800-900°C, which is at the upper boundary for pyroxene hornfels. As there is no sanidine found, the hornfels did not reach the sanidinite facies, which is not to be expected, the protolith being basaltic.

## 8. SUMMARY AND CONCLUSION

Hrossatungur gabbro was the heat source for a high-temperature system and is surrounded by a hornfels contact zone. The evidence suggests that the gabbro is the last intrusive phase in the Hafnarfjall-Skardsheidi central volcano which influenced by multiple inflation and deflation events, became fractured, and increased the permeability of the rocks to allow magmatic gases, like sulphide volatiles, to escape from the magma chamber. The hornfels is badly exposed on the northern side of the caldera, but well exposed on the southern side, which allowed us to study the southern part in detail.

Loss-on-ignition analyses show that the hornfels is the least hydrous part of the rocks around the intrusion, due to the mineral assemblage being dominantly water-free. This was caused by thermal conduction from the gabbro intrusion, which also prevented fluid heat-mining from the molten magma.

The hornfels rocks have a composition range that is almost identical to the equivalent fresh rocks of the volcano, although the hornfels appears to have suffered some $Na_2O$ depletion. $SiO_2$ content shows a wide range, which can be explained partly by diorite to felsic veining of late-stage melts from the intrusion, but also quartz and a possible andesitic composition of some of the protolith rocks, while samples that have anomalously low $SiO_2$ content come from locations of late sulphide volatile migration, which in turn indicates rock dissolution and formation of secondary permeability.

The main minerals analyzed were pyroxene, plagioclase and oxides. The pyroxene composition range is dominantly salite-augite-ferrosalite with slight diopside and hedenbergite. The pyroxene in the zone nearest the hornfels is more recrystallized and dominantly of salite-augite composition, while further away from the gabbro, it becomes dominantly ferrosalite. Orthopyroxene is mostly as Mg-rich vesicle fillings. Pyroxene within vesicles and veins tends to have more Fe-rich outer boundary.

Plagioclase shows a wide range of compositions in the hornfels contact zone around HTG, dominantly with labradorite to andesine composition, which extends to anorthite composition in some cases.

A comparison between the hornfels compositions around HTG and well HE-42 at Hellisheidi indicates that the pyroxene composition is within the salite–augite field and the plagioclase is more Ca-rich labradorite and extends to pure anorthite in well HE-42. The crystallization is more pronounced and tends to be granoblastic, which is indicative of more intense hornfels crystallization, leading to less Fe-rich pyroxene and more common orthopyroxene. Plagioclase will probably become more anorthitic under those conditions.

The similarity between the bulk chemical composition of the hornfels and primary basalts is probably due to the similar compositional ranges of the pyroxene, plagioclase and oxides in both types.

## REFERENCES


Armstrong, J. 1991: Quantitative elemental analysis of individual microparticles with electron beam instruments. In: Heinrich, K.F.J., and Newbury, D.E. (eds.), *Electron probe quantitation*. Plenum, NY, 261-315.

Bird, D.K., Schiffman, P., Elders, W.A., Williams, A.E. and McDowell, S.D. 1984: Calcic-silicate mineralization in active geothermal systems. *Economic Geology, 79,* 671-695

Brett, J., Franzson, H., and Alnethary, M., 2016: *Hafnarfjall-Skardsheidi central volcano, W Iceland. The Hrossatungur gabbro intrusion and its derivative geothermal system*. Unpublished manuscript, prepared for GEORG, 2016, Reykjavík.

Deer, H. 1965: *An introduction to the rock forming minerals*. Chaucer Press, Richard Clay Ltd, Bungay, Suffolk, Britain.

Deer, H and Zussman. 1997: *Rock forming minerals, single chain silicates* (2nd ed.). Geological Society, London, 680 pp.

Eskola, P., 1914: On the petrology of the Orijärvi region in southwestern Finland. *Bull. Comm. Geol., Finland, 40.*

Eskola, P., 1920: The mineral facies of rocks. *Norsk. Geol. Tidsskr, 6,* 143-194.

Franzson, H. 1979: *Structure and petrochemistry of the Hafnarfjall-Skardsheidi central volcano and the surrounding basalt succession, W-Iceland*. University of Edinburgh, Faculty of Science, Edinburgh, PhD thesis, 264 pp.

Franzson, H., Gudlaugsson, S.T., and Fridleifsson, G.Ó., 2001: Petrophysical properties of Icelandic rocks. *Proceedings of the 6th Nordic Symposium on Petrophysics, Throndheim, Norway.*

Franzson, H., Zierenberg, R., and Schiffman, P., 2008: Chemical transport in geothermal systems in Iceland, Evidence from hydrothermal alteration. *J. Volcanology and Geothermal Res., 173,* 217-229.

Fridleifsson, G.Ó., 1983: *The geology and the alteration history of the Geitafell central volcano, southeast Iceland*. University of Edinburgh, Faculty of Science, Edinburgh, 371 pp.

Goldschmidt, V.M., 1911: *Die kontaktmetamorphose in kristianagebiet, vidensk.* Meddr. Dansk naturh. Foren., 11.

Gunnarsdóttir, S H. 2012: *Geology and alteration in the vicinity of Reykjafell, Hellisheidi, occurrence, formation and composition of sulfides and oxides in well 42, Hellisheidi geothermal field, SW-Iceland*., University of Iceland, Faculty of Science, Reykjavik.

Harker, A. 1909. *The natural history of igneous rocks*. Macmillan, NY, 384 pp.

Harker, A. 1964: *Petrology for students: an introduction to the study of rocks under the microscop* (8th ed., revised by Tilley, C.E., Nockolds, S.R., and Black, M.). Cambridge University Press, 283 pp.

Helgadóttir, H., Ruggieri, G., and Rimondi, V., 2017: *Geitafell, core-alteration minerals and fluid inclusions in garnet*. Report prepared for IMAGE, ÍSOR - Iceland GeoSurvey, Reykjavík.

Hjartarson, Á., and Saemundsson, K. 2014: *Geological map of Iceland: bedrock, 1:600 000*. ÍSOR - Iceland GeoSurvey, Reykjavik.

Marks, N., Schiffman, P., and Zierenberg, R.A., 2011: *High-grade contact metamorphism in the Reykjanes geothermal system: Implications for fluid-rock interactions at mid-oceanic ridge spreading centers*. AGU Publications, 12-8, CA.

Moore, J.G., 1970: Water content of basalt erupted on the ocean floor. *Contrib. Mineral. Petrol., 28*, 272-279.

Schiffman, P., Zierenberg, R.A., Mortensen, A.K., Fridleifsson, G.Ó., and Elders, W.A., 2014: High temperature metamorphism in the conductive boundary layer adjacent to a rhyolite intrusion in the Krafla geothermal system, Iceland. *Geothermics, 49,* 23-30.

Sigurjónsson, H. 2016: *The composition of garnet in the fossil geothermal system of Hafnarfjall*. University of Iceland, Faculty of Earth Sciences, BSc thesis.

White, W.M., 2013: *Geochemistry.* Cornell University, Ithaca, John Wiley & Sons, Ltd., NY, 672 pp.

Winter, J., 2014: *Principle of igneous and metamorphic petrology* (2nd ed.). Pearson Education, Ltd., 720 pp.

Xiandeng, H., and Bradley, T., 2000: Inductively coupled plasma/optical emission spectrometry. In: Meyers, R.A. (ed.), *Encyclopedia of analytical chemistry*. John Wiley & Sons, Ltd, Chichester, 9468-9485.

## APPENDIX I: Procedures and samples preparations for ICP-OES analysis

The main procedures to prepare the samples for ICP-OES analysis are as the following:

1. Crush the samples using laboratory jaw crusher to fine gravel and sieve them to finer chips.

2. Grind the chip samples using an agate mortar to a fine powder of about 100-mesh.
   Note: It is important to keep the mortar and pestle as clean as possible after grinding each sample using acetone to avoid contamination.

3. Weigh 100 mg ± 2 mg of the sample into epicure graphite crucible. After re-zeroing the balance, add 200 mg ±2 mg of lithium metaborate (LiBO2) flux to the sample. Carefully mix the sample with the flux and make sure that the mixture does not stick to the wall of the crucible.
   Note: The flux of lithium metaborate is added to facilitate the melting process in the oven.

4. Preparation of a chemical solution, which will be used to dissolve the sample, by mixing the $HNO_3$ (5%), HCl (1.33%) with a semi-saturated oxalic acid, $C_2H_2O_4$ (1.33%), and de-ionized water.
   Note: Keep everything clean and avoid contamination.

5. Prepare the working standard samples. The four standard samples prepared are K9119, ATHO, BTHO and BAIK by mixing 250 mg ±1 mg of each sample and 500 mg ±1 mg of the lithium flux. Then standard bottles prepared by weighing 30 ml of the prepared chemical solution and 75 ml of the solution into individual bottles.

6. The sample melted in an electric furnace at 1000ºC for 30 minutes and then to cool down for another 20 minutes. Transfer the glassy pellet (the solidified sample after melting) into a 30 mg bottle mixture.

7. The new solution (glassy pellets in their mixtures) immediately run in a carousel to avoid any silica precipitations by completing the solution. The shaking process take 3-4 hours until the solution become homogenous. By now, samples are ready for ICP-OES instrument analysis.

8. Initially, ICP-OES instrument calibration, then analysis starts by running four-calibration standards. The instrumental reference sample (REF) is made of the same parts of internal calibration standards, which are used to monitor drift during the process of analysis. In addition, spectra software used in the calculation of 3-4 points for every single element. As the beginning of the session, REF was analyzed at 4 or 5 samples interval across the whole analytical samples (30 samples). The four other calibration standard (K9119, ATHO, BTHO and BAIK) were individually and alternatively used in between a batch of 4-5 samples.

9. The output raw data then copied for correction to a spreadsheet. Thereafter, all the samples values normalized to 100%. Then time variation calculated to each sample, in order to obtain correction for the batch results to be equal to the absolute values of the references samples.

# APPENDIX II: Scanning electron microscope (SEM) analyses

**Table 1.Quantitive analysis results for pyroxene (SEM)**

| | 1 | 2 | 3 | 4 | 5 | 6 | 7 | 8 | 9 | 10 | 11 | 12 | 13 | 14 | 15 | 16 | 17 | 18 | 19 | 20 | 21 | 22 | 23 | 24 | 25 | 26 |
|---|---|---|---|---|---|---|---|---|---|---|---|---|---|---|---|---|---|---|---|---|---|---|---|---|---|---|
| **SiO2** | 54 | 54 | 55 | 52.5 | 54 | 54 | 53.8 | 53.79 | 55.62 | 55.74 | 49.85 | 55.11 | 40.62 | 54.8 | 54.18 | 64.65 | 37.02 | 45.97 | 35.73 | 36.23 | 36.48 | 54.12 | 51.74 | 49.74 | 55.25 | 54.83 |
| **FeO** | 10 | 20 | 9.7 | 19.1 | 18.6 | 9.66 | 8.4 | 9.43 | 6.07 | 7.26 | 22.08 | 6.25 | 25.23 | 15.53 | 15.53 | 8.69 | 25.96 | 23.45 | 27.45 | 25.94 | 26.98 | 22.12 | 11.74 | 21.14 | 10.43 | 21.42 |
| **MgO** | 12 | 22.5 | 12.9 | 21.89 | 22.7 | 14.81 | 13.6 | 12.97 | 8.98 | 14.87 | 4.08 | 15.21 | 0.23 | 12.16 | 12.16 | 4.76 | 16.65 | 21.51 | 17.3 | 17.41 | 17.06 | 21.85 | 11.08 | 5.6 | 13.09 | 21.52 |
| **CaO** | 23 | 1.4 | 22.4 | 1.32 | 1.3 | 18.64 | 22.4 | 21.16 | 15.68 | 21.83 | 20.41 | 21.47 | 32.85 | 13.26 | 13.26 | 9.18 | | | | | | 1.6 | 22.45 | 21.94 | 19.62 | 1.93 |
| **MnO** | | 1.69 | | 1.09 | 1.3 | 0.8 | | | | | | | 0.25 | 1.39 | 1.39 | 6.52 | | | | | | | | | | |
| **TiO2** | | | | | | | | | | | | | 0.2 | 0.04 | | | | | | | | | | | | |
| **Na2O** | | | | | | | | | 2.52 | 0.17 | 0.19 | 0.17 | 0.21 | 0.43 | 0.43 | 1.84 | 0.17 | 0.24 | 0.17 | 0.17 | 0.17 | 0.17 | 0.18 | 0.19 | 0.17 | 0.17 |
| **Al2O3** | | | 1.29 | 3.2 | 1.55 | 1.17 | 15 | 2.02 | 11.13 | | 2.48 | 1.81 | 0.37 | 2.9 | 2.9 | 0.14 | 20.13 | 8.73 | 19.55 | 20.18 | 19.24 | 0.14 | 2.82 | 1.4 | 1.44 | 0.14 |
| **K2O** | | | | | | | | | | | 0.92 | | 0.03 | 0.1 | 0.1 | 0.07 | | | | | | | | | | |
| **Sample NO.** | 230-pyx1 | 230-pyx2 | 230-pyx-3 | 230-pyx4 | 230-pyx5 | 230-pyx6 | 230-pyx7 | 230-pyx8 | 230-pyx9 | 226-vesfilling3-pyx2-centre-zonation | 226-vesfilling3-pyx2-margin | 226-vesfilling3-pyx-centre-crystal 5 | 226-vesfilling3-pyx-margin-crystal 9 | 226-vesfilling3-pyx-thread-crystal 3 | 226-vesfilling3-pyx-thread-crystal 24 | 226-vesfilling3-pyx-thread-crystal 18 | 248-veinfilling1 | 248-veinfilling2 | 248-veinfilling3 | 248-veinfilling4 | 248-veinfilling5 | 290-groundmass 1 | 290-vesfilling1 | 290-groundmass | 290-cpx1vesfilling2 | 290-cpx2-groundmass |
| | **1** | **2** | **3** | **4** | **5** | **6** | **7** | **8** | **9** | **10** | **11** | **12** | **13** | **14** | **15** | **16** | **17** | **18** | **19** | **20** | **21** | **22** | **23** | **24** | **25** | **26** |
| **SiO2** | 53.9 | 51.04 | 55 | 52.97 | 52.31 | 48.52 | 53.5 | 50.76 | 51 | 49.16 | 51.59 | 50.28 | 53.34 | 54.16 | 52.84 | 52.15 | 52.48 | 55.81 | 55.42 | 53.17 | 53.58 | 53.8 | 53.22 | 51.77 | 54.29 | 52.16 |
| **FeO** | 13.1 | 20.58 | 12.3 | 23.47 | 14.41 | 21.62 | 13.03 | 18.05 | 22.94 | 21.77 | 16.73 | 16.58 | 9.77 | 10.13 | 10.35 | 8.22 | 8.51 | 8.34 | 9.93 | 8.26 | 10.54 | 9.99 | 8.68 | 19 | 22.25 | 25.16 |
| **MgO** | 12.1 | 6.6 | 13.2 | 20.14 | 10.38 | 6.25 | 12.8 | 6.86 | 4.19 | 4.4 | 6.71 | 7.07 | 12.57 | 13.79 | 12.54 | 15.76 | 13.53 | 14.31 | 12.3 | 13.12 | 14.14 | 12.56 | 12.52 | 14.59 | 20.57 | 20.99 |
| **CaO** | 20.6 | 19.65 | 17.9 | 1.56 | 19.9 | 19.93 | 19.1 | 21.37 | 19.98 | 21.14 | 21.88 | 22.94 | 21.07 | 19.75 | 21.21 | 19.69 | 19.31 | 19.31 | 22.03 | 22.33 | 19.59 | 20.5 | 21.84 | 9.39 | 1.28 | 1.39 |
| **MnO** | | 1.78 | | 1.55 | | 1.74 | | 1.41 | 1.54 | 2.12 | 1.54 | 1.2 | | | | | | | | | | | | | | |
| **TiO2** | | | | | | | | | | | | | | | | | | | | | | | | | | |
| **Na2O** | 0.18 | 0.19 | 0.17 | 0.17 | | | 0.18 | 0.18 | | | | | | | | | | | | | | | | | | |
| **Al2O3** | 0.15 | 0.16 | 1.43 | 0.14 | 2.83 | 1.75 | 1.39 | 1.37 | 0.15 | 1.23 | 1.36 | 1.75 | 3.09 | 2.01 | 2.89 | 4.01 | 6 | 2.07 | 0.15 | 2.96 | 1.98 | 2.98 | 3.57 | 5.08 | 1.45 | 0.14 |
| **K2O** | | | | | | | | | | | | | | | | | | | | | | | | | | |
| **Sample NO.** | 290-cpx2-vesfilling1a | 290-cpx2-vesfilling1 | 290-cpx2-vesfilling2 | 290-cpx3-groundmass | 290-cpx3-vesfillingground | 290-cpx3-vesfillingmass | 290-cpx3-vesfilling1g1f | 290-cpx4-vesfilling1g2b | 290-cpx5-vesfilling1ng1c | 290-cpx6-vesfilling1ng1 | 290-cpx7-vesfilling1ng1 | 290-cpx8-vesfilling1ng1 | HE-cpx1-loc1-vesl | HE-cpx1-loc2-groundmass | HE-cpx1-loc2-vesl | HE-cpx1-loc1-margin-ves1 | HE-cpx2-loc1-vesl | HE-cpx2-loc2-groundmass | HE-cpx2-loc2-vesl | HE-cpx3-loc2-vesl | HE-cpx3-loc2grounmass | HE-cpx3-loc2-vesl | HE-cpx4-loc1-ves1 | HE-cpx4-loc2-groundmass | HE-opx1-loc3-ves1 | HE-opx2-loc3-ves1 |
| | **1** | **2** | **3** | **4** | **5** | **6** | **7** | **8** | **9** | **10** | **11** | **12** | **13** | **14** | **15** | **16** | **17** | **18** | **19** | **20** | **21** | **22** | **23** | **24** | **25** | **26** |
| **SiO2** | 54.3 | 52.04 | 64.4 | 53.84 | 54.29 | 53.81 | 52.69 | 53.19 | 53.73 | 54.32 | 52.67 | 53.59 | 34.44 | 35.48 | 33.94 | 34.24 | 32.17 | 37.79 | 42.22 | 36.54 | 45.53 | 54.77 | 52.17 | 53.56 | 53.19 | 52.48 |
| **FeO** | 23 | 25.26 | 10.2 | 22.39 | 7.43 | 7.42 | 9.39 | 7.53 | 7.94 | 8.21 | 9.51 | 8.19 | 33.41 | 30.9 | 37.21 | 34.86 | 60 | 29.31 | 16.65 | 25.89 | 7.31 | 6.68 | 10.73 | 10.08 | 10.57 | 9.87 |
| **MgO** | 21.2 | 19.18 | 22.2 | 20.7 | 14.54 | 13.74 | 13.69 | 15.19 | 15.4 | 13.88 | 13.69 | 13.64 | 13.85 | 16.23 | 11.59 | 13.34 | 1.88 | 12.75 | 8.98 | 17.02 | 9.72 | 16.68 | 16.96 | 13.27 | 13.63 | 15.25 |
| **CaO** | 1.24 | 1.08 | 0.99 | 1.22 | 20.61 | 22.32 | 20.97 | 21.17 | 19.87 | 20.73 | 21.23 | 21.63 | 0.08 | 0.07 | 0.9 | 0 | 2.24 | 1.25 | 9.47 | 1.52 | 9.69 | 19.98 | 4.65 | 18.61 | 19.01 | 17.66 |
| **MnO** | | | | | 1.5 | 1.01 | 1.36 | 1.07 | 1.61 | 1.22 | 1.31 | 1.13 | | | | | | | | | | | | 1.44 | 1.58 | 1.47 |
| **TiO2** | | | | | | | | | | | | | | | | | | | | | | | | | | |
| **Na2O** | | | | | | | | | | | | | | | | | | | | | 1.83 | 0.17 | 2.58 | | | |
| **Al2O3** | 0.14 | 1.64 | 2.05 | 1.68 | 1.46 | 1.53 | 1.71 | 1.68 | 1.27 | 1.46 | 1.42 | 1.64 | 17.9 | 17.01 | 16.04 | 17.18 | 3.52 | 17.76 | 22.51 | 18.87 | 23.5 | 1.72 | 12.92 | 2.87 | 1.84 | 3.1 |
| **K2O** | | | | | | | | | | | | | | | | | | | | | 2.42 | | | | | |
| **Sample NO.** | HE-opx3-loc3-ves1 | HE-opx4-loc3-ves1 | HE-opx5-loc2-groundmass | HE-opx5-loc3-ves1 | 251-ves1-centre-cpx1 | 251-ves1-centre-cpx2 | 251-ves1-groundmass-cpx1 | 251-ves1-groundmass-cpx2 | 251-ves1-groundmass-cpx3 | 251-ves1-groundmass-cpx4 | 251-ves1m-margin-cpx1 | 251-margin-cpx2 | 271-margin-1-cpx1 | 271-margin-1-cpx2 | 271-margin-1-cpx3 | 271-margin-1-cpx4 | 271-margin-1-cpx5 | 271-vesfilling1-cpx1 | 271-vesfilling1-cpx2 | 271-vesfilling1-cpx3 | 274-groundmass-s1-cpx1 | 274-vesfilling-ng-cpx5 | 274-vesfilling-cpx7 | 291-groundmass-ass-cpx1 | 291-groundmass-ass-cpx2 | 291-groundmass-ass-cpx5 |

**Table 2.Quantitive analysis results for plagioclase (SEM)**

| | 1 | 2 | 3 | 4 | 5 | 6 | 7 | 8 | 9 | 10 | 11 | 12 | 13 | 14 | 15 | 16 | 17 | 18 | 19 | 20 | 21 | 22 | 23 | 24 | 25 |
|---|---|---|---|---|---|---|---|---|---|---|---|---|---|---|---|---|---|---|---|---|---|---|---|---|---|
| **SiO2** | 57 | 53 | 54 | 57 | 57 | 59 | 57.2 | 55.6 | 57.89 | 57.1 | 57.17 | 57.09 | 53.1 | 54 | 54.8 | 55.81 | 71.77 | 66.56 | 64.06 | 82.83 | 63.33 | 54.21 | 52.17 | 58.89 | 56.69 |
| **Al2O3** | 26.7 | 29.3 | 28.7 | 26.1 | 25 | 2.5 | 26.3 | 26.7 | 26.74 | 26.79 | 26.79 | 26.55 | 28.89 | 28.1 | 26.9 | 27.66 | 16.1 | 4.8 | 22.44 | 11.28 | 20.66 | 26.46 | 24.89 | 24.35 | 25.69 |
| **CaO** | 6.64 | 9.13 | 8.7 | 8.7 | 8.66 | 40.53 | 8 | 9.6 | 9.4 | 8.96 | 8.96 | 8.56 | 12.62 | 11.62 | 10.11 | 7.64 | 3.67 | 11.77 | 2 | 1.66 | 1.32 | 10.23 | 16.44 | 6.99 | 9.1 |
| **Na2O** | 8.75 | 7.37 | 8.4 | 9.08 | 9.9 | 0.57 | 8.5 | 8.02 | 6.8 | 8 | 8 | 8.7 | 6.29 | 7.14 | 9.07 | 8.74 | 9 | 11.14 | 12.39 | 5.13 | 4.99 | 8.26 | 7.52 | 9.24 | 9.26 |
| **K2O** | 1.4 | 0.4 | 0.6 | | | 0.02 | | | | | | | | | | | 0.37 | | | | 10.63 | | | | |
| **MgO** | 0.26 | | 0.59 | | | | | | | | | | | | | 0.19 | 0.19 | | | | | | | | |
| **FeO** | 0.6 | | | 1.3 | 1.3 | 4.5 | | | | | | | | | | | | | | | | | | 0.34 | |
| **Sample NO.** | 230-feld1 | 230-feld2 | 230-feld3 | 230-feld4 | 230-feld5 | 230-feld6 | 230-feld7 | 230-feld8 | 230-feld9 | 230-feld10 | 230-feld11 | 230-feld12 | 230-feld13 | 230-feld14 | 230-feld15 | 226-groundmass3 | 226-vesfilling1 | 226-vesfilling-margin | 248-feld3-ves1-veinfilling | 248-feld4-ves1-veinfilling | 248-feld2-ves1-veinfilling | 290-feld1-groundmass | 290-feld1-vesfilling1 | 290-feld1-vesfilling2 | 290-feld2-groundmass |

| | 1 | 2 | 3 | 4 | 5 | 6 | 7 | 8 | 9 | 10 | 11 | 12 | 13 | 14 | 15 | 16 | 17 | 18 | 19 | 20 | 21 | 22 | 23 | 24 | 25 |
|---|---|---|---|---|---|---|---|---|---|---|---|---|---|---|---|---|---|---|---|---|---|---|---|---|---|
| **SiO2** | 54.02 | 55.6 | 56.67 | 56.42 | 55.64 | 54.45 | 50.42 | 52.12 | 53.89 | 54.33 | 52.4 | 51.33 | 53.94 | 50.25 | 53.8 | 47.11 | 53.98 | 64.23 | 58.03 | 56.91 | 57.63 | 55.93 | 55.56 | 57.15 | 44.62 |
| **Al2O3** | 28.78 | 28.04 | 26.58 | 26.51 | 25.35 | 28.9 | 31.44 | 30.63 | 30.49 | 27.95 | 29.27 | 29.93 | 27.91 | 30.19 | 28.77 | 32.49 | 29.39 | 20.64 | 24.98 | 24.96 | 24.6 | 26.46 | 25.97 | 25.52 | 34.13 |
| **CaO** | 9.71 | 8.83 | 8.71 | 10.14 | 8.06 | 10.49 | 15.02 | 13.1 | 10.96 | 12.13 | 12.83 | 14.64 | 11.78 | 15.36 | 11.69 | 18.04 | 11.46 | | 7.52 | 8.61 | 8.18 | 9.67 | 9.64 | 8.6 | 19.29 |
| **Na2O** | 8.41 | 6.96 | 7.49 | 7.85 | 9.63 | 7.08 | 4.06 | 5.07 | 5.58 | 6.52 | 6.42 | 5.03 | 7.29 | 5.14 | 6.66 | 3.3 | 6.09 | 2.04 | 10.39 | 10.44 | 10.51 | 8.86 | 9.75 | 9.65 | 1.67 |
| **K2O** | | | | | 0.73 | | | | | | | | | | | | | 13.97 | | | | | | | |
| **MgO** | | | | | | | | | | | | | | | | | | | | | | | | | |
| **FeO** | | 0.39 | 0.37 | | 0.4 | | | | | | | | | | | | | | | | | | | | |
| **Sample NO.** | 290-feld2-vesfilling1 | 290-feld2-vesfilling2 | 290-feld3-groundmass | 290-feld3-vesfilling1 | 290-feld4-groundmass | HE-feld1-loc1-groundmass | HE-feld1-loc1-ves1 | HE-feld1-loc2-groundmass | HE-feld1-loc2-ves1 | HE-feld1--margin-loc1-groundmass | HE-feld2-loc1-groundmass | HE-feld2-loc1-ves1 | HE-feld2-loc2-groundmass | HE-feld2-loc2-ves1 | HE-feld3-loc1-groundmass | He-feld3-loc1-ves1 | HE-feld3-loc2-ves1 | HE-feld1-loc2-ves1 | 251-ves1-groundmass-feld1 | 251-ves1-groundmass-feld2 | 251-ves1-groundmass-feld3 | 251-ves1-groundmass-feld4 | 251-ves1-margin-feld1 | 251-ves1-margin-feld2 | 271-groundmass-feld1 |

| | 1 | 2 | 3 | 4 | 5 | 6 | 7 | 8 | 9 | 10 | 11 | 12 | 13 | 14 | 15 | 16 | 17 | 18 | 19 | 20 | 21 | 22 | 23 | 24 | |
|---|---|---|---|---|---|---|---|---|---|---|---|---|---|---|---|---|---|---|---|---|---|---|---|---|---|
| **SiO2** | 44.62 | 45.3 | 45.38 | 44.84 | 43.91 | 44.64 | 45.37 | 45.24 | 44.96 | 45.86 | 48.93 | 60.5 | 59.36 | 59.53 | 59.97 | 59.49 | 56.08 | 55.97 | 56.27 | 63.19 | 63.75 | 55.06 | 55.89 | 72.53 | |
| **Al2O3** | 34.44 | 33.62 | 33.88 | 34.36 | 36.46 | 33.19 | 33.45 | 32.95 | 34.35 | 33.53 | 33.12 | 21.86 | 24.65 | 24.02 | 23.6 | 23.34 | 25.03 | 26.05 | 25.84 | 19.99 | 18.76 | 28.21 | 26.23 | 14.68 | |
| **CaO** | 18.96 | 18.87 | 18.4 | 18.9 | 17.17 | 20.03 | 19.11 | 19.57 | 18.91 | 19.62 | 15.38 | 3.46 | 5.85 | 5.54 | 5.13 | 5.83 | 9.28 | 9.66 | 8.64 | 0.7 | 0.82 | 8.67 | 10.2 | 5.89 | |
| **Na2O** | 1.43 | 1.39 | 1.67 | 1.15 | 1.52 | 1.53 | 1.32 | 1.63 | 1.35 | 0.17 | 15.38 | 5.57 | 9.93 | 10.53 | 10.4 | 10.88 | 8.73 | 8.33 | 8 | 0.38 | 0.99 | 7.8 | 7.82 | 0.16 | |
| **K2O** | | | | | | | | | | | | 9.56 | 1.13 | 1.29 | 1.82 | 1.37 | 0.73 | 0.91 | 0.82 | 16.71 | 16.66 | | 0.78 | 7.68 | |
| **MgO** | | | | | | | | | | | | | | | | | | | | | | | | | |
| **FeO** | | | | | | | | | | | | | | | | | | | 0.23 | | | | | | |
| **Sample NO.** | 271-groundmass-feld2 | 271-groundmass-feld3 | 271-groundmass-feld4 | 271-groundmass-feld5 | 271-groundmass-feld6 | 271-margin1-feld1 | 271-margin1-feld2 | 271-vesfilling-feld1 | 271-vesfilling-feld2 | 271-vesfilling-feld3 | 274-groundmass1-feld1 | 274-groundmass1-feld2 | 274-vesfilling-feld1 | 274-vesfilling-feld2 | 274-vesfilling-feld3 | 274-vesfilling-feld4 | 291-groundmass-feld1 | 291-groundmass-feld2 | 291-groundmass-feld3 | 291-vesfilling-inner-centre-feld1 | 291-vesfilling-inner-centre-feld3 | 291-vesfilling-outer-centre-feld1 | 291-vesfilling-outer-centre-feld2 | 291-vesfilling-outer-centre-feld3 | |

**Table 3.Quantitive analysis results for oxides (SEM)**

| | 1 | 2 | 3 | 4 | 5 | 6 | 7 | 8 | 9 | 10 | 11 | 12 | 13 | 14 | 15 | 16 | 17 | 18 |
|---|---|---|---|---|---|---|---|---|---|---|---|---|---|---|---|---|---|---|
| **FeO** | 94.4 | 87.5 | 96.8 | 91.72 | 57.5 | 47.75 | 96.6 | 94.16 | 94.3 | 55.44 | 55.68 | 96.81 | 98.61 | 97.23 | 96.38 | 96.66 | 97.11 | 97.22 |
| **TiO2** | 2.4 | 10.5 | 3 | 6.1 | 40.48 | 49.6 | 2.53 | 4.7 | 2.5 | 42.39 | 42.57 | 1.75 | 0 | 1.81 | 2.48 | 2.15 | 1.78 | 1.75 |
| **Al2O3** | 1.9 | 1.18 | 0.15 | 1.51 | 0.1 | 0.14 | 0.89 | 1.16 | 1.97 | 0.56 | 0.14 | 1.49 | 0.99 | 1 | 1.18 | 1.24 | 1.16 | 1.07 |
| **MgO** | 0.7 | 0.09 | 0.03 | 0.06 | | | | | 0.7 | | | | | | | | | |
| **MnO** | 0.54 | 1.04 | | 0.6 | 1.9 | 2.54 | | | 0.5 | 1.65 | 1.65 | | 0.47 | | | | | |
| **Sample No.** | 230-ox2 | 230-ox3 | 230-ox4 | 230-ox5 | 230-ox6 | 230-ox7 | 230-ox8 | 230-ox9 | 230-ox10 | 230-ox11 | 230-ox12 | 230-ox14 | 230-ox15 | 230-ox16 | 248-ox3-veinfilling | 248-ox4-veinfilling | 248-ox5-veinfilling | 248-ox6-veinfilling |

| | 1 | 2 | 3 | 4 | 5 | 6 | 7 | 8 | 9 | 10 | 11 | 12 | 13 | 14 | 15 | 16 | 17 | 18 | 19 |
|---|---|---|---|---|---|---|---|---|---|---|---|---|---|---|---|---|---|---|---|
| **FeO** | 96.94 | 93.46 | 97.21 | 96.73 | 96.94 | 96.9 | 97.56 | 93.29 | 94.67 | 73.83 | 94.2 | 42.9 | 94.56 | 88.63 | 88.35 | 84.46 | 84.68 | 84.2 | 78.15 |
| **TiO2** | 1.47 | 0 | 2.69 | 1.94 | 1.79 | 2.01 | 1.4 | 5.3 | 4.12 | 23.3 | 2.94 | 55.37 | 2.82 | 4.76 | 7.97 | 6.67 | 7.96 | 7.32 | 9.71 |
| **Al2O3** | 1.63 | 2.52 | 0.14 | 1.38 | 1.31 | 1.14 | 1.08 | 1.45 | 1.25 | 0.97 | 2.91 | 0.14 | 2.66 | 5 | 3.72 | | | | 1.16 |
| **MgO** | | | | | | | | | | | | | | 1.62 | | | | | |
| **MnO** | | 4.16 | | | | | | | | 1.95 | | 1.63 | | | | | | | |
| **Sample No.** | 290-ox1-groundmass | 290-ox1-vesfilling1 | 248-ox2-veinfilling | 290-ox1-vesfilling2 | 290-ox2-groundmass | 290-ox2-vesfilling2 | 290-ox3-vesfilling2 | 290-ox4-vesfilling1 | 290-ox5-vesfilling1 | 290-ox7-vesfilling1 | HE-ox1-loc2-ves1 | HE-ox2-loc2-groundm | HE-ox2-loc2-ves1 | HE-ox3-loc2-groundm | HE-ox4-loc2-groundm | HE-sulfde1-loc1- | HE-sulfde2-loc1- | HE-sulfde3-loc1- | HE-sulfde3-loc1-ves1 |

| | 1 | 2 | 3 | 4 | 5 | 6 | 7 | 8 | 9 | 10 | 11 | 12 | 13 | 14 | 15 | 16 | 17 | 18 |
|---|---|---|---|---|---|---|---|---|---|---|---|---|---|---|---|---|---|---|
| **FeO** | 96.97 | 85.66 | 82.34 | 96.25 | 91.03 | 91.03 | 89.95 | 91.03 | 85.33 | 92.19 | 91.57 | 91.25 | 72.82 | 70.97 | 65.45 | 88.2 | 65 | 51.32 |
| **TiO2** | 1.81 | 6.37 | 7.27 | 2.57 | 6.68 | 6.68 | 7.31 | 6.68 | 6.64 | 6.05 | 6.79 | 6.45 | 27.08 | 28.93 | 34.46 | 10.71 | 34.9 | 46.69 |
| **Al2O3** | 1.27 | 1.39 | | 1.22 | 2.34 | 2.34 | 2.79 | 2.34 | 6.4 | 1.8 | 1.69 | 2.35 | 0.14 | 0.14 | 0.14 | 0.14 | 0.14 | 0.14 |
| **MgO** | | 4.66 | | | | | | | 1.64 | | | | | | | | | |
| **MnO** | | 1.92 | | | | | | | | | | | | | | | | 1.88 |
| **Sample No.** | 251-ves1-groundmass-ox1 | 251-ves1-margin-ox1 | HE-sulfde4-loc1-groundmass | 251-ves1-margin-ox2 | 271-groundmass1-ox40 | 271-groundmass-ox1 | 271-groundmass-ox2 | 271-groundmass-ox3 | 271-groundmass-ox7 | 271-vesfilling1-ox1 | 271-vesfilling1-ox2 | 271-vesfilling1-ox3 | 274-vesfilling-ox1 | 274-vesfilling-ox3 | 274-vesfilling-ox4 | 274-groundmass1-ox1 | 274-groundmass1-ox2 | 291-groundmass-ox1 |

**Table 4.Quantitive analysis results for apatite (SEM)**

| | 1 | 2 | 3 | 4 | 5 | 6 | 7 | 8 | 9 | 10 | 11 | 12 | 13 | 14 |
|---|---|---|---|---|---|---|---|---|---|---|---|---|---|---|
| **CaO** | 65.47 | 66.29 | 68.97 | 65.04 | 67.6 | 70.04 | 68.68 | 69.88 | 65.88 | 68.37 | 66.89 | 70.08 | 71.33 | 70.83 |
| **P2O5** | 21.15 | 20.8 | 27.26 | 22.23 | 20.61 | 24.65 | 25.91 | 24.2 | 21.24 | 24.91 | 25.69 | 24.1 | 24.31 | 25.63 |
| **F** | 4.44 | 4.19 | 3.77 | 1.95 | 4.7 | 4.7 | 4.57 | 3 | 2.4 | 2.48 | 3.58 | 3.95 | 4.35 | 2.73 |
| **Cl** | | | | | | | | | 2.68 | 3.22 | 0.96 | | | |
| **Zr** | 7.58 | 7.42 | | 7.46 | 6.47 | | | | 6.96 | | | | | |
| **SiO2** | 1.37 | 1.35 | | 1.93 | | | 0.84 | 0.89 | 0.84 | 1.02 | 1.85 | 1.86 | | 0.81 |
| **Sample No.** | 226-ves5 | 230 | HE-42 | 271-margin-sulfide1 | 271-margin1-sulfide2 | 271-margin1-carbonate 1 | 271-margin1-carbonat2 | 271-margin1-carbonat6 | 274-vesfilling-sulfite2 | 274-vesfilling-carbonate-sulfite3 | 290-ccpo1-vesfilling1 | 290-ccpo2-vesfilling1 | 290-ccpo3-vesfilling1 | 290-ccpo4-vesfilling1 |

| | 1 | 2 | 3 | 4 | 5 | 6 | 7 | 8 | 9 | 10 | 11 | 12 | 13 | 14 |
|---|---|---|---|---|---|---|---|---|---|---|---|---|---|---|
| **CaO** | 72.18 | 67.25 | 68.04 | 72.24 | 66.89 | 70.08 | 71.33 | 70.83 | 72.18 | 67.25 | 70.04 | 68.68 | 65.88 | 68.37 |
| **P2O5** | 24.85 | 26.64 | 23.43 | 26.88 | 25.69 | 24.1 | 24.31 | 25.63 | 24.85 | 26.64 | 24.65 | 25.91 | 21.24 | 24.91 |
| **F** | 0.92 | 4.84 | | | 3.58 | 3.95 | 4.35 | 2.73 | 0.92 | 4.84 | 4.7 | 4.57 | 2.4 | 2.48 |
| **Cl** | 0.54 | | | | 0.96 | | | | 0.54 | | | | 2.68 | 3.22 |
| **Zr** | | | 7.23 | | | | | | | | | | | |
| **SiO2** | 1.51 | 1.28 | 0.93 | | 1.85 | 1.86 | | 0.81 | 1.51 | 1.28 | | 0.84 | 0.84 | 1.02 |
| **Sample No.** | 290-ccpo5-vesfilling1 | 251-ves1-center-carbonate-P2 | 251-ves1-center-carbonate-p1 | 251-ves1-margin-carbonate-p1 | 290-cc-po1-vesfilling1 | 290-cc-po2-vesfilling1 | 290-cc-po3-vesfilling1 | 290-cc-po4-vesfilling1 | 290-cc-po5-vesfilling1 | 251-ves1-center-carbonate-with- p2 | 271-margin1-carbonate1 | 271-margin1-carbonate 2 | 274-vesfilling-carbonate-sulfitde2 | 274-vesfilling-carbonate-sulfitde3 |

**Table 5.Quantitive analysis results for titanite (SEM)**

| | 1 | 2 | 3 | 4 | 5 | 6 | 7 | 8 | 9 | 10 | 11 |
|---|---|---|---|---|---|---|---|---|---|---|---|
| **SiO2** | 21.8 | 21.59 | 22.66 | 22.57 | 22.9 | 24.58 | 22.47 | 22.64 | 26.64 | 24.42 | 22.64 |
| **CaO** | 35.7 | 35.09 | 35.7 | 34.43 | 33.93 | 34.74 | 35.13 | 34.98 | 33.19 | 34.29 | 34.98 |
| **TiO2** | 38.25 | 39.54 | 37.5 | 38.73 | 38.82 | 32.29 | 38.26 | 34.97 | 31.04 | 32.72 | 34.97 |
| **FeO** | 2.99 | 2.69 | 2.78 | 2.52 | 2.57 | 3.79 | 2.71 | 3.95 | 3.52 | 3.87 | 3.95 |
| **Al2O3** | 1.16 | 1.09 | 1.32 | 1.75 | 1.78 | 4.47 | 1.28 | 3.45 | 5.6 | 4.69 | 3.45 |
| **MgO** | | | | | | 0.1 | 0.05 | | | | |
| **Na2O** | | | | | | | 0.05 | | | | |
| **MnO** | | | | | | | 0.05 | | | | |
| **Sample No.** | 230-SI-As-sphene | 230-SI-As-sphene3 | 230-16-sphene-230-2 | 230-sphene-2 | 230-sphene-4 | 226-groundmass4-sphene | 226-vesfilling 5-sphene-crystal-2 | 248-sphene1-veinfilling | 248-sphene2-veinfilling | 248-sphene3-veinfilling | 248-sphene 1-veinfilling |

| | 1 | 2 | 3 | 4 | 5 | 6 | 7 | 8 | 9 | 10 | 11 |
|---|---|---|---|---|---|---|---|---|---|---|---|
| **SiO2** | 26.64 | 24.42 | 24.77 | 24.47 | 23.47 | 20.57 | 21.55 | 20.61 | 24.14 | 23.69 | 33.56 |
| **CaO** | 33.19 | 34.29 | 33.3 | 33.49 | 32.56 | 36.45 | 36.21 | 36.7 | 33.6 | 32.88 | 28.85 |
| **TiO2** | 31.04 | 32.72 | 32.65 | 33.37 | 33.95 | 38.33 | 38 | 39.1 | 36.27 | 34.23 | 11.38 |
| **FeO** | 3.52 | 3.87 | 4.48 | 4.66 | 5.14 | 3.12 | 2.8 | 2.37 | 3.05 | 5.54 | 3.45 |
| **Al2O3** | 5.6 | 4.69 | 3.73 | 3.15 | 3.67 | 1.41 | 1.45 | 1.21 | 2.74 | 3.67 | 22.77 |
| **MgO** | | | 1.07 | 0.87 | 1.21 | | | | | | |
| **Na2O** | | | | | | | | | | | |
| **MnO** | | | | | | | | | | | |
| **Sample No.** | 248-sphene2-veinfilling | 248-sphene3-veinfilling | HE-sphene1-loc1-groundmass | HE-sphene2-loc1-groundmass | HE-sphene3-loc1-groundmass | 251-ves1-center-sphene1 | 251-ves1-center-sphene2 | 251-ves1-center-sphene3 | 271-vesfilling 1-shene1 | 271-vesfilling 1-shene2 | 271-vesfilling 1-shene3 |

**Table 6.Quantitive analysis results for sulphides (SEM)**

| | 1 | 2 | 3 | 4 | 5 | 6 | 7 | 8 | 9 | 10 | 11 | 12 | 13 | 14 | 15 | 16 | 17 | 18 | 19 | 20 |
|---|---|---|---|---|---|---|---|---|---|---|---|---|---|---|---|---|---|---|---|---|
| S | 46.8 | 46.43 | 46.44 | 45.56 | 43.49 | 54.61 | 45.96 | 47.33 | 47.33 | 46 | 47.3 | 46.35 | 47.55 | 45.1 | 44.6 | 44.75 | 46.8 | 44.74 | 44.74 | 44.74 |
| Fe | 45.8 | 46.44 | 45.55 | 46.06 | 49.23 | 45.18 | 46.61 | 45.12 | 45.12 | 45.88 | 45.08 | 46.27 | 44.73 | 47.12 | 48.51 | 47.03 | 44.88 | 42.66 | 42.66 | 42.66 |
| Pb | 7.29 | 7.09 | 7.56 | 7.67 | 7.24 | | 7.33 | 7.46 | 7.46 | 7.38 | 7.62 | 7.39 | 7.25 | 7.69 | 6.66 | 8.05 | 8.15 | 11.72 | 11.72 | 11.72 |
| Ti | 0.03 | | 0.14 | 0.12 | 0.04 | | | | | 0.01 | | | | | 0.1 | | | 0.08 | 0.08 | 0.08 |
| SiO2 | | | | | | | | | | | | | | | | | | | | |
| As | 0.07 | 6.05 | 0.04 | 0.15 | | 0.03 | | | | | | | | 0.09 | 0.04 | 0.12 | | | | |
| Zn | | | 0.12 | 0.31 | | | | | | 0.09 | | | 0.28 | | | | | 0.51 | 0.51 | 0.51 |
| Sb | | | 0.15 | | | | 0.1 | 0.09 | 0.09 | 0.33 | | | | | 0.05 | | | | | |
| Au | | | | | | | | | | | | | | | | | | | | |
| Cu | | | | 0.15 | | 0.06 | | | | 0.31 | | | 0.14 | | 0.03 | | 0.17 | 0.29 | 0.29 | 0.29 |
| Ag | | | | | | 0.11 | | | | | | | 0.05 | | | | | | | |
| Ca | | | | | | | | | | | | | | | | | | | | |
| Sample No. | 252-groundmass-sulfite-grain2-zoom15000-1 | 252-groundmass-sulfite-grain2-zoom15000-2 | 252-groundmass-sulfite-grain3-zoom9000-1 | 252-groundmass-sulfite-grain3-zoom9000-2 | 252-groundmass-sulfite-grain3-zoom9000-3 | 252-groundmass-sulfite-grain4-zoom2500-1 | 252-groundmass-sulfite-grain4-zoom2500-2 | 252-groundmass-sulfite-grain4-zoom2500-3 | 252-groundmass-sulfite-grain4-zoom2500-4 | 252-groundmass-sulfite-grain4-zoom2500-5 | 252-groundmass-sulfite-grain4-zoom2500-6 | 252-groundmass-sulfite-grain4-zoom2500-7 | 252-groundmass-sulfite-grain5-zoom3000-1 | 252-groundmass-sulfite-grain5-zoom3000-2 | 252-groundmass-sulfite-grain5-zoom3000-3 | 252-groundmass-sulfite-grain5-zoom3000-4 | 252-groundmass-sulfite-grain5-zoom3000-5 | 252-groundmass-sulfite-grain5-zoom3000-6 | 252-groundmass-sulfite-grain5-zoom3000-7 | 252-groundmass-sulfite-grain5-zoom3000-8 |

| | 1 | 2 | 3 | 4 | 5 | 6 | 7 | 8 | 9 | 10 | 11 | 12 | 13 | 14 | 15 | 16 | 17 | 18 | 19 | 20 |
|---|---|---|---|---|---|---|---|---|---|---|---|---|---|---|---|---|---|---|---|---|
| S | 43.89 | 46.27 | 44.82 | 41.5 | 47.86 | 43.81 | 44.41 | 48.75 | 45.52 | 43.56 | 44.38 | 45.5 | 43.95 | 49 | 46.33 | 45.07 | 46.4 | 9.76 | 32.03 | 29.98 |
| Fe | 48.51 | 45.47 | 47.03 | 50.5 | 47.95 | 48.81 | 47.04 | 42.55 | 46.62 | 49.51 | 48.42 | 47.69 | 48.17 | 41.77 | 46.6 | 46.28 | 44.8 | 26.94 | 30.44 | 29.42 |
| Pb | 7.16 | 7.55 | 7.8 | 7.5 | 7.53 | 7.11 | 7.7 | 8.47 | 7.62 | 6.67 | 6.77 | 6.67 | 7.82 | 8.3 | 6.95 | 7.97 | 8.66 | | 5.46 | 5.58 |
| Ti | 0.04 | 0.2 | 0.05 | | | | 0.01 | | | | 0.07 | | 0.02 | | 0.01 | 0.11 | | | 0.12 | 0.25 |
| SiO2 | | | | | | | | | | | | | | | | | | | 1.32 | 2.36 |
| As | 0.13 | 0.03 | | 0.04 | | 0.03 | 0.14 | 0.03 | 0.07 | 0.07 | 0.15 | 0.07 | 0.02 | 0.14 | 0.11 | | 0.14 | | | |
| Zn | 0.02 | | | 0.45 | 0.28 | 0.23 | 0.28 | | 0.02 | 0.19 | | 0.06 | | | | 0.17 | | | 0.17 | |
| Sb | | | 0.23 | | | | 0.03 | 0.13 | | | 0.14 | | | | | | | | | |
| Au | | 0.18 | 0.05 | | 0.04 | | | | 0.05 | | | | | | | 0.03 | | | 0.29 | |
| Cu | 0.27 | 0.3 | 0.01 | 0.02 | 0.11 | | 0.38 | 0.05 | 0.1 | | | | | | | 0.38 | | | 28.37 | 29.81 |
| Ag | | | | | | | | 0.02 | | 0.03 | 0.04 | | | | | | | | | |
| Ca | | | | | | | | | | | | | | | | | | | 0.81 | 1.46 |
| Sample No. | 252-groundmass-sulfite-grain6-zoom15000-1 | 252-groundmass-sulfite-grain6-zoom15000-2 | 252-groundmass-sulfite-grain6-zoom15000-3 | 252-groundmass-sulfite-grain6-zoom15000-4 | 252-groundmass-sulfite-grain-zoom4000-1 | 252-groundmass-sulfite-grain-zoom4000-3 | 252-vein2-sulfite-grain-zoom5000-1 | 252-vein2-sulfite-grain-zoom5000-2 | 252-vein2-sulfite-grain-zoom5000-3 | 252-vein2-sulfite-grain-zoom5000-4 | 252-vein2-sulfite-grain-zoom5000-5 | 252-vein2-sulfite-grain-zoom5000-6 | 252-vein2-sulfite-grain-zoom5000-7 | 252-vein-sulfite-grain-zoom3000-2 | 252-vein-sulfite-grain-zoom3000-3 | 252-vein-sulfite-grain-zoom3000-4 | 252-vein-sulfite-grain-zoom3000-5 | 252-vein-sulfite-grain-zoom3000-1 | HE-sulfde1-loc1-ves1 | HE-sulfde2-loc1-ves1 |

| Table 7.Quantitive analysis results for amphibole (SEM) | | | | | | | | |
|---|---|---|---|---|---|---|---|---|
| | | | | | | | | |
| | 1 | 2 | 3 | 4 | 5 | 6 | 7 | 8 |
| Na2O | 4.21 | | | | | | | |
| MgO | 6.52 | 17.07 | 12.77 | 9.47 | 5.89 | 14.67 | 12.49 | 15.03 |
| Al2O3 | 22.28 | 14.1 | 21.78 | 17.82 | 23.41 | 13.83 | 13.13 | 14.47 |
| SiO2 | 43.65 | 31 | 39.79 | 23.78 | 39.73 | 30.67 | 31.41 | 32.14 |
| CaO | 12.4 | 1.6 | 1.26 | 0.51 | 2.15 | 2.27 | 2.19 | 1.95 |
| FeO | 10.92 | 36.22 | 22.72 | 48.41 | 25.01 | 38.56 | 40.77 | 36.41 |
| K2O | | | 1.68 | | 3.81 | | | |
| Sample No. | HE-amph1-loc2-groundmass | HE-amph2-loc1-groundmass | HE-amph1-loc1-groundmass | HE-amph1-loc2-ves1 | HE-amph2-loc2-ves1 | HE-amph4-loc1-groundmass | HE-amph5-loc1-groundmass | HE-amph3-loc1-groundmass |

| Table 8.Quantitive analysis results for carbonate (SEM) | | | | | | | | | | | |
|---|---|---|---|---|---|---|---|---|---|---|---|
| | | | | | | | | | | | |
| | 1 | 2 | 3 | 4 | 5 | 6 | 7 | 8 | 9 | 10 | 11 |
| Si | 2.89 | 2.7 | | 38.86 | 38.51 | 37.65 | 39.34 | 0.89 | 0.7 | 1.27 | 2.44 |
| P | | | | | | | | 18.63 | | | |
| S | | | | | | | | | 1.99 | 1.41 | 0.2 |
| Cl | | | | | | | | 2.64 | | | |
| Ca | 90.22 | 91.86 | 94.39 | 28.03 | 29.78 | 29.5 | 23.84 | 55.86 | 89.59 | 89.6 | 92.32 |
| Al | 1.69 | 1.69 | | 30.72 | 29.58 | 29.51 | 32.69 | | | | |
| Fe | 5.2 | 3.76 | 2.66 | 2.39 | 2.13 | 2.46 | 4.14 | | 3.21 | 3.26 | 1.56 |
| Mn | | | 2.95 | | | | | | | | |
| Sample No. | 251-ves1-center-carbonate-no p1 | 251-ves1-center-carbonate-no p2 | 251-ves1-margin-carbonate1 | 271-groundmass-carbonate1 | 271-margin1-carbonate3 | 271-margin1-carbonate4 | 271-margin1-carbonate5 | 274-vesfilling-carbonate-sulfitde1 | 291-veinfilling-inner-rim-carbonate1 | 291-veinfilling-inner-rim-carbonate2 | 291-veinfilling-inner-rim-carbonate3 |

# APPENDIX III: Electron microprobe (EMP) analyses

**Table 9.Quantitive analysis results for amphibole (EMP)**

| | 1 | 2 | 3 | 4 | 5 | 6 | 7 | 8 | 9 | 10 | 11 | 12 | 13 | 14 | 15 | 16 | 17 | 18 | 19 | 20 | 21 | 22 |
|---|---|---|---|---|---|---|---|---|---|---|---|---|---|---|---|---|---|---|---|---|---|---|
| **SiO2** | 51.220 | 49.920 | 72.020 | 46.660 | 49.040 | 48.360 | 49.800 | 49.030 | 48.810 | 48.740 | 49.400 | 49.530 | 48.380 | 48.220 | 48.450 | 48.880 | 49.170 | 49.350 | 50.850 | 50.600 | 50.120 | 49.440 |
| **TiO2** | 0.029 | 0.073 | 0.097 | 0.126 | 0.038 | 0.110 | 0.161 | 0.202 | 0.034 | 0.157 | 0.184 | 0.163 | 0.314 | 0.296 | 0.333 | 0.268 | 0.208 | 0.226 | 0.147 | 0.146 | 0.158 | 0.220 |
| **Al2O3** | 1.315 | 2.160 | 1.484 | 2.040 | 4.480 | 5.120 | 4.260 | 4.470 | 4.500 | 5.410 | 5.080 | 5.090 | 5.930 | 5.820 | 5.750 | 5.660 | 5.360 | 4.960 | 3.740 | 4.200 | 4.430 | 5.240 |
| **FeO** | 17.250 | 21.190 | 11.650 | 21.810 | 23.800 | 23.370 | 22.340 | 24.070 | 25.520 | 20.790 | 20.050 | 20.440 | 21.090 | 21.000 | 21.030 | 19.760 | 19.360 | 20.120 | 19.990 | 18.410 | 18.220 | 18.280 |
| **MnO** | 0.873 | 0.743 | 0.261 | 0.695 | 0.429 | 0.429 | 0.421 | 0.409 | 0.456 | 0.421 | 0.390 | 0.514 | 0.479 | 0.468 | 0.482 | 0.488 | 0.552 | 0.551 | 0.325 | 0.371 | 0.338 | 0.461 |
| **MgO** | 12.280 | 9.590 | 3.730 | 6.340 | 8.730 | 8.600 | 9.530 | 8.240 | 7.530 | 10.280 | 10.960 | 10.640 | 9.870 | 10.040 | 9.970 | 10.940 | 11.590 | 10.880 | 11.670 | 12.610 | 12.810 | 11.940 |
| **CaO** | 11.800 | 11.600 | 5.530 | 16.550 | 11.630 | 11.690 | 11.750 | 11.690 | 11.600 | 11.690 | 11.520 | 11.360 | 11.620 | 11.720 | 11.650 | 11.550 | 11.210 | 11.410 | 11.540 | 11.160 | 10.700 | 11.640 |
| **Na2O** | 0.167 | 0.247 | 0.181 | 0.302 | 0.497 | 0.625 | 0.481 | 0.533 | 0.534 | 0.709 | 0.557 | 0.659 | 0.724 | 0.732 | 0.729 | 0.664 | 0.646 | 0.598 | 0.485 | 0.495 | 0.379 | 0.625 |
| **K2O** | 0.108 | 0.144 | 0.218 | 0.093 | 0.097 | 0.067 | 0.050 | 0.072 | 0.074 | 0.075 | 0.070 | 0.066 | 0.052 | 0.040 | 0.052 | 0.055 | 0.060 | 0.038 | 0.047 | 0.050 | 0.076 | 0.048 |
| **Cl** | 0.093 | 0.082 | 0.089 | 0.089 | 0.058 | 0.096 | 0.070 | 0.080 | 0.110 | 0.136 | 0.058 | 0.103 | 0.153 | 0.149 | 0.154 | 0.106 | 0.099 | 0.096 | 0.028 | 0.060 | 0.038 | 0.069 |
| **Cr2O3** | 0.000 | 0.000 | 0.000 | 0.016 | 0.000 | 0.000 | 0.014 | 0.000 | 0.000 | 0.024 | 0.000 | 0.013 | 0.027 | 0.010 | 0.009 | 0.000 | 0.000 | 0.000 | 0.024 | 0.000 | 0.000 | 0.004 |
| **NiO** | 0.019 | 0.039 | 0.000 | 0.025 | 0.000 | 0.000 | 0.001 | 0.003 | 0.010 | 0.000 | 0.000 | 0.003 | 0.000 | 0.005 | 0.007 | 0.000 | 0.000 | 0.004 | 0.001 | 0.006 | 0.000 | 0.000 |
| **Total** | 95.155 | 95.787 | 95.260 | 94.746 | 98.798 | 98.466 | 98.878 | 98.798 | 99.179 | 98.432 | 98.268 | 98.580 | 98.640 | 98.499 | 98.616 | 98.377 | 98.256 | 98.231 | 98.846 | 98.107 | 97.270 | 97.968 |
| **Sample NO.** | 226-ves rim 2-3-amph grn 1 pnt1 | 226-ves rim 2-3-amph grn 1 pnt4 | 226-ves rim 5-amph grn 1 pnt1 | 226-ves center 5-amph grn 1 pnt2 | HE-vein-loc2-amph grn1 | HE-vein-loc2-amph grn2 | HE-vein-loc2-amph grn3 | HE-vein-loc2-amph grn4 | HE-vein-loc2-amph grn5 | HE-vein-loc2-amph grn6 | HE-vein-loc2-amph grn7 | HE-vein-loc2-amph grn8 | HE-vein-loc2-amph grn9 | HE-vein-loc2-amph grn10 | HE-vein-loc2-amph grn11 | HE-vein-loc2-amph grn12 | HE-vein-loc2-amph grn13 | HE-vein-loc2-amph grn14 | HE-vein-loc2-amph grn15 | HE-vein-loc2-amph grn16 | HE-vein-loc2-amph grn17 | HE-vein-loc2-amph grn18 |

**Table 10.Quantitive analysis results for plagioclase (EMP)**

| | 1 | 2 | 3 | 4 | 5 | 6 | 7 | 8 | 9 | 10 | 11 | 12 | 13 | 14 | 15 | 16 | 17 | 18 | 19 | 20 | 21 | 22 | 23 | 24 | 25 | 26 | 27 | 28 | 29 |
|---|---|---|---|---|---|---|---|---|---|---|---|---|---|---|---|---|---|---|---|---|---|---|---|---|---|---|---|---|---|
| **SiO2** | 55.660 | 54.720 | 57.600 | 58.350 | 51.380 | 53.120 | 54.720 | 52.670 | 52.930 | 56.120 | 55.420 | 55.860 | 55.750 | 56.650 | 57.780 | 57.340 | 57.180 | 57.490 | 62.780 | 56.570 | 55.450 | 54.550 | 46.920 | 47.050 | 51.870 | 50.480 | 46.080 | 47.030 | 45.820 |
| **TiO2** | 0.008 | 0.026 | 0.000 | 0.039 | 0.085 | 0.108 | 0.036 | 0.082 | 0.037 | 0.028 | 0.027 | 0.111 | 0.168 | 0.180 | 0.038 | 0.041 | 0.053 | 0.117 | 0.098 | 0.103 | 0.012 | 0.057 | 0.029 | 0.009 | 0.030 | 0.115 | 0.012 | 0.028 | 0.042 |
| **Al2O3** | 27.650 | 28.170 | 26.480 | 26.240 | 30.060 | 29.100 | 28.220 | 30.110 | 29.230 | 27.570 | 27.940 | 27.510 | 27.690 | 26.690 | 26.610 | 26.860 | 26.100 | 26.110 | 19.920 | 26.400 | 27.740 | 28.380 | 33.430 | 33.240 | 30.540 | 26.160 | 34.250 | 33.600 | 34.270 |
| **FeO** | 0.457 | 0.689 | 0.062 | 0.096 | 0.894 | 0.702 | 0.719 | 0.565 | 1.031 | 0.733 | 0.637 | 0.737 | 0.790 | 1.042 | 0.812 | 0.574 | 1.112 | 0.811 | 0.713 | 0.626 | 0.393 | 0.448 | 0.590 | 0.481 | 0.567 | 1.760 | 0.536 | 0.575 | 0.630 |
| **MnO** | 0.021 | 0.000 | 0.019 | 0.016 | 0.004 | 0.008 | 0.020 | 0.016 | 0.038 | 0.007 | 0.038 | 0.009 | 0.032 | 0.025 | 0.001 | 0.015 | 0.014 | 0.028 | 0.027 | 0.043 | 0.017 | 0.028 | 0.000 | 0.000 | 0.005 | 0.017 | 0.000 | 0.000 | 0.035 |
| **MgO** | 0.032 | 0.029 | 0.000 | 0.000 | 0.036 | 0.037 | 0.048 | 0.046 | 0.067 | 0.033 | 0.033 | 0.032 | 0.034 | 0.040 | 0.038 | 0.029 | 0.038 | 0.039 | 0.292 | 0.066 | 0.016 | 0.048 | 0.086 | 0.035 | 0.069 | 2.040 | 0.031 | 0.043 | 0.063 |
| **CaO** | 9.970 | 10.680 | 7.910 | 7.710 | 12.780 | 12.100 | 10.820 | 12.510 | 12.500 | 9.960 | 10.200 | 9.590 | 9.720 | 8.900 | 8.210 | 8.800 | 8.460 | 8.600 | 1.389 | 8.810 | 9.980 | 10.530 | 16.570 | 16.300 | 12.880 | 15.080 | 17.090 | 16.450 | 17.360 |
| **Na2O** | 5.770 | 5.250 | 6.890 | 6.990 | 3.990 | 4.380 | 5.060 | 4.230 | 4.250 | 5.390 | 5.340 | 5.820 | 5.480 | 5.940 | 6.020 | 5.820 | 6.740 | 6.010 | 1.019 | 6.030 | 5.360 | 5.140 | 2.130 | 2.270 | 4.090 | 3.300 | 1.540 | 2.190 | 1.530 |
| **K2O** | 0.251 | 0.215 | 0.097 | 0.152 | 0.156 | 0.171 | 0.233 | 0.164 | 0.189 | 0.468 | 0.394 | 0.395 | 0.466 | 0.521 | 0.778 | 0.637 | 0.698 | 0.768 | 13.650 | 0.672 | 0.501 | 0.453 | 0.082 | 0.087 | 0.208 | 0.163 | 0.068 | 0.084 | 0.051 |
| **BaO** | 0.045 | 0.013 | 0.000 | 0.005 | 0.046 | 0.000 | 0.010 | 0.000 | 0.014 | 0.000 | 0.006 | 0.034 | 0.034 | 0.000 | 0.077 | 0.027 | 0.041 | 0.008 | 0.409 | 0.024 | 0.008 | 0.024 | 0.000 | 0.000 | 0.000 | 0.013 | 0.033 | 0.000 | 0.000 |
| **Total** | 99.864 | 99.792 | 99.058 | 99.597 | 99.431 | 99.726 | 99.887 | 100.393 | 100.286 | 100.308 | 100.035 | 100.098 | 100.164 | 99.987 | 100.364 | 100.142 | 100.436 | 99.980 | 100.295 | 99.344 | 99.478 | 99.656 | 99.838 | 99.472 | 100.258 | 99.128 | 99.639 | 100.000 | 99.802 |
| **Sample NO.** | 226 rim 5 gr 1 pt1-feld | 226ves 2-3 gr 2 pt1-feld | 226 ves 2-3 gr 3 pt1-feld | 226 ves 2-3 gr 4 pt1-feld | 226 groundmass 2-3 gr 1 pt1-feld | 226 groundmass 2-3 gr 2 pt1-feld | 226 groundmass 2-3 gr 3 pt1-feld | 226 groundmass 5 gr 3 pt1-feld | 226 ves 5 gr 2 pt1-feld | 230 rim 1 gr 2 pt1-feld | 230 rim 1 gr 2 pt1-feld | 230 groundmass1 gr 1 pt1-feld | 230 groundmass1 gr 2 pt1-feld | 230 groundmass1 gr 3 pt1-feld | 230 ves 2 gr 1 pt1-feld | 230 ves 2 gr 2 pt1-feld | 230 groundmass 2 gr 1 pt1-feld | 291 groundmass gr 1 pt1-feld | 291 groundmass gr 2 with zone pt1-feld | 291 groundmass gr 3 with zone pt1-feld | 291-feldspar phenocrysts 1 | 291-feldspar phenocrysts 2 | HE-loc1-inner-grn1 | HE-loc1-inner-grn2 | HE-loc1-inner-grn3 | HE-loc1-inner-grn4 | HE-loc1-inner-grn5 | HE-loc1-inner-grn6 | HE-loc1-inner-grn7 |

| | 1 | 2 | 3 | 4 | 5 | 6 | 7 | 8 | 9 | 10 | 11 | 12 | 13 | 14 | 15 | 16 | 17 | 18 | 19 | 20 | 21 | 22 | 23 | 24 | 25 | 26 | 27 | 28 | 29 |
|---|---|---|---|---|---|---|---|---|---|---|---|---|---|---|---|---|---|---|---|---|---|---|---|---|---|---|---|---|---|
| **SiO2** | 49.250 | 47.560 | 48.750 | 53.180 | 50.390 | 52.740 | 54.330 | 51.140 | 50.600 | 54.790 | 53.900 | 49.550 | 51.210 | 52.210 | 51.780 | 49.540 | 51.800 | 51.750 | 53.020 | 53.620 | 54.320 | 53.760 | 54.110 | 53.090 | 54.220 | 53.820 | 48.680 | 52.320 | 51.890 |
| **TiO2** | 0.056 | 0.025 | 0.019 | 0.063 | 0.038 | 0.078 | 0.072 | 0.040 | 0.080 | 0.066 | 0.047 | 0.052 | 0.079 | 0.064 | 0.016 | 0.013 | 0.042 | 0.068 | 0.091 | 0.100 | 0.092 | 0.074 | 0.055 | 0.114 | 0.073 | 0.044 | 0.045 | 0.045 | 0.038 |
| **Al2O3** | 32.490 | 33.390 | 32.490 | 29.550 | 31.670 | 29.740 | 28.540 | 30.500 | 30.790 | 28.090 | 29.020 | 31.050 | 30.370 | 30.140 | 30.200 | 31.530 | 29.890 | 30.290 | 29.160 | 25.540 | 28.510 | 28.800 | 28.540 | 29.270 | 28.230 | 28.600 | 31.920 | 29.860 | 29.890 |
| **FeO** | 0.569 | 0.453 | 0.535 | 0.579 | 0.547 | 0.606 | 0.624 | 0.555 | 0.612 | 0.643 | 0.637 | 0.642 | 0.644 | 0.623 | 0.463 | 0.458 | 0.506 | 0.417 | 0.795 | 2.300 | 0.784 | 0.681 | 0.809 | 0.879 | 0.709 | 0.612 | 0.493 | 0.512 | 0.493 |
| **MnO** | 0.009 | 0.000 | 0.000 | 0.024 | 0.001 | 0.047 | 0.010 | 0.021 | 0.000 | 0.005 | 0.000 | 0.000 | 0.006 | 0.000 | 0.022 | 0.027 | 0.005 | 0.016 | 0.014 | 0.047 | 0.024 | 0.015 | 0.019 | 0.005 | 0.007 | 0.008 | 0.012 | 0.013 | 0.005 |
| **MgO** | 0.024 | 0.026 | 0.030 | 0.091 | 0.085 | 0.046 | 0.057 | 0.053 | 0.045 | 0.060 | 0.051 | 0.047 | 0.046 | 0.044 | 0.049 | 0.030 | 0.059 | 0.062 | 0.064 | 1.840 | 0.060 | 0.050 | 0.076 | 0.050 | 0.103 | 0.053 | 0.042 | 0.036 | 0.046 |
| **CaO** | 15.150 | 16.450 | 15.260 | 11.790 | 14.090 | 12.140 | 11.350 | 13.430 | 13.560 | 10.490 | 11.290 | 14.070 | 13.190 | 12.140 | 13.100 | 14.310 | 12.350 | 12.790 | 11.480 | 10.890 | 10.670 | 11.060 | 10.980 | 11.710 | 10.570 | 11.230 | 14.770 | 12.360 | 12.820 |
| **Na2O** | 2.740 | 2.320 | 2.800 | 4.700 | 3.400 | 4.460 | 4.900 | 3.680 | 3.670 | 5.090 | 4.910 | 3.390 | 3.820 | 4.350 | 3.970 | 3.370 | 4.160 | 3.980 | 4.750 | 4.710 | 5.050 | 4.940 | 5.090 | 4.610 | 5.230 | 4.930 | 2.810 | 4.240 | 4.020 |
| **K2O** | 0.125 | 0.073 | 0.118 | 0.265 | 0.143 | 0.288 | 0.355 | 0.193 | 0.200 | 0.388 | 0.335 | 0.177 | 0.219 | 0.276 | 0.203 | 0.135 | 0.209 | 0.197 | 0.272 | 0.301 | 0.291 | 0.293 | 0.307 | 0.249 | 0.318 | 0.280 | 0.123 | 0.217 | 0.184 |
| **BaO** | 0.000 | 0.000 | 0.002 | 0.000 | 0.000 | 0.005 | 0.000 | 0.000 | 0.029 | 0.016 | 0.000 | 0.000 | 0.022 | 0.000 | 0.002 | 0.000 | 0.013 | 0.007 | 0.000 | 0.025 | 0.009 | 0.029 | 0.000 | 0.026 | 0.014 | 0.027 | 0.021 | 0.013 | 0.000 |
| **Total** | 100.413 | 100.297 | 100.004 | 100.242 | 100.365 | 100.149 | 100.237 | 99.612 | 99.586 | 99.637 | 100.190 | 98.978 | 99.606 | 99.847 | 99.805 | 99.413 | 99.034 | 99.576 | 99.646 | 99.373 | 99.809 | 99.702 | 99.986 | 100.003 | 99.473 | 99.604 | 98.917 | 99.616 | 99.386 |
| **Sample NO.** | HE-loc1-inner-grn8 | HE-loc1-inner-grn9 | HE-loc1-inner-grn10 | HE-loc1-rim-grn1 | HE-loc1-rim-grn2 | HE-loc1-rim-grn3 | HE-loc1-rim-grn4 | HE-loc1-rim-grn5 | HE-loc1-groundmass-grn1 | HE-loc1-groundmass-grn2 | HE-loc1-groundmass-grn3 | HE-loc1-groundmass-grn4 | HE-loc1-groundmass-grn5 | HE-loc1-groundmass-grn6 | HE-loc2-inner-grn1 | HE-loc2-inner-grn2 | HE-loc2-inner-grn3 | HE-loc2-inner-grn4 | HE-loc2-rim-grn1 | HE-loc2-rim-grn2 | HE-loc2-rim-grn3 | HE-loc2-rim-grn4 | HE-loc2-rim-grn5 | HE-loc2-groundmass-grn1 | HE-loc2-groundmass-grn2 | HE-loc2-groundmass-grn4 | HE-loc3-inner-grn1 | HE-loc3-inner-grn2 | HE-loc3-inner-grn3 |

| | 1 | 2 | 3 | 4 | 5 | 6 | 7 | 8 | 9 | 10 | 11 | 12 | 13 | 14 | 15 | 16 | 17 | 18 | 19 | 20 | 21 | 22 | 23 | 24 | 25 | 26 | 27 | 28 |
|---|---|---|---|---|---|---|---|---|---|---|---|---|---|---|---|---|---|---|---|---|---|---|---|---|---|---|---|---|
| **SiO2** | 53.240 | 46.740 | 52.200 | 44.190 | 44.710 | 52.440 | 52.300 | 53.640 | 52.920 | 53.370 | 54.220 | 53.990 | 54.030 | 52.990 | 51.750 | 55.760 | 53.270 | 56.600 | 55.280 | 56.230 | 56.130 | 55.380 | 57.180 | 56.310 | 58.380 | 58.700 | 58.340 | 58.700 |
| **TiO2** | 0.000 | 0.030 | 0.000 | 0.021 | 0.000 | 0.046 | 0.048 | 0.087 | 0.042 | 0.040 | 0.037 | 0.075 | 0.031 | 0.091 | 0.029 | 0.451 | 0.139 | 0.094 | 0.054 | 0.000 | 0.023 | 0.043 | 0.263 | 0.269 | 0.193 | 0.129 | 0.047 | 0.085 |
| **Al2O3** | 29.320 | 34.010 | 29.830 | 35.400 | 34.840 | 29.600 | 29.530 | 29.130 | 29.330 | 29.170 | 28.370 | 28.690 | 28.940 | 29.920 | 29.700 | 26.440 | 24.250 | 25.590 | 26.430 | 26.780 | 26.710 | 26.750 | 24.430 | 24.420 | 25.190 | 25.060 | 25.460 | 25.310 |
| **FeO** | 0.525 | 0.551 | 0.550 | 0.532 | 0.505 | 0.505 | 0.638 | 0.678 | 0.698 | 0.658 | 0.734 | 0.797 | 0.683 | 0.678 | 0.726 | 1.029 | 3.030 | 1.228 | 1.490 | 1.043 | 1.108 | 1.390 | 2.940 | 4.220 | 1.201 | 0.965 | 1.017 | 0.971 |
| **MnO** | 0.010 | 0.008 | 0.000 | 0.019 | 0.000 | 0.000 | 0.010 | 0.005 | 0.018 | 0.000 | 0.020 | 0.036 | 0.004 | 0.013 | 0.004 | 0.010 | 0.143 | 0.025 | 0.036 | 0.000 | 0.018 | 0.056 | 0.018 | 0.037 | 0.023 | 0.024 | 0.017 | 0.015 |
| **MgO** | 0.056 | 0.024 | 0.059 | 0.038 | 0.016 | 0.046 | 0.089 | 0.048 | 0.043 | 0.051 | 0.059 | 0.077 | 0.046 | 0.056 | 0.035 | 0.048 | 1.163 | 0.151 | 0.255 | 0.048 | 0.099 | 0.208 | 0.272 | 0.362 | 0.216 | 0.146 | 0.135 | 0.157 |
| **CaO** | 12.160 | 17.150 | 12.500 | 18.840 | 18.260 | 12.410 | 12.090 | 11.310 | 11.810 | 11.440 | 10.850 | 10.910 | 11.190 | 11.330 | 12.510 | 10.090 | 12.440 | 9.170 | 10.540 | 9.870 | 9.880 | 10.870 | 7.190 | 7.260 | 7.410 | 7.680 | 7.700 | 7.650 |
| **Na2O** | 4.640 | 1.860 | 4.420 | 0.751 | 1.106 | 4.350 | 4.520 | 4.920 | 4.930 | 4.750 | 5.450 | 5.020 | 5.000 | 4.820 | 4.300 | 5.430 | 4.510 | 5.780 | 5.230 | 5.520 | 5.580 | 5.210 | 6.670 | 6.480 | 6.530 | 6.700 | 6.490 | 6.600 |
| **K2O** | 0.230 | 0.066 | 0.241 | 0.021 | 0.035 | 0.209 | 0.195 | 0.237 | 0.247 | 0.235 | 0.289 | 0.290 | 0.264 | 0.253 | 0.216 | 0.480 | 0.376 | 0.630 | 0.437 | 0.492 | 0.506 | 0.414 | 0.833 | 0.872 | 0.990 | 0.665 | 0.944 | 0.708 |
| **BaO** | 0.000 | 0.000 | 0.000 | 0.000 | 0.022 | 0.002 | 0.000 | 0.012 | 0.000 | 0.000 | 0.000 | 0.000 | 0.000 | 0.000 | 0.002 | 0.035 | 0.043 | 0.045 | 0.033 | 0.040 | 0.023 | 0.008 | 0.012 | 0.050 | 0.032 | 0.033 | 0.004 | 0.000 |
| **Total** | 100.181 | 100.439 | 99.800 | 99.812 | 99.494 | 99.606 | 99.419 | 100.066 | 100.037 | 99.714 | 100.029 | 99.885 | 100.188 | 100.152 | 99.272 | 99.773 | 99.364 | 99.313 | 99.784 | 100.023 | 100.076 | 100.328 | 99.807 | 100.279 | 100.164 | 100.103 | 100.155 | 100.196 |
| **Sample NO.** | HE-loc3-inner-grn4 | HE-loc3-inner-grn5 | HE-loc3-inner-grn6 | HE-loc3-inner-grn7 | HE-loc3-inner-grn8 | HE-loc3-inner-grn9 | HE-loc3-rim-grn1 | HE-loc3-rim-grn2 | HE-loc3-rim-grn3 | HE-loc3-rim-grn5 | HE-loc3-groundmass-grn1 | HE-loc3-groundmass-grn2 | HE-loc3-groundmass-grn3 | HE-loc3-groundmass-grn4 | HE-loc3-groundmass-grn5 | 290-ves1-rim-grn1 | 290-ves1-rim-grn2 | 290-ves1-rim-grn3 | 290-ves1-rim-grn4 | 290-ves1-rim-grn5 | 290-ves1-rim-grn6 | 290-ves1-rim-grn7 | 290-ves1-groundmass-grn1 | 290-ves1-groundmass-grn2 | 290-ves1-groundmass-grn3 | 290-ves1-groundmass-grn4 | 290-ves1-groundmass-grn5 | 290-ves1-groundmass-grn6 |

**Table 11.Quantitive analysis results for garnet (EMP)**

| | 1 | 2 | 3 | 4 | 5 | 6 | 7 | 8 | 9 | 10 | 11 | 12 | 13 | 14 | 15 | 16 | 17 | 18 | 19 | 20 | 21 | 22 | 23 | 24 | 25 | 26 | 27 |
|---|---|---|---|---|---|---|---|---|---|---|---|---|---|---|---|---|---|---|---|---|---|---|---|---|---|---|---|
| SiO2 | 35.840 | 35.730 | 35.700 | 35.480 | 35.820 | 35.620 | 35.660 | 35.700 | 35.150 | 35.470 | 34.750 | 35.050 | 38.370 | 35.540 | 35.700 | 35.230 | 34.530 | 35.770 | 35.950 | 35.610 | 35.600 | 35.860 | 35.760 | 35.770 | 35.640 | 35.660 | 35.540 |
| TiO2 | 0.036 | 0.035 | 0.007 | 0.022 | 0.027 | 0.043 | 0.004 | 0.042 | 1.970 | 1.171 | 2.950 | 0.000 | 0.003 | 0.021 | 0.050 | 1.218 | 2.720 | 0.131 | 0.257 | 0.090 | 0.077 | 0.084 | 1.506 | 0.037 | 0.000 | 0.026 | 0.019 |
| Al2O3 | 0.000 | 0.013 | 0.018 | 0.011 | 0.015 | 0.010 | 0.000 | 0.000 | 2.490 | 2.500 | 3.970 | 1.665 | 0.645 | 0.440 | 0.242 | 1.440 | 2.330 | 0.633 | 0.579 | 0.251 | 0.051 | 0.241 | 1.473 | 0.374 | 0.004 | 0.012 | 0.047 |
| FeO | 28.940 | 28.800 | 29.040 | 29.430 | 28.950 | 28.990 | 29.360 | 29.270 | 26.550 | 25.920 | 23.160 | 26.580 | 24.050 | 27.590 | 28.370 | 27.070 | 25.760 | 28.180 | 27.930 | 28.520 | 29.180 | 28.640 | 27.240 | 28.930 | 29.420 | 29.900 | 29.270 |
| MnO | 0.334 | 0.396 | 0.383 | 0.414 | 0.284 | 0.285 | 0.458 | 0.416 | 0.305 | 0.921 | 1.164 | 0.245 | 0.418 | 0.317 | 0.220 | 1.223 | 1.146 | 0.856 | 0.502 | 0.508 | 1.300 | 0.526 | 0.817 | 1.760 | 0.467 | 0.544 | 0.405 |
| MgO | 0.083 | 0.043 | 0.029 | 0.010 | 0.125 | 0.093 | 0.002 | 0.012 | 0.071 | 0.135 | 0.255 | 0.035 | 2.120 | 0.077 | 0.049 | 0.157 | 0.248 | 0.034 | 0.050 | 0.045 | 0.021 | 0.041 | 0.116 | 0.082 | 0.030 | 0.024 | 0.014 |
| CaO | 32.530 | 32.650 | 32.520 | 31.820 | 32.710 | 32.890 | 32.370 | 32.480 | 31.200 | 31.610 | 31.560 | 32.950 | 32.290 | 32.670 | 32.710 | 31.170 | 31.160 | 32.080 | 32.690 | 32.380 | 31.250 | 32.210 | 30.900 | 30.680 | 31.890 | 31.860 | 32.370 |
| Na2O | 0.009 | 0.027 | 0.009 | 0.007 | 0.025 | 0.019 | 0.019 | 0.000 | 0.006 | 0.014 | 0.007 | 0.008 | 0.003 | 0.016 | 0.002 | 0.010 | 0.007 | 0.019 | 0.018 | 0.013 | 0.005 | 0.002 | 0.000 | 0.017 | 0.008 | 0.014 | 0.001 |
| Cr2O3 | 0.000 | 0.000 | 0.012 | 0.000 | 0.003 | 0.000 | 0.000 | 0.000 | 0.010 | 0.000 | 0.000 | 0.000 | 0.000 | 0.013 | 0.000 | 0.017 | 0.000 | 0.010 | 0.000 | 0.014 | 0.000 | 0.000 | 0.000 | 0.000 | 0.000 | 0.000 | 0.020 |
| NiO | 0.004 | 0.007 | 0.004 | 0.000 | 0.006 | 0.003 | 0.000 | 0.005 | 0.024 | 0.003 | 0.000 | 0.007 | 0.025 | 0.008 | 0.021 | 0.000 | 0.000 | 0.000 | 0.000 | 0.000 | 0.000 | 0.000 | 0.000 | 0.009 | 0.004 | 0.006 | 0.004 |
| Total | 97.775 | 97.699 | 97.722 | 97.194 | 97.965 | 97.953 | 97.873 | 97.925 | 97.776 | 97.744 | 97.815 | 96.540 | 97.924 | 96.691 | 97.363 | 97.534 | 97.902 | 97.713 | 97.978 | 97.430 | 97.483 | 97.604 | 97.813 | 97.660 | 97.464 | 98.046 | 97.689 |
| Sample NO. | 291- ves 2-3 garnet inner rim gr 1 pt1 | 226- ves 2-3 garnet inner rim gr 1 pt1 | 291- ves 2-3 garnet inner rim gr 1 pt3 | 226- ves 2-3 garnet inner rim gr 1 pt3 | 291- ves 2-3 garnet inner rim gr 1 pt5 | 226- ves 2-3 garnet inner rim gr 1 pt6 | 226- ves 5 garnet center gr 1 pt1 | 226- ves 5 garnet center gr 1 pt2 | 226- ves 5 garnet center gr 1 pt3 | 291- vein rim garnet gr 1 pt2 | 291- vein rim garnet gr 1 pt3 | 291- vein center garnet gr 1 pt1 | 291- vein center garnet gr 1 pt2 | 291- vein center garnet gr 1 pt3 | 291- vein center garnet gr 1 pt4 | 291- vein rim garnet gr 1 pt4 | 291- vein rim garnet gr 1 pt5 | 290-rim-ves1-garnet-grn1 | 290-rim-ves1-garnet-grn2 | 290-rim-ves1-garnet-grn3 | 290-rim-ves1-garnet-grn4 | 290-rim-ves1-garnet-grn5 | 290-rim-ves1-garnet-grn6 | 290-rim-ves1-garnet-grn7 | 290-rim-ves1-garnet-grn8 | 290-rim-ves1-garnet-grn10 | 290-rim-ves1-garnet-grn11 |

**Table 12.Quantitive analysis results for oxides (EMP)**

| | 1 | 2 | 3 | 4 | 5 | 6 | 7 | 8 | 9 | 10 | 11 | 12 | 13 | 14 | 15 | 16 | 17 | 18 | 19 | 20 | 21 | 22 | 23 | 24 | 25 | 26 |
|---|---|---|---|---|---|---|---|---|---|---|---|---|---|---|---|---|---|---|---|---|---|---|---|---|---|---|
| **SiO2** | 0.042 | 0.400 | 0.068 | 1.061 | 0.667 | 1.528 | 4.044 | 2.116 | 0.315 | 0.128 | 1.226 | 0.185 | 0.103 | 0.261 | 0.150 | 0.178 | 0.258 | 4.585 | 0.221 | 1.448 | 0.276 | 0.235 | 0.886 | 0.084 | 0.189 | 3.909 |
| **TiO2** | 38.574 | 1.115 | 2.200 | 0.714 | 0.549 | 0.346 | 1.609 | 0.924 | 12.919 | 4.340 | 29.080 | 0.178 | 3.225 | 2.818 | 5.373 | 42.448 | 9.641 | 4.110 | 3.838 | 4.671 | 10.259 | 9.428 | 3.665 | 44.018 | 43.397 | 42.482 |
| **Al2O3** | 0.112 | 0.865 | 2.236 | 1.317 | 0.408 | 0.939 | 2.072 | 0.621 | 1.110 | 1.335 | 0.796 | 0.021 | 1.504 | 1.632 | 1.295 | 0.114 | 0.953 | 2.034 | 1.206 | 1.513 | 0.956 | 1.007 | 1.570 | 0.085 | 0.150 | 0.080 |
| **FeO** | 50.249 | 85.274 | 79.901 | 81.495 | 86.216 | 84.684 | 77.780 | 84.843 | 77.419 | 85.532 | 59.496 | 58.576 | 86.357 | 84.454 | 84.011 | 50.679 | 78.146 | 77.924 | 85.025 | 79.374 | 78.954 | 80.315 | 83.362 | 50.496 | 49.702 | 49.193 |
| **MnO** | 5.304 | 0.140 | 1.103 | 0.303 | 0.096 | 0.068 | 0.064 | 0.130 | 0.788 | 0.325 | 1.746 | 0.020 | 0.322 | 0.269 | 0.432 | 2.017 | 0.737 | 0.308 | 0.272 | 0.332 | 0.790 | 0.706 | 0.286 | 1.407 | 1.206 | 1.462 |
| **MgO** | 0.051 | 0.015 | 0.013 | 0.069 | 0.060 | 0.034 | 0.515 | 0.199 | 0.042 | 0.037 | 0.631 | 0.025 | 0.055 | 0.073 | 0.030 | 0.059 | 0.018 | 0.109 | 0.025 | 0.247 | 0.086 | 0.064 | 0.383 | 0.464 | 0.960 | 0.589 |
| **Cr2O3** | 0.119 | 0.688 | 7.188 | 3.085 | 0.614 | 0.544 | 0.644 | 1.331 | 0.020 | 0.024 | 0.011 | 0.009 | 0.000 | 0.004 | 0.006 | 0.000 | 0.014 | 0.213 | 0.004 | 0.036 | 0.007 | 0.000 | 0.012 | 0.002 | 0.000 | 0.005 |
| **NiO** | 0.015 | 0.088 | 0.126 | 0.057 | 0.115 | 0.057 | 0.109 | 0.177 | 0.010 | 0.000 | 0.000 | 0.000 | 0.000 | 0.008 | 0.009 | 0.000 | 0.027 | 0.082 | 0.014 | 0.041 | 0.025 | 0.013 | 0.000 | 0.015 | 0.000 | 0.002 |
| **Total** | 94.466 | 88.585 | 92.835 | 88.101 | 88.725 | 88.200 | 86.837 | 90.341 | 92.623 | 91.721 | 92.986 | 59.014 | 91.566 | 89.519 | 91.306 | 95.495 | 89.794 | 89.365 | 90.605 | 87.662 | 91.353 | 91.768 | 90.164 | 96.571 | 95.604 | 97.722 |
| **Sample NO.** | 226 oxide groundmass gr1 | 226 oxide groundmass gr 2 | 226 oxide groundmass gr 3 | 226 oxide groundmass gr 4 | 226 oxide groundmass gr 5 | 226 oxide groundmass gr 6 | 226 oxide groundmass gr 7 | 226 oxide groundmass gr 8 | 230 oxide groundmass gr 1 | 230 oxide groundmass gr 2 | 230 oxide groundmass gr 3 | 230 oxide groundmass gr 4 | 230 oxide rim 1 grain3 | 230 oxide rim 1 grain4 | 230 oxide rim 1 grain5 | 230 oxide center1 grain1 | 230 oxide center1 grain2 | 230 oxide center1 grain3 | 230 oxide center1 grain4 | 230 oxide groundmass 2 grain5 | 230 oxide groundmass 2 grain1 | 230 oxide groundmass 2 grain3 | 230 oxide groundmass 2 grain4 | 291 oxide groundmass 1 grain1 | 291 oxide groundmass 1 grain2 | 291 oxide groundmass 1 grain3 |

| | 1 | 2 | 3 | 4 | 5 | 6 | 7 | 8 | 9 | 10 | 11 | 12 | 13 | 14 | 15 | 16 | 17 | 18 | 19 | 20 | 21 | 22 | 23 | 24 | 25 | 26 |
|---|---|---|---|---|---|---|---|---|---|---|---|---|---|---|---|---|---|---|---|---|---|---|---|---|---|---|
| **SiO2** | 0.737 | 0.107 | 0.105 | 0.139 | 0.102 | 29.388 | 29.750 | 29.839 | 0.130 | 0.179 | 0.107 | 0.088 | 2.914 | 0.409 | 0.780 | 0.327 | 0.120 | 0.096 | 1.694 | 0.115 | 0.102 | 27.029 | 4.921 | 0.154 | 0.543 | 1.369 |
| **TiO2** | 42.666 | 41.358 | 39.456 | 4.729 | 4.912 | 33.876 | 32.989 | 34.432 | 48.627 | 5.335 | 37.842 | 7.036 | 22.022 | 47.067 | 45.997 | 47.162 | 46.952 | 47.442 | 8.496 | 7.167 | 7.035 | 14.688 | 12.553 | 6.186 | 22.206 | 9.033 |
| **Al2O3** | 0.383 | 0.077 | 0.089 | 0.984 | 1.025 | 1.312 | 1.450 | 1.239 | 0.217 | 3.138 | 0.986 | 3.507 | 3.181 | 0.170 | 0.516 | 0.077 | 0.114 | 0.100 | 1.587 | 3.967 | 3.950 | 9.504 | 3.537 | 4.243 | 2.031 | 2.940 |
| **FeO** | 50.137 | 53.043 | 53.773 | 84.891 | 84.226 | 1.971 | 2.508 | 1.762 | 46.334 | 79.473 | 53.840 | 78.799 | 59.751 | 46.147 | 45.446 | 46.400 | 46.700 | 46.074 | 72.035 | 78.446 | 78.759 | 25.573 | 66.286 | 78.491 | 65.719 | 75.127 |
| **MnO** | 1.662 | 1.752 | 1.613 | 0.179 | 0.212 | 0.037 | 0.020 | 0.058 | 1.321 | 0.102 | 1.078 | 0.134 | 0.504 | 2.551 | 2.494 | 2.516 | 2.498 | 2.728 | 0.663 | 0.184 | 0.174 | 0.147 | 0.446 | 0.154 | 0.949 | 0.476 |
| **MgO** | 0.278 | 0.174 | 0.330 | 0.042 | 0.078 | 0.029 | 0.006 | 0.016 | 0.149 | 0.111 | 0.091 | 0.216 | 2.029 | 0.100 | 0.456 | 0.128 | 0.095 | 0.102 | 0.157 | 0.098 | 0.098 | 0.613 | 1.953 | 0.121 | 0.246 | 0.888 |
| **Cr2O3** | 0.000 | 0.012 | 0.010 | 0.000 | 0.014 | 0.018 | 0.028 | 0.006 | 0.007 | 0.093 | 0.027 | 0.082 | 0.055 | 0.084 | 0.123 | 0.099 | 0.123 | 0.142 | 2.547 | 0.030 | 0.050 | 0.017 | 0.054 | 0.078 | 0.451 | 0.460 |
| **NiO** | 0.030 | 0.001 | 0.003 | 0.009 | 0.015 | 0.018 | 0.000 | 0.000 | 0.041 | 0.072 | 0.043 | 0.067 | 0.051 | 0.022 | 0.000 | 0.021 | 0.033 | 0.005 | 0.072 | 0.122 | 0.111 | 0.065 | 0.107 | 0.128 | 0.056 | 0.101 |
| **Total** | 95.893 | 96.524 | 95.379 | 90.973 | 90.584 | 66.649 | 66.751 | 67.352 | 96.826 | 88.503 | 94.014 | 89.929 | 90.507 | 96.550 | 95.812 | 96.730 | 96.635 | 96.689 | 87.251 | 90.129 | 90.279 | 77.636 | 89.857 | 89.555 | 92.201 | 90.394 |
| **Sample NO.** | 291 oxide groundmass 1 grain4 | 291 oxide groundmass 2 grain1 | 291 oxide groundmass 2 grain2 | 291 oxide groundmass 2 grain3 | 291 oxide groundmass 2 grain4 | 226 sphene ves 5 grain1 | 226 sphene ves 5 grain2 | 226 sphene ves 5 grain3 | HE-oxide-center-loc1-grain1 | HE-oxide-center-loc1-grain2 | HE-oxide-center-loc1-grain3 | HE-oxide-center-loc1-grain4 | HE-oxide-center-loc1-grain5 | HE-oxide-rim-loc1-grain1 | HE-oxide-rim-loc1-grain2 | HE-oxide-rim-loc1-grain3 | HE-oxide-rim-loc1-grain4 | HE-oxide-rim-loc1-grain5 | HE-oxide-groundmass-loc1-grain6 | HE-oxide-inner-loc2-grain1 | HE-oxide-inner-loc2-grain2 | HE-oxide-inner-loc2-grain3 | HE-oxide-inner-loc2-grain4 | HE-oxide-inner-loc2-grain5 | HE-oxide-rim-loc2-grain1 | HE-oxide-rim-loc2-grain2 |

| | 1 | 2 | 3 | 4 | 5 | 6 | 7 | 8 | 9 | 10 | 11 | 12 | 13 | 14 | 15 | 16 | 17 | 18 | 19 | 20 | 21 | 22 | 23 | 24 | 25 | 26 |
|---|---|---|---|---|---|---|---|---|---|---|---|---|---|---|---|---|---|---|---|---|---|---|---|---|---|---|
| **SiO2** | 0.784 | 0.283 | 0.110 | 10.028 | 2.114 | 0.130 | 0.317 | 0.893 | 6.057 | 21.281 | 2.548 | 0.728 | 0.079 | 1.039 | 0.878 | 0.087 | 0.305 | 0.160 | 14.586 | 12.306 | 0.168 | 0.164 | 0.242 | 0.162 | 0.123 | 0.153 |
| **TiO2** | 11.702 | 47.300 | 8.684 | 11.726 | 46.416 | 9.106 | 8.572 | 3.431 | 10.316 | 0.797 | 46.087 | 2.943 | 47.477 | 44.099 | 22.779 | 48.579 | 28.685 | 4.884 | 29.723 | 1.179 | 5.254 | 2.064 | 3.933 | 45.033 | 2.066 | 2.047 |
| **Al2O3** | 2.543 | 0.086 | 3.182 | 7.736 | 0.126 | 3.010 | 2.644 | 2.565 | 2.482 | 16.070 | 0.918 | 2.920 | 0.087 | 0.418 | 1.587 | 0.035 | 1.037 | 2.056 | 10.337 | 8.717 | 1.193 | 1.194 | 0.955 | 0.056 | 1.305 | 1.148 |
| **FeO** | 73.632 | 45.887 | 77.071 | 52.085 | 46.381 | 77.123 | 77.546 | 81.616 | 67.962 | 43.645 | 45.331 | 82.434 | 48.260 | 49.035 | 66.755 | 47.765 | 62.500 | 82.804 | 32.810 | 64.588 | 83.539 | 85.595 | 85.515 | 47.743 | 86.839 | 86.891 |
| **MnO** | 0.609 | 1.898 | 0.445 | 0.536 | 1.850 | 0.528 | 0.402 | 0.089 | 0.140 | 0.022 | 1.014 | 0.047 | 0.967 | 0.939 | 0.375 | 0.802 | 1.336 | 0.286 | 1.294 | 0.119 | 0.368 | 0.198 | 0.357 | 2.027 | 0.203 | 0.199 |
| **MgO** | 0.540 | 0.116 | 0.053 | 2.960 | 0.687 | 0.062 | 0.173 | 0.092 | 0.192 | 1.849 | 0.124 | 0.358 | 0.113 | 0.286 | 0.291 | 0.128 | 0.123 | 0.127 | 0.340 | 4.996 | 0.098 | 0.070 | 0.119 | 0.343 | 0.071 | 0.076 |
| **Cr2O3** | 0.414 | 0.072 | 0.750 | 0.574 | 0.127 | 1.014 | 0.656 | 0.076 | 0.064 | 0.031 | 0.000 | 0.161 | 0.014 | 0.031 | 0.293 | 0.038 | 0.866 | 0.565 | 0.047 | 0.804 | 0.009 | 0.013 | 0.035 | 0.001 | 0.000 | 0.015 |
| **NiO** | 0.059 | 0.004 | 0.082 | 0.014 | 0.000 | 0.091 | 0.111 | 0.106 | 0.063 | 0.044 | 0.023 | 0.120 | 0.011 | 0.031 | 0.026 | 0.000 | 0.000 | 0.099 | 0.000 | 0.047 | 0.023 | 0.000 | 0.025 | 0.029 | 0.000 | 0.025 |
| **Total** | 90.283 | 95.646 | 90.377 | 85.659 | 97.701 | 91.064 | 90.421 | 88.868 | 87.276 | 83.739 | 96.045 | 89.711 | 97.008 | 95.878 | 92.984 | 97.434 | 94.852 | 90.981 | 89.137 | 92.756 | 90.652 | 89.298 | 91.181 | 95.394 | 90.607 | 90.554 |
| **Sample NO.** | HE-oxide-rim-loc2-grain3 | HE-oxide-rim-loc2-grain4 | HE-oxide-rim-loc2-grain5 | HE-oxide-groundmass-loc2-grain1 | HE-oxide-groundmass-loc2-grain2 | HE-oxide-groundmass-loc2-grain3 | HE-oxide-groundmass-loc2-grain4 | HE-oxide-inner-loc3-grain1 | HE-oxide-inner-loc3-grain2 | HE-oxide-inner-loc3-grain3 | HE-oxide-inner-loc3-grain4 | HE-oxide-rim-loc3-grain1 | HE-oxide-rim-loc3-grain2 | HE-oxide-rim-loc3-grain3 | HE-oxide-rim-loc3-grain4 | HE-oxide-rim-loc3-grain5 | HE-oxide-groundmass-loc3-grain1 | HE-oxide-groundmass-loc3-grain2 | HE-oxide-groundmass-loc3-grain3 | HE-oxide-groundmass-loc3-grain4 | 290-oxide-groundmass-ves1-grn1 | 290-oxide-groundmass-ves1-grn2 | 290-oxide-groundmass-ves1-grn3 | 290-oxide-groundmass-ves1-grn4 | 290-oxide-groundmass-ves1-grn5 | 290-oxide-groundmass-ves1-grn6 |

**Table 13.Quantitive analysis results for pyroxene (EMP)**

| | 1 | 2 | 3 | 4 | 5 | 6 | 7 | 8 | 9 | 10 | 11 | 12 | 13 | 14 | 15 | 16 | 17 | 18 | 19 | 20 | 21 | 22 | 23 | 24 | 25 | 26 | 27 | 28 | 29 |
|---|---|---|---|---|---|---|---|---|---|---|---|---|---|---|---|---|---|---|---|---|---|---|---|---|---|---|---|---|---|
| SiO2 | 52.240 | 52.290 | 52.550 | 47.140 | 46.370 | 46.750 | 52.390 | 52.520 | 52.720 | 46.480 | 47.310 | 47.710 | 53.510 | 52.470 | 52.610 | 45.770 | 47.130 | 49.200 | 52.910 | 53.350 | 53.100 | 45.770 | 48.580 | 51.970 | 52.790 | 52.140 | 47.160 | 47.780 | 46.650 |
| TiO2 | 0.313 | 0.309 | 0.243 | 0.311 | 0.297 | 0.273 | 0.236 | 0.274 | 0.168 | 0.323 | 0.272 | 0.269 | 0.096 | 0.223 | 0.258 | 0.323 | 0.296 | 0.151 | 0.250 | 0.142 | 0.149 | 0.440 | 0.293 | 0.254 | 0.133 | 0.268 | 0.383 | 0.329 | 0.358 |
| Al2O3 | 1.454 | 1.419 | 1.378 | 2.120 | 1.586 | 1.488 | 1.305 | 1.327 | 1.041 | 2.140 | 1.367 | 1.394 | 0.689 | 1.308 | 1.414 | 2.330 | 2.070 | 1.375 | 1.400 | 0.822 | 0.850 | 3.020 | 2.250 | 1.449 | 0.702 | 1.352 | 2.720 | 2.280 | 2.770 |
| FeO | 8.700 | 8.540 | 8.130 | 22.870 | 25.140 | 25.140 | 8.020 | 7.800 | 7.330 | 24.090 | 23.510 | 23.340 | 7.450 | 8.710 | 7.990 | 25.750 | 24.060 | 20.020 | 8.280 | 7.640 | 7.840 | 23.320 | 18.890 | 8.670 | 7.670 | 9.340 | 20.380 | 19.530 | 22.160 |
| MnO | 0.493 | 0.471 | 0.478 | 0.701 | 0.769 | 0.735 | 0.477 | 0.383 | 0.403 | 0.695 | 0.760 | 0.757 | 0.449 | 0.493 | 0.466 | 0.633 | 0.593 | 0.454 | 0.486 | 0.453 | 0.496 | 0.388 | 0.383 | 0.374 | 0.461 | 0.345 | 0.362 | 0.361 | 0.385 |
| MgO | 14.870 | 14.930 | 14.710 | 4.430 | 3.180 | 3.270 | 14.920 | 14.310 | 14.970 | 3.890 | 4.240 | 4.290 | 14.300 | 14.210 | 14.610 | 2.940 | 4.080 | 6.150 | 14.950 | 15.120 | 15.150 | 4.410 | 6.930 | 13.550 | 14.560 | 12.750 | 6.270 | 6.670 | 5.190 |
| CaO | 21.090 | 21.200 | 22.150 | 22.070 | 22.060 | 21.920 | 21.480 | 22.920 | 22.490 | 22.180 | 22.280 | 22.150 | 23.300 | 21.910 | 22.230 | 22.200 | 22.350 | 22.440 | 21.330 | 22.330 | 21.820 | 22.180 | 22.540 | 23.040 | 22.900 | 23.400 | 22.470 | 22.330 | 22.320 |
| Na2O | 0.288 | 0.268 | 0.274 | 0.275 | 0.250 | 0.248 | 0.271 | 0.234 | 0.268 | 0.227 | 0.225 | 0.235 | 0.224 | 0.284 | 0.257 | 0.175 | 0.218 | 0.287 | 0.256 | 0.248 | 0.204 | 0.275 | 0.277 | 0.268 | 0.217 | 0.255 | 0.270 | 0.260 | 0.273 |
| Cr2O3 | 0.000 | 0.000 | 0.000 | 0.010 | 0.014 | 0.000 | 0.000 | 0.018 | 0.000 | 0.000 | 0.000 | 0.006 | 0.000 | 0.002 | 0.009 | 0.000 | 0.007 | 0.000 | 0.000 | 0.000 | 0.000 | 0.000 | 0.000 | 0.000 | 0.003 | 0.009 | 0.005 | 0.000 | 0.010 |
| NiO | 0.028 | 0.046 | 0.035 | 0.034 | 0.067 | 0.059 | 0.025 | 0.020 | 0.010 | 0.033 | 0.026 | 0.028 | 0.000 | 0.012 | 0.018 | 0.060 | 0.023 | 0.049 | 0.022 | 0.036 | 0.018 | 0.046 | 0.042 | 0.020 | 0.006 | 0.010 | 0.071 | 0.057 | 0.054 |
| Total | 99.475 | 99.472 | 99.947 | 99.961 | 99.733 | 99.883 | 99.123 | 99.806 | 99.401 | 100.058 | 99.990 | 100.180 | 100.019 | 99.624 | 99.863 | 100.180 | 100.827 | 100.126 | 99.883 | 100.141 | 99.627 | 99.848 | 100.185 | 99.595 | 99.443 | 99.869 | 100.089 | 99.597 | 100.170 |
| Sample NO. | 226_ves 2-3 gr a center pt1 | 226_ves 2-3 gr a center pt2 | 226_ves 2-3 gr a center pt3 | 226_ves 2-3 gr a rim pt1 | 226_ves 2-3 gr a rim pt2 | 226_ves 2-3 gr a rim pt3 | 226_ves 2-3 gr b center pt1 | 226_ves 2-3 gr b center pt2 | 226_ves 2-3 gr b center pt3 | 226_ves 2-3 gr b rim pt1 | 226_ves 2-3 gr b rim pt2 | 226_ves 2-3 gr b rim pt3 | 226_ves 2-3 gr c center pt1 | 226_ves 2-3 gr c center pt2 | 226_ves 2-3 gr c center pt3 | 226_ves 2-3 gr c rim pt1 | 226_ves 2-3 gr c rim pt2 | 226_ves 2-3 gr c rim pt3 | 226_ves 2-3 gr d center pt1 | 226_ves 2-3 gr d center pt2 | 226_ves 2-3 gr d center pt3 | 226_ves 2-3 gr d rim pt1 | 226_ves 2-3 gr d rim pt2 | 226_ves 2-3 gr d rim pt3 | 226_ves 2-3 gr e center pt1 | 226_ves 2-3 gr e center pt2 | 226_ves 2-3 gr e center pt3 | 226_ves 2-3 gr e rim pt1 | 226_ves 2-3 gr e rim pt2 | 226_ves 2-3 gr e rim pt3 |

| | 1 | 2 | 3 | 4 | 5 | 6 | 7 | 8 | 9 | 10 | 11 | 12 | 13 | 14 | 15 | 16 | 17 | 18 | 19 | 20 | 21 | 22 | 23 | 24 | 25 | 26 | 27 | 28 | 29 |
|---|---|---|---|---|---|---|---|---|---|---|---|---|---|---|---|---|---|---|---|---|---|---|---|---|---|---|---|---|---|
| SiO2 | 53.070 | 52.680 | 52.660 | 48.150 | 48.440 | 52.520 | 52.230 | 53.340 | 49.550 | 49.810 | 52.830 | 52.440 | 52.680 | 51.160 | 52.180 | 50.620 | 52.590 | 52.490 | 52.150 | 49.010 | 47.400 | 48.140 | 52.260 | 53.420 | 52.800 | 51.180 | 51.010 | 48.370 | 52.550 |
| TiO2 | 0.203 | 0.257 | 0.145 | 0.266 | 0.252 | 0.192 | 0.209 | 0.131 | 0.380 | 0.413 | 0.186 | 0.235 | 0.161 | 0.254 | 0.184 | 0.352 | 0.254 | 0.208 | 0.201 | 0.189 | 0.450 | 0.281 | 0.205 | 0.116 | 0.202 | 0.271 | 0.257 | 0.602 | 0.243 |
| Al2O3 | 0.976 | 1.263 | 0.664 | 2.060 | 2.180 | 1.176 | 1.347 | 0.351 | 2.460 | 2.390 | 1.125 | 1.388 | 1.180 | 1.226 | 1.181 | 1.639 | 1.436 | 1.175 | 1.301 | 1.267 | 2.080 | 1.468 | 1.267 | 0.731 | 1.195 | 1.458 | 1.448 | 3.290 | 1.120 |
| FeO | 8.310 | 8.230 | 8.780 | 18.550 | 17.880 | 8.870 | 9.260 | 9.100 | 12.770 | 12.470 | 7.760 | 8.180 | 7.770 | 11.930 | 8.870 | 12.350 | 8.040 | 8.200 | 9.460 | 19.950 | 21.120 | 22.020 | 8.710 | 7.650 | 7.870 | 11.710 | 11.770 | 14.370 | 8.020 |
| MnO | 0.553 | 0.451 | 0.397 | 0.378 | 0.638 | 0.413 | 0.347 | 0.383 | 0.341 | 0.331 | 0.407 | 0.419 | 0.415 | 0.359 | 0.408 | 0.336 | 0.440 | 0.409 | 0.345 | 0.487 | 0.483 | 0.508 | 0.428 | 0.431 | 0.394 | 0.281 | 0.336 | 0.342 | 0.420 |
| MgO | 15.250 | 14.600 | 13.870 | 7.610 | 7.340 | 13.940 | 13.630 | 13.960 | 11.140 | 11.280 | 15.000 | 14.650 | 14.950 | 11.630 | 13.780 | 11.600 | 14.800 | 14.000 | 12.530 | 6.300 | 5.550 | 5.040 | 14.000 | 15.280 | 14.910 | 11.660 | 11.500 | 9.990 | 15.240 |
| CaO | 21.400 | 22.110 | 22.740 | 22.500 | 21.850 | 22.070 | 22.260 | 22.730 | 22.120 | 22.280 | 22.050 | 21.960 | 21.910 | 22.910 | 22.540 | 22.650 | 21.550 | 23.030 | 23.620 | 22.930 | 22.340 | 22.540 | 22.250 | 21.610 | 22.130 | 22.800 | 22.520 | 22.110 | 21.650 |
| Na2O | 0.239 | 0.256 | 0.224 | 0.287 | 0.217 | 0.260 | 0.264 | 0.220 | 0.310 | 0.318 | 0.241 | 0.291 | 0.268 | 0.253 | 0.276 | 0.290 | 0.277 | 0.255 | 0.272 | 0.199 | 0.239 | 0.194 | 0.278 | 0.215 | 0.257 | 0.257 | 0.281 | 0.355 | 0.235 |
| Cr2O3 | 0.000 | 0.000 | 0.000 | 0.006 | 0.013 | 0.000 | 0.000 | 0.008 | 0.000 | 0.004 | 0.000 | 0.003 | 0.000 | 0.000 | 0.006 | 0.000 | 0.002 | 0.005 | 0.000 | 0.000 | 0.000 | 0.005 | 0.000 | 0.000 | 0.027 | 0.000 | 0.017 | 0.000 | 0.019 |
| NiO | 0.013 | 0.026 | 0.005 | 0.056 | 0.011 | 0.012 | 0.015 | 0.026 | 0.059 | 0.032 | 0.017 | 0.018 | 0.017 | 0.015 | 0.018 | 0.030 | 0.024 | 0.014 | 0.000 | 0.045 | 0.034 | 0.015 | 0.028 | 0.009 | 0.000 | 0.016 | 0.000 | 0.037 | 0.031 |
| Total | 100.014 | 99.873 | 99.486 | 99.863 | 98.821 | 99.453 | 99.562 | 100.249 | 99.130 | 99.329 | 99.616 | 99.584 | 99.350 | 99.736 | 99.443 | 99.867 | 99.413 | 99.786 | 99.880 | 100.377 | 99.696 | 100.212 | 99.426 | 99.462 | 99.785 | 99.632 | 99.141 | 99.466 | 99.528 |
| Sample NO. | 226_ves 2-3 gr F center pt1 | 226_ves 2-3 gr F center pt2 | 226_ves 2-3 gr F center pt3 | 226_ves 2-3 gr F rim pt1 | 226_ves 2-3 gr F rim pt2 | 226_ves 5 gr a center pt1 | 226_ves 5 gr a center pt2 | 226_ves 5 gr a center pt3 | 226_ves 5 gr a rim pt1 | 226_ves 5 gr a rim pt2 | 226_ves 5 gr b center pt1 | 226_ves 5 gr b center pt2 | 226_ves 5 gr b center pt3 | 226_ves 5 gr b rim pt1 | 226_ves 5 gr b rim pt2 | 226_ves 5 gr b rim pt3 | 226_ves 5 gr c center pt1 | 226_ves 5 gr c center pt2 | 226_ves 5 gr c center pt3 | 226_ves 5 gr c rim pt1 | 226_ves 5 gr c rim pt2 | 226_ves 5 gr c rim pt3 | 226_ves 5 gr d center pt1 | 226_ves 5 gr d center pt2 | 226_ves 5 gr d center pt3 | 226_ves 5 gr d rim pt1 | 226_ves 5 gr d rim pt2 | 226_ves 5 gr d rim pt3 | 226_grou ndmass gr a pt1 |

| | 1 | 2 | 3 | 4 | 5 | 6 | 7 | 8 | 9 | 10 | 11 | 12 | 13 | 14 | 15 | 16 | 17 | 18 | 19 | 20 | 21 | 22 | 23 | 24 | 25 | 26 | 27 | 28 | 29 | 30 |
|---|---|---|---|---|---|---|---|---|---|---|---|---|---|---|---|---|---|---|---|---|---|---|---|---|---|---|---|---|---|---|
| SiO2 | 52.700 | 52.690 | 52.730 | 52.410 | 52.520 | 50.300 | 50.750 | 50.170 | 51.870 | 51.730 | 52.730 | 51.600 | 52.180 | 52.690 | 51.920 | 50.730 | 50.400 | 51.050 | 50.680 | 49.270 | 52.040 | 51.540 | 52.890 | 52.300 | 51.130 | 52.450 | 51.900 | 52.590 | 51.680 | 52.180 |
| TiO2 | 0.241 | 0.249 | 0.276 | 0.376 | 0.359 | 0.611 | 0.467 | 0.418 | 0.275 | 0.362 | 0.283 | 0.338 | 0.401 | 0.208 | 0.189 | 0.291 | 0.326 | 0.701 | 0.771 | 0.973 | 0.460 | 1.390 | 0.345 | 0.448 | 0.793 | 0.415 | 0.684 | 0.434 | 0.496 | 0.378 |
| Al2O3 | 1.102 | 1.212 | 1.188 | 1.411 | 1.421 | 2.060 | 1.576 | 1.474 | 1.144 | 1.472 | 0.948 | 1.488 | 1.169 | 0.494 | 1.004 | 1.039 | 2.560 | 1.980 | 2.290 | 2.610 | 1.374 | 1.324 | 1.029 | 1.299 | 2.120 | 1.166 | 1.578 | 1.201 | 1.408 | 1.409 |
| FeO | 8.540 | 8.420 | 8.420 | 9.050 | 8.940 | 13.300 | 13.230 | 13.010 | 11.050 | 10.460 | 9.790 | 9.960 | 9.570 | 9.110 | 8.860 | 13.540 | 11.690 | 9.680 | 9.730 | 12.950 | 8.780 | 7.990 | 8.210 | 8.730 | 9.280 | 8.730 | 9.200 | 8.290 | 8.880 | 9.780 |
| MnO | 0.372 | 0.395 | 0.349 | 0.382 | 0.373 | 0.486 | 0.507 | 0.514 | 0.484 | 0.531 | 0.656 | 0.582 | 0.592 | 0.540 | 1.116 | 1.203 | 0.184 | 0.215 | 0.193 | 0.211 | 0.198 | 0.215 | 0.237 | 0.215 | 0.201 | 0.195 | 0.243 | 0.181 | 0.220 | 0.287 |
| MgO | 15.070 | 15.070 | 15.040 | 14.860 | 14.670 | 10.740 | 10.780 | 10.860 | 12.940 | 13.070 | 13.910 | 13.420 | 13.810 | 13.840 | 12.720 | 9.230 | 12.280 | 13.750 | 13.740 | 11.050 | 14.440 | 14.110 | 14.870 | 14.800 | 13.360 | 15.110 | 14.760 | 15.040 | 14.600 | 14.550 |
| CaO | 21.350 | 21.590 | 21.440 | 21.330 | 21.680 | 22.070 | 22.220 | 22.710 | 21.990 | 21.630 | 21.230 | 21.700 | 21.350 | 22.060 | 23.270 | 23.410 | 21.730 | 21.400 | 21.460 | 21.620 | 21.570 | 21.790 | 21.350 | 21.010 | 21.960 | 21.040 | 20.850 | 21.280 | 21.160 | 20.330 |
| Na2O | 0.232 | 0.294 | 0.239 | 0.269 | 0.262 | 0.317 | 0.316 | 0.311 | 0.263 | 0.260 | 0.277 | 0.290 | 0.304 | 0.161 | 0.205 | 0.148 | 0.255 | 0.306 | 0.285 | 0.344 | 0.281 | 0.289 | 0.264 | 0.286 | 0.319 | 0.251 | 0.291 | 0.274 | 0.276 | 0.230 |
| Cr2O3 | 0.032 | 0.026 | 0.028 | 0.050 | 0.016 | 0.006 | 0.006 | 0.015 | 0.009 | 0.000 | 0.000 | 0.015 | 0.000 | 0.006 | 0.006 | 0.001 | 0.017 | 0.000 | 0.006 | 0.000 | 0.115 | 0.091 | 0.118 | 0.077 | 0.070 | 0.024 | 0.063 | 0.056 | 0.043 | 0.008 |
| NiO | 0.004 | 0.014 | 0.019 | 0.019 | 0.022 | 0.000 | 0.000 | 0.027 | 0.000 | 0.001 | 0.000 | 0.000 | 0.000 | 0.000 | 0.002 | 0.000 | 0.013 | 0.000 | 0.001 | 0.019 | 0.026 | 0.005 | 0.000 | 0.000 | 0.029 | 0.000 | 0.003 | 0.000 | 0.000 | 0.000 |
| Total | 99.643 | 99.959 | 99.729 | 100.156 | 100.263 | 99.889 | 99.853 | 99.508 | 100.025 | 99.516 | 99.824 | 99.392 | 99.375 | 99.109 | 99.292 | 99.592 | 99.455 | 99.082 | 99.157 | 99.046 | 99.283 | 98.743 | 99.313 | 99.165 | 99.261 | 99.381 | 99.571 | 99.346 | 98.763 | 99.151 |
| Sample NO. | 226_grou ndmass gr a pt2 | 226_grou ndmass gr b pt1 | 226_grou ndmass gr b pt2 | 226_grou ndmass gr c pt1 | 226_grou ndmass gr c pt2 | 230 ves1 gr a pt1 | 230 ves1 gr b pt1 | 230 ves1 gr c pt1 | 230 ves1 gr d pt1 | 230 ves1 gr e rim pt1 | 230 ves 2 gr a center pt1 | 230 ves 2 gr b center pt1 | 230 ves 2 gr c rim pt1 | 230 ves 2 gr d rim pt1 | 291 vein margingr e pt1 | 291 vein margin gr f pt2 | HE-pyx-loc1-grn1-pnt1 | HE-pyx-loc1-inner-grn2 | HE-pyx-loc1-inner-grn4 | HE-pyx-loc1-phenocrysts-inner-grn5 | HE-pyx-loc1-phenocrysts-rim-grn1 | HE-pyx-loc1-phenocrysts-rim-grn2 | HE-pyx-loc1-phenocrysts-rim-grn3 | HE-pyx-loc1-phenocrysts-rim-grn4 | HE-pyx-loc1-phenocrysts-rim-grn5 | HE-pyx-loc1-groundmass-grn1 | HE-pyx-loc1-groundmass-grn2 | HE-pyx-loc1-groundmass-grn3 | HE-pyx-loc1-groundmass-grn4 | HE-pyx-loc2-inner-grn1 |

| | 1 | 2 | 3 | 4 | 5 | 6 | 7 | 8 | 9 | 10 | 11 | 12 | 13 | 14 | 15 | 16 | 17 | 18 | 19 | 20 | 21 | 22 | 23 | 24 | 25 | 26 | 27 | 28 | 29 | 30 |
|---|---|---|---|---|---|---|---|---|---|---|---|---|---|---|---|---|---|---|---|---|---|---|---|---|---|---|---|---|---|---|
| SiO2 | 51.570 | 52.350 | 52.240 | 51.850 | 51.920 | 51.830 | 51.830 | 51.870 | 52.300 | 51.600 | 50.730 | 51.160 | 50.130 | 50.860 | 51.610 | 51.880 | 52.190 | 51.770 | 51.750 | 51.820 | 49.930 | 48.250 | 47.380 | 44.630 | 42.970 | 51.110 | 52.490 | 52.370 | 53.590 | 52.040 |
| TiO2 | 0.455 | 0.300 | 0.344 | 0.579 | 0.538 | 0.517 | 0.501 | 0.505 | 0.669 | 0.538 | 0.552 | 0.485 | 0.363 | 0.509 | 0.656 | 0.367 | 0.322 | 0.524 | 0.548 | 0.506 | 0.064 | 0.272 | 0.325 | 6.710 | 9.300 | 0.091 | 0.317 | 0.331 | 0.364 | 0.487 |
| Al2O3 | 1.686 | 1.081 | 1.283 | 1.473 | 1.517 | 1.502 | 1.436 | 1.506 | 1.073 | 1.361 | 3.290 | 2.240 | 14.360 | 2.130 | 1.719 | 1.174 | 1.121 | 1.472 | 1.471 | 1.358 | 0.430 | 1.733 | 1.950 | 1.970 | 2.090 | 0.367 | 0.856 | 0.920 | 0.939 | 1.108 |
| FeO | 10.560 | 9.230 | 9.370 | 10.510 | 10.660 | 10.420 | 10.320 | 10.600 | 10.220 | 10.670 | 10.440 | 10.840 | 6.560 | 10.980 | 10.360 | 10.030 | 9.800 | 10.870 | 10.590 | 10.610 | 23.650 | 20.960 | 21.740 | 18.270 | 16.680 | 15.730 | 11.120 | 11.310 | 11.000 | 11.890 |
| MnO | 0.281 | 0.250 | 0.243 | 0.323 | 0.313 | 0.294 | 0.306 | 0.303 | 0.309 | 0.332 | 0.185 | 0.194 | 0.110 | 0.219 | 0.205 | 0.182 | 0.200 | 0.211 | 0.220 | 0.250 | 1.520 | 1.281 | 1.166 | 0.975 | 0.887 | 2.060 | 0.784 | 0.754 | 0.707 | 0.837 |
| MgO | 14.250 | 14.690 | 14.390 | 14.410 | 14.160 | 14.140 | 14.070 | 14.290 | 14.420 | 14.480 | 12.830 | 13.410 | 7.810 | 12.850 | 14.200 | 14.300 | 14.400 | 14.390 | 14.480 | 14.510 | 2.400 | 4.880 | 4.180 | 3.700 | 3.290 | 8.080 | 13.750 | 13.720 | 13.280 | 14.170 |
| CaO | 19.710 | 20.770 | 20.750 | 20.210 | 20.040 | 20.370 | 20.620 | 20.040 | 20.430 | 19.910 | 20.690 | 20.550 | 18.490 | 21.020 | 20.420 | 20.770 | 20.800 | 19.950 | 20.000 | 19.880 | 22.220 | 22.490 | 22.310 | 23.160 | 23.770 | 23.170 | 19.920 | 19.880 | 19.500 | 18.970 |
| Na2O | 0.252 | 0.213 | 0.237 | 0.261 | 0.277 | 0.272 | 0.256 | 0.298 | 0.256 | 0.273 | 0.433 | 0.277 | 1.336 | 0.248 | 0.239 | 0.239 | 0.266 | 0.248 | 0.242 | 0.230 | 0.166 | 0.257 | 0.263 | 0.211 | 0.182 | 0.132 | 0.311 | 0.329 | 0.286 | 0.328 |
| Cr2O3 | 0.033 | 0.000 | 0.008 | 0.015 | 0.000 | 0.011 | 0.012 | 0.026 | 0.026 | 0.026 | 0.000 | 0.006 | 0.007 | 0.003 | 0.035 | 0.060 | 0.094 | 0.061 | 0.069 | 0.072 | 0.000 | 0.000 | 0.006 | 0.018 | 0.000 | 0.017 | 0.020 | 0.000 | 0.008 | 0.000 |
| NiO | 0.009 | 0.014 | 0.012 | 0.003 | 0.027 | 0.025 | 0.039 | 0.025 | 0.007 | 0.029 | 0.016 | 0.019 | 0.000 | 0.013 | 0.026 | 0.006 | 0.044 | 0.020 | 0.030 | 0.022 | 0.015 | 0.000 | 0.003 | 0.000 | 0.000 | 0.000 | 0.003 | 0.004 | 0.000 | 0.002 |
| Total | 98.807 | 98.898 | 98.876 | 99.633 | 99.451 | 99.381 | 99.389 | 99.462 | 99.710 | 99.219 | 99.167 | 99.182 | 99.165 | 98.832 | 99.470 | 99.008 | 99.236 | 99.516 | 99.400 | 99.258 | 100.394 | 100.123 | 99.324 | 99.644 | 99.169 | 100.756 | 99.570 | 99.617 | 99.674 | 99.832 |
| Sample NO. | HE-pyx-loc2-inner-grn2 | HE-pyx-loc2-inner-grn3 | HE-pyx-loc2-inner-grn4 | HE-pyx-loc2-rim-grn1 | HE-pyx-loc2-rim-grn2 | HE-pyx-loc2-rim-grn3 | HE-pyx-loc2-rim-grn4 | HE-pyx-loc2-groundmass-grn1 | HE-pyx-loc2-groundmass-grn2 | HE-pyx-loc2-groundmass-grn3 | HE-pyx-loc3-inner-grn1 | HE-pyx-loc3-inner-grn2 | HE-pyx-loc3-inner-grn3 | HE-pyx-loc3-inner-grn4 | HE-pyx-loc3-rim-grn1 | HE-pyx-loc3-rim-grn2 | HE-pyx-loc3-rim-grn3 | HE-pyx-loc3-groundmass-grn1 | HE-pyx-loc3-groundmass-grn2 | HE-pyx-loc3-groundmass-grn3 | 290-pyx-ves1-inner-grn1 | 290-pyx-ves1-rim-grn1 | 290-pyx-ves1-rim-grn2 | 290-pyx-ves1-rim-grn3 | 290-pyx-ves1-rim-grn4 | 290-pyx-ves1-rim-grn5 | 290-pyx-ves1-groundmass-grn1 | 290-pyx-ves1-groundmass-grn2 | 290-pyx-ves1-groundmass-grn3 | 290-pyx-ves1-groundmass-grn4 |

**Table 14.Quantitive analysis results for titanite (EMP)**

| | 1 | 2 | 3 | 4 | 5 | 6 | 7 | 8 | 9 | 10 | 11 | 12 | 13 | 14 | 15 | 16 | 17 | 18 | 19 |
|---|---|---|---|---|---|---|---|---|---|---|---|---|---|---|---|---|---|---|---|
| **SiO2** | 29.645 | 29.836 | 29.662 | 29.907 | 29.767 | 29.879 | 29.868 | 29.755 | 30.065 | 44.584 | 46.641 | 29.751 | 32.000 | 31.140 | 30.480 | 30.810 | 31.230 | 30.840 | 30.440 |
| **TiO2** | 36.060 | 34.638 | 35.666 | 34.093 | 34.254 | 34.291 | 35.346 | 33.840 | 33.478 | 0.386 | 0.276 | 34.291 | 30.470 | 29.420 | 27.480 | 32.560 | 28.950 | 31.620 | 31.790 |
| **Al2O3** | 1.201 | 1.392 | 1.265 | 1.575 | 1.422 | 1.575 | 1.363 | 1.640 | 1.915 | 2.512 | 1.337 | 1.489 | 3.720 | 3.660 | 4.100 | 2.930 | 3.530 | 3.140 | 2.920 |
| **FeO** | 1.833 | 2.365 | 1.642 | 2.697 | 2.417 | 2.595 | 1.979 | 2.750 | 3.172 | 25.396 | 23.867 | 2.374 | 3.570 | 5.420 | 6.130 | 2.610 | 4.120 | 2.840 | 3.000 |
| **MnO** | 0.059 | 0.030 | 0.029 | 0.024 | 0.025 | 0.020 | 0.037 | 0.050 | 0.037 | 0.631 | 0.577 | 0.016 | 0.018 | 0.077 | 0.050 | 0.007 | 0.044 | 0.040 | 0.010 |
| **MgO** | 0.039 | 0.003 | 0.016 | 0.011 | 0.000 | 0.003 | 0.012 | 0.009 | 0.020 | 2.479 | 3.279 | 0.011 | 0.535 | 1.980 | 2.160 | 0.333 | 0.855 | 0.692 | 1.062 |
| **CaO** | 28.432 | 28.829 | 28.344 | 28.873 | 28.686 | 28.930 | 28.802 | 28.525 | 28.807 | 22.286 | 22.565 | 28.755 | 27.140 | 24.630 | 25.260 | 28.030 | 26.540 | 27.090 | 26.390 |
| **Cr2O3** | 0.016 | 0.000 | 0.030 | 0.000 | 0.004 | 0.010 | 0.000 | 0.004 | 0.000 | 0.011 | 0.000 | 0.005 | 0.012 | 0.017 | 0.059 | 0.118 | 0.000 | 0.000 | 0.028 |
| **NiO** | 0.007 | 0.024 | 0.029 | 0.002 | 0.017 | 0.000 | 0.011 | 0.014 | 0.007 | 0.035 | 0.061 | 0.007 | 0.000 | 0.000 | 0.004 | 0.004 | 0.000 | 0.027 | 0.000 |
| **Na2O** | 0 | 0 | 0 | 0 | 0 | 0 | 0 | 0 | 0 | 0 | 0 | 0 | 0.031 | 0.067 | 0.038 | 0.016 | 0.024 | 0.035 | 0.062 |
| **K2O** | 0 | 0 | 0 | 0 | 0 | 0 | 0 | 0 | 0 | 0 | 0 | 0 | 0.034 | 0.043 | 0.040 | 0.023 | 0.027 | 0.011 | 0.016 |
| **F** | 0 | 0 | 0 | 0 | 0 | 0 | 0 | 0 | 0 | 0 | 0 | 0 | 0.185 | 0.053 | 0.032 | 0.130 | 0.123 | 0.177 | 0.118 |
| **Cl** | 0 | 0 | 0 | 0 | 0 | 0 | 0 | 0 | 0 | 0 | 0 | 0 | 0.006 | 0.000 | 0.004 | 0.011 | 0.000 | 0.003 | 0.000 |
| **Total** | 97.292 | 97.117 | 96.683 | 97.182 | 96.592 | 97.303 | 97.418 | 96.587 | 97.501 | 98.320 | 98.603 | 96.699 | 97.721 | 96.507 | 95.835 | 97.582 | 95.443 | 96.516 | 95.837 |
| **Sample NO.** | 226 sphene ves 5 grain1 | 226 sphene ves 5 grain2 | 226 sphene ves 5 grain3 | 226 sphene ves 5 grain4 | 226 sphene ves 5 grain5 | 226 sphene ves 5 grain6 | 226 sphene ves 5 grain7 | 226 sphene ves 2-3 grain1 | 226 sphene ves 2-3 grain2 | 226 sphene ves 2-3 grain3 | 226 sphene ves 2-3 grain4 | 226 sphene ves 2-3 grain5 | HE-ves-loc1-sphene grn1 | HE-ves-loc1-sphene grn4 | HE-ves-loc1-sphene grn5 | HE-ves-loc1-sphene grn6 | HE-ves-loc1-sphene grn7 | HE-ves-loc1-sphene grn8 | HE-ves-loc1-sphene grn10 |

| | 1 | 2 | 3 | 4 | 5 | 6 | 7 | 8 | 9 | 10 | 11 | 12 | 13 | 14 | 15 | 16 | 17 | 18 |
|---|---|---|---|---|---|---|---|---|---|---|---|---|---|---|---|---|---|---|
| **SiO2** | 30.600 | 29.860 | 30.750 | 34.060 | 29.980 | 29.630 | 30.160 | 30.580 | 30.010 | 30.120 | 29.620 | 30.550 | 30.720 | 30.120 | 30.030 | 29.430 | 30.460 | 30.590 |
| **TiO2** | 30.830 | 29.380 | 31.710 | 27.200 | 33.960 | 35.550 | 30.580 | 35.350 | 36.180 | 34.330 | 34.590 | 34.070 | 34.030 | 35.440 | 35.050 | 35.730 | 33.520 | 34.250 |
| **Al2O3** | 3.250 | 3.940 | 3.110 | 1.191 | 0.676 | 1.121 | 0.894 | 1.763 | 1.071 | 1.570 | 1.561 | 1.613 | 0.946 | 1.052 | 1.523 | 0.939 | 1.527 | 1.053 |
| **FeO** | 2.440 | 4.130 | 3.010 | 4.670 | 3.570 | 2.100 | 2.580 | 2.190 | 1.840 | 2.450 | 2.240 | 2.700 | 2.710 | 2.020 | 2.320 | 2.270 | 3.100 | 3.020 |
| **MnO** | 0.022 | 0.025 | 0.008 | 0.254 | 0.102 | 0.128 | 0.168 | 0.100 | 0.131 | 0.192 | 0.153 | 0.153 | 0.172 | 0.075 | 0.128 | 0.114 | 0.141 | 0.130 |
| **MgO** | 1.082 | 3.040 | 1.034 | 2.000 | 0.139 | 0.072 | 1.178 | 0.104 | 0.024 | 0.082 | 0.061 | 0.171 | 0.341 | 0.027 | 0.051 | 0.042 | 0.033 | 0.249 |
| **CaO** | 25.950 | 23.390 | 26.190 | 27.020 | 28.030 | 28.120 | 29.480 | 27.920 | 28.290 | 28.030 | 27.350 | 27.590 | 27.460 | 28.130 | 28.110 | 28.310 | 28.120 | 28.080 |
| **Cr2O3** | 0.019 | 0.004 | 0.000 | 0.000 | 0.000 | 0.043 | 0.004 | 0.000 | 0.048 | 0.005 | 0.051 | 0.000 | 0.000 | 0.021 | 0.012 | 0.000 | 0.000 | 0.007 |
| **NiO** | 0.000 | 0.009 | 0.000 | 0.028 | 0.000 | 0.000 | 0.000 | 0.000 | 0.021 | 0.013 | 0.000 | 0.035 | 0.000 | 0.000 | 0.000 | 0.037 | 0.000 | 0.017 |
| **Na2O** | 0.073 | 0.257 | 0.050 | 0.103 | 0.036 | 0.034 | 0.048 | 0.131 | 0.012 | 0.033 | 0.039 | 0.045 | 0.029 | 0.008 | 0.044 | 0.033 | 0.023 | 0.006 |
| **K2O** | 0.034 | 0.032 | 0.039 | 0.000 | 0.005 | 0.008 | 0.007 | 0.023 | 0.009 | 0.051 | 0.041 | 0.020 | 0.005 | 0.009 | 0.025 | 0.004 | 0.003 | 0.007 |
| **F** | 0.130 | 0.178 | 0.183 | 0.570 | 0.540 | 0.470 | 0.214 | 0.547 | 0.423 | 0.582 | 0.484 | 0.585 | 0.294 | 0.336 | 0.520 | 0.177 | 0.598 | 0.367 |
| **Cl** | 0.007 | 0.002 | 0.000 | 0.000 | 0.001 | 0.008 | 0.018 | 0.004 | 0.000 | 0.005 | 0.003 | 0.006 | 0.001 | 0.000 | 0.002 | 0.004 | 0.001 | 0.000 |
| **Total** | 94.437 | 94.246 | 96.083 | 97.095 | 97.038 | 97.283 | 95.331 | 98.713 | 98.057 | 97.463 | 96.192 | 97.537 | 96.707 | 97.237 | 97.814 | 97.089 | 97.525 | 97.776 |
| **Sample NO.** | HE-ves-loc1-sphene grn11 | HE-ves-loc1-sphene grn12 | HE-ves-loc1-sphene grn13 | 290-ves1-sphene grn1 | 290-ves1-sphene grn2 | 290-ves1-sphene grn3 | 290-ves1-sphene grn4 | 290-ves1-sphene grn5 | 290-ves1-sphene grn6 | 290-ves1-sphene grn7 | 290-ves1-sphene grn8 | 290-ves1-sphene grn9 | 290-ves1-sphene grn10 | 290-ves1-sphene grn11 | 290-ves1-sphene grn12 | 290-ves1-sphene grn13 | 290-ves1-sphene grn14 | 290-ves1-sphene grn16 |

| Table 15.Quantitive analysis results for apatite (EMP) | | | | | | | |
|---|---|---|---|---|---|---|---|
| | | | | | | | |
| | 1 | 2 | 3 | 4 | 5 | 6 | |
| CaO | 55.520 | 56.130 | 55.250 | 55.220 | 55.930 | 54.960 | |
| P2O5 | 39.160 | 41.200 | 41.440 | 40.590 | 41.120 | 41.460 | |
| F | 3.740 | 2.640 | 3.320 | 3.930 | 3.030 | 3.610 | |
| Cl | 0.065 | 0.049 | 0.045 | 0.068 | 0.053 | 0.035 | |
| FeO | 0.198 | 0.239 | 0.283 | 0.284 | 0.239 | 0.277 | |
| MgO | 0.149 | 0.145 | 0.123 | 0.124 | 0.106 | 0.184 | |
| SiO2 | 0.304 | 0.234 | 0.104 | 0.617 | 0.130 | 0.275 | |
| MnO | 0.050 | 0.064 | 0.078 | 0.043 | 0.048 | 0.060 | |
| SO3 | 0.002 | 0.007 | 0.000 | 0.002 | 0.016 | 0.003 | |
| Total | 99.187 | 100.708 | 100.643 | 100.878 | 100.671 | 100.864 | |
| Sample NO. | HE-apatite-loc1-inner-ves-grn4 | HE-apatite-loc1-inner-ves-grn7 | HE-apatite-loc3-rim-ves-grn1 | HE-apatite-loc3-rim-ves-grn5 | HE-apatite-loc3-rim-ves-grn6 | HE-apatite-loc3-rim-ves-grn10 | |

| Table 16.Quantitive analysis results for unpure composition of apatite (EMP) | | | | | | | | | | | |
|---|---|---|---|---|---|---|---|---|---|---|---|
| | | | | | | | | | | | |
| | 1 | 2 | 3 | 4 | 5 | 6 | 7 | 8 | 9 | 10 | 11 |
| SiO2 | 0.166 | 3.000 | 0.353 | 0.141 | 0.239 | 0.235 | 0.209 | 0.083 | 0.205 | 0.447 | 0.313 |
| FeO | 0.202 | 0.372 | 0.200 | 0.196 | 0.263 | 0.323 | 0.319 | 0.277 | 0.245 | 0.236 | 0.453 |
| MnO | 0.054 | 0.069 | 0.045 | 0.072 | 0.053 | 0.064 | 0.040 | 0.054 | 0.048 | 0.046 | 0.043 |
| MgO | 0.109 | 0.864 | 0.114 | 0.149 | 0.125 | 0.154 | 0.131 | 0.125 | 0.139 | 0.115 | 0.109 |
| CaO | 55.750 | 55.010 | 56.570 | 56.340 | 55.940 | 55.850 | 56.250 | 56.080 | 56.270 | 55.050 | 56.120 |
| P2O5 | 41.960 | 38.680 | 41.220 | 40.750 | 41.180 | 40.690 | 41.310 | 41.410 | 41.390 | 41.670 | 41.390 |
| F | 3.350 | 3.160 | 3.290 | 4.180 | 3.660 | 3.920 | 2.990 | 3.660 | 4.910 | 3.980 | 3.930 |
| SO3 | 0.000 | 0.002 | 0.000 | 0.000 | 0.000 | 0.003 | 0.000 | 0.000 | 0.000 | 0.005 | 0.003 |
| Cl | 0.044 | 0.055 | 0.040 | 0.051 | 0.041 | 0.047 | 0.046 | 0.041 | 0.052 | 0.056 | 0.051 |
| Total | 101.635 | 101.212 | 101.832 | 101.880 | 101.501 | 101.286 | 101.295 | 101.731 | 103.259 | 101.604 | 102.412 |
| Sample NO. | HE-apatite-loc1-inner-ves-grn1 | HE-apatite-loc1-inner-ves-grn2 | HE-apatite-loc1-inner-ves-grn3 | HE-apatite-loc1-inner-ves-grn5 | HE-apatite-loc1-inner-ves-grn6 | HE-apatite-loc3-rim-ves-grn2 | HE-apatite-loc3-rim-ves-grn3 | HE-apatite-loc3-rim-ves-grn4 | HE-apatite-loc3-rim-ves-grn9 | HE-apatite-loc3-rim-ves-grn11 | HE-apatite-loc3-rim-ves-grn15 |

## APPENDIX IV: Procedures and sample preparation for Loss-on-Ignition (LOI) analyses

1. Grind the samples to a very fine (100 mesh) powder before starting the LOI analysis.

2. Clean white ceramic crucibles and completely dry them in one of low-temperature (0 – 400ºC) ovens. Let them cool down to room temperature (ideally in a desiccator) for 20 minutes before continuing to next step.

3. Label and weigh empty white ceramic crucible, note the weight and label in notebook as shown in Table 17.
   i. Put one of samples in the crucible, weigh both crucible and the sample and note weight and sample number. Repeat this step for all samples.
   ii. Note: The weight of samples is supposed to be in the range 1-5 g.

4. Put the crucibles in the low-temperature oven (0-400 ºC) and heat them up to 105ºC for about 10 hours (the purpose of this step is to remove initial pore water). Let them cool down for 20 minutes to room temperature.

5. Weigh crucibles after the 10 hours heating, and note the weight.

6. Put the crucible in the high-temperature furnace (0 - 1000 ºC). Heat the oven gradually, in small steps, at a rate of 200 ºC /hrs (smaller increments make the temperature gradient smoother, otherwise the crucible breaks) up to 1000 ºC. Leave the crucibles at 1000 ºC for 10 - 12 hours and cool thereafter again at the same rate (200 ºC /hrs in increments of 15 or 30 minutes).
   i. Note: The permanent marking will evaporate by heating to 1000 ºC, so it is important to note the position of the crucibles in the oven. Then can be re-labelled when taking them out of the oven.

7. Weigh the crucibles after these procedures one more time and note the weight.

8. Now calculate the loss on ignition to be able to obtain the percent of mass lost on ignition from the following formulas:
   i. Sample weight = (Crucible + Sample) – Crucible empty
   ii. Loss-on-ignition = Heated 105 ºC – Heated to 1000 ºC
   iii. Percent of mass lost on ignition = (Loss on ignition /Sample weight)*100

| Table 17. The weights of the ceramic crucibles and samples during loss on ignition | | | | | | | | |
|---|---|---|---|---|---|---|---|---|
| **Crucible number** | **Sample (thin section) No.** | **Crucible empty** | **Crucible + Sample** | **Heated 105°C** | **Heated to 1000°C** | **Sample weight** | **Loss on Ignition** | **Precent of Mass Lost on Ignition** |
| **1** | 225 (121) | 19.255 | 20.397 | 20.395 | 20.377 | 1.142 | 0.018 | 1.61 |
| **2** | 226 (118) | 19.456 | 20.628 | 20.619 | 20.609 | 1.171 | 0.010 | 0.84 |
| **3** | 227 (124) | 20.281 | 21.901 | 21.897 | 21.887 | 1.620 | 0.010 | 0.64 |
| **4** | 228 (120) | 19.932 | 21.222 | 21.217 | 21.210 | 1.290 | 0.007 | 0.53 |
| **5** | 229 (119) | 19.698 | 20.812 | 20.810 | 20.809 | 1.114 | 0.001 | 0.12 |
| **6** | 230 (123) | 18.920 | 20.027 | 20.025 | 20.027 | 1.107 | -0.002 | -0.16 |
| **7** | 231 (125) | 18.899 | 19.927 | 19.926 | 19.924 | 1.029 | 0.002 | 0.20 |
| **8** | 248A (101) | 18.945 | 19.935 | 19.935 | 19.928 | 0.991 | 0.007 | 0.70 |
| **9** | 250 (103) | 19.866 | 20.891 | 20.888 | 20.867 | 1.025 | 0.021 | 2.09 |
| **10** | 251 (102) | 19.195 | 20.210 | 20.207 | 20.191 | 1.015 | 0.016 | 1.58 |
| **11** | 252 (106) | 18.353 | 19.447 | 19.446 | 19.432 | 1.094 | 0.014 | 1.25 |
| **12** | 271 (105) | 21.270 | 22.593 | 22.591 | 22.576 | 1.324 | 0.015 | 1.13 |
| **13** | 272A | 21.365 | 22.397 | 22.395 | 22.385 | 1.033 | 0.010 | 0.98 |
| **14** | 272B | 19.801 | 21.076 | 21.072 | 21.047 | 1.275 | 0.025 | 2.00 |
| **15** | 272C (108) | 19.256 | 20.631 | 20.614 | 20.538 | 1.375 | 0.076 | 5.51 |
| **16** | 272D (109) | 19.454 | 20.477 | 20.471 | 20.469 | 1.022 | 0.002 | 0.18 |
| **17** | 273 (112) | 20.279 | 21.698 | 21.695 | 21.697 | 1.419 | -0.002 | -0.18 |
| **18** | 274 (111) | 19.932 | 20.993 | 20.991 | 20.989 | 1.061 | 0.001 | 0.12 |
| **19** | 292 (114) | 19.698 | 20.721 | 20.714 | 20.701 | 1.022 | 0.013 | 1.31 |
| **20** | 293 (116) | 18.919 | 19.973 | 19.968 | 19.951 | 1.054 | 0.017 | 1.59 |
| **21** | 20592 | 18.898 | 20.099 | 20.095 | 20.065 | 1.201 | 0.030 | 2.53 |
| **22** | 20603 | 19.394 | 20.566 | 20.565 | 20.554 | 1.172 | 0.011 | 0.95 |
| **23** | 20604 | 18.944 | 20.042 | 20.038 | 20.022 | 1.097 | 0.017 | 1.53 |
| **24** | 20605 | 19.865 | 21.016 | 21.012 | 20.990 | 1.151 | 0.023 | 1.95 |
| **25** | 20606 | 19.195 | 20.425 | 20.421 | 20.406 | 1.229 | 0.015 | 1.22 |
| **26** | 20608 | 21.269 | 22.506 | 22.504 | 22.506 | 1.236 | -0.003 | -0.21 |
| **27** | 20622 | 21.365 | 22.540 | 22.535 | 22.498 | 1.175 | 0.036 | 3.07 |
| **28** | 25 | 19.802 | 21.158 | 21.151 | 21.119 | 1.356 | 0.032 | 2.37 |
| **29** | 26 | 18.353 | 19.477 | 19.477 | 19.475 | 1.125 | 0.002 | 0.19 |
| **30** | 27-Gabbro | 19.394 | 20.788 | 20.785 | 20.773 | 1.394 | 0.012 | 0.83 |

# APPENDIX V: End-member composition of garnet

Table 18. Garnet end-member compositions calculated from the result of EMP analysis, numbers in mole %

| | | mole% | | | | | | | |
|---|---|---|---|---|---|---|---|---|---|
| **point** | **Sample** | **Almandine** | **Pyrope** | **Grossular** | **Spessartine** | **Uvarovite** | **Andradite** | **Ca-Ti Gt** | **Total** |
| **1** | 115- ves 2-3 garnet inner rim gr 1 pt1 | 1.70 | 0.34 | 0.00 | 0.79 | 0.00 | 97.06 | 0.11 | 100.00 |
| **2** | 118- ves 2-3 garnet inner rim gr 1 pt1 | 1.05 | 0.18 | 0.06 | 0.94 | 0.00 | 97.67 | 0.11 | 100.00 |
| **3** | 115- ves 2-3 garnet inner rim gr 1 pt3 | 1.39 | 0.12 | 0.09 | 0.91 | 0.04 | 97.43 | 0.02 | 100.00 |
| **4** | 118- ves 2-3 garnet inner rim gr 1 pt3 | 2.93 | 0.04 | 0.05 | 0.99 | 0.00 | 95.92 | 0.07 | 100.00 |
| **5** | 115- ves 2-3 garnet inner rim gr 1 pt5 | 1.03 | 0.52 | 0.07 | 0.67 | 0.01 | 97.62 | 0.08 | 100.00 |
| **6** | 118- ves 2-3 garnet inner rim gr 1 pt6 | 1.03 | 0.52 | 0.07 | 0.67 | 0.01 | 97.62 | 0.08 | 100.00 |
| **7** | 118- ves 5 garnet center gr 1 pt1 | 1.66 | 0.01 | 0.00 | 1.09 | 0.00 | 97.24 | 0.01 | 100.00 |
| **8** | 118- ves 5 garnet center gr 1 pt2 | 1.57 | 0.05 | 0.00 | 0.99 | 0.00 | 97.26 | 0.13 | 100.00 |
| **9** | 118- ves 5 garnet center gr 1 pt3 | 7.75 | 0.29 | 11.26 | 0.71 | 0.03 | 74.29 | 5.68 | 100.00 |
| **10** | 115- vein rim garnet gr 1 pt2 | 4.13 | 0.55 | 11.44 | 2.15 | 0.00 | 78.31 | 3.42 | 100.00 |
| **11** | 115- vein rim garnet gr 1 pt3 | 4.84 | 1.03 | 17.48 | 2.67 | 0.00 | 65.69 | 8.29 | 100.00 |
| **12** | 115- vein center garnet gr 1 pt2 | 0.68 | 8.24 | 3.32 | 0.92 | 0.00 | 86.83 | 0.01 | 100.00 |
| **13** | 115- vein center garnet gr 1 pt3 | 0.68 | 8.24 | 3.32 | 0.92 | 0.00 | 86.83 | 0.01 | 100.00 |
| **14** | 115- vein center garnet gr 1 pt4 | 1.21 | 0.20 | 1.18 | 0.52 | 0.00 | 96.72 | 0.16 | 100.00 |
| **15** | 115- vein rim garnet gr 1 pt4 | 4.10 | 0.65 | 6.59 | 2.86 | 0.05 | 82.19 | 3.56 | 100.00 |
| **16** | 115- vein rim garnet gr 1 pt5 | 5.06 | 1.01 | 10.24 | 2.65 | 0.00 | 73.42 | 7.63 | 100.00 |
| **17** | 117-rim-ves1-garnet-grn1 | 2.01 | 0.14 | 3.02 | 2.02 | 0.03 | 92.38 | 0.40 | 100.00 |
| **18** | 117-rim-ves1-garnet-grn2 | 1.71 | 0.21 | 2.80 | 1.18 | 0.00 | 93.31 | 0.79 | 100.00 |
| **19** | 117-rim-ves1-garnet-grn3 | 1.37 | 0.19 | 1.21 | 1.21 | 0.04 | 95.71 | 0.28 | 100.00 |
| **20** | 117-rim-ves1-garnet-grn4 | 2.93 | 0.09 | 0.24 | 3.09 | 0.00 | 93.43 | 0.23 | 100.00 |
| **21** | 117-rim-ves1-garnet-grn5 | 2.52 | 0.17 | 1.17 | 1.24 | 0.00 | 94.64 | 0.26 | 100.00 |
| **22** | 117-rim-ves1-garnet-grn6 | 7.92 | 0.47 | 6.86 | 1.88 | 0.00 | 78.41 | 4.47 | 100.00 |
| **23** | 117-rim-ves1-garnet-grn7 | 3.67 | 0.34 | 1.73 | 4.16 | 0.00 | 89.98 | 0.11 | 100.00 |
| **24** | 117-rim-ves1-garnet-grn8 | 2.90 | 0.13 | 0.02 | 1.11 | 0.00 | 95.85 | 0.00 | 100.00 |
| **25** | 117-rim-ves1-garnet-grn10 | 2.93 | 0.10 | 0.05 | 1.29 | 0.00 | 95.54 | 0.08 | 100.00 |
| **26** | 117-rim-ves1-garnet-grn11 | 1.43 | 0.06 | 0.23 | 0.96 | 0.06 | 97.20 | 0.06 | 100.00 |

## APPENDIX VI: The standards used for EMP analyses

TABLE 19a: Standards, spectrometers and analytical crystals used, counting times on peak and background on each side of peak for apatite analyses

| Element | Spec. | Crystal | Standard | Peak (sec) | Backgr. (sec) |
|---|---|---|---|---|---|
| Si | 5 | TAP | Plagioclase (NMNH 115900) | 60 | 60 |
| Fe | 4 | LIFL | Garnet (NMNH 87375) | 60 | 60 |
| Mn | 4 | LIFL | Bustamite (Astimex Standards Ltd.) | 60 | 60 |
| Mg | 5 | TAP | Diopside Glass (NASA) | 60 | 60 |
| Ca | 2 | PETJ | Apatite (Astimex Standards Ltd.) | 60 | 15 |
| P | 2 | PETJ | Apatite (Astimex Standards Ltd.) | 60 | 15 |
| F | 1 | LDE1 | Topaz (Astimex Standards Ltd.) | 120 | 60 |
| S | 3 | PETH | Pyrite (Astimex Standards Ltd.) | 60 | 60 |
| Cl | 3 | PETH | Scapolite (Meionite) (NMNH R6600) | 60 | 60 |

TABLE 19b: Standards, spectrometers and analytical crystals used, counting times on peak and background on each side of peak for amphibole analyses

| Element | Spec. | Crystal | Standard | Peak (sec) | Backgr. (sec) |
|---|---|---|---|---|---|
| Si | 1 | TAP | Augite (NMNH 122142) | 20 | 10 |
| Ti | 2 | PETJ | Hornblende (Kakanui) (NMNH 143965) | 45 | 45 |
| Al | 1 | TAP | Pyrope (NMNH 143968) | 30 | 15 |
| Fe | 3 | LIFH | Hornblende (Kakanui) (NMNH 143965) | 30 | 15 |
| Mn | 3 | LIFH | Bustamite (Astimex Standards Ltd.) | 30 | 30 |
| Mg | 5 | TAP | Hypersthene (USNM 746) | 30 | 15 |
| Ca | 2 | PETJ | Diopside (NMNH 117733) | 30 | 15 |
| Na | 5 | TAP | Omphacite (NMNH 110607) | 30 | 15 |
| K | 4 | PETL | Corning Glass D (NMNH 117218-3) | 30 | 15 |
| F | 1 | LDE1 | Topaz (Astimex Standards Ltd.) | 45 | 45 |
| Cl | 4 | PETL | Scapolite (Meionite) (NMNH R6600) | 45 | 45 |
| Cr | 4 | LIFL | Chromite (NMNH 117075) | 30 | 15 |
| Ni | 3 | LIFH | Pentlandite (Astimex Standards Ltd.) | 30 | 30 |

TABLE 19c: Standards, spectrometers and analytical crystals used, counting times on peak and background on each side of peak for garnet analyses

| Element | Spec. | Crystal | Standard | Peak (sec) | Backgr. (sec) |
|---|---|---|---|---|---|
| Si | 1 | TAP | Pyrope (NMNH 143968) | 30 | 15 |
| Ti | 2 | PETJ | Hornblende (Kakanui) (NMNH 143965) | 30 | 30 |
| Al | 1 | TAP | Pyrope (NMNH 143968) | 30 | 15 |
| Fe | 3 | LIFH | Garnet (NMNH 87375) | 30 | 15 |
| Mn | 4 | LIFL | Bustamite (Astimex Standards Ltd.) | 30 | 15 |
| Mg | 5 | TAP | Pyrope (NMNH 143968) | 30 | 15 |
| Ca | 2 | PETJ | Garnet (NMNH 87375) | 30 | 15 |
| Na | 5 | TAP | Omphacite (NMNH 110607) | 30 | 30 |
| Cr | 4 | LIFL | Chromite (NMNH 117075) | 30 | 30 |

TABLE 19d: Standards, spectrometers and analytical crystals used, counting times on peak and background on each side of peak for oxide analyses

| Element | Spec. | Crystal | Standard | Peak (sec) | Backgr. (sec) |
|---|---|---|---|---|---|
| Si | 1 | TAP | Pyrope (NMNH 143968) | 30 | 30 |
| Ti | 2 | PETJ | Rutile (Astimex Standards Ltd.) | 30 | 30 |
| Al | 1 | TAP | Garnet (NMNH 87375) | 30 | 15 |
| Fe | 3 | LIFH | Hematite (Astimex Standards Ltd.) | 30 | 15 |
| Mn | 4 | LIFL | Bustamite (Astimex Standards Ltd.) | 30 | 30 |
| Mg | 5 | TAP | Hypersthene (USNM 746) | 30 | 30 |
| Cr | 4 | LIFL | Chromite (NMNH 117075) | 30 | 15 |
| Ni | 3 | LIFH | Pentlandite (Astimex Standards Ltd.) | 30 | 30 |

TABLE 19e: Standards, spectrometers and analytical crystals used, counting times on peak and background on each side of peak for plagioclase analyses

| Element | Spec. | Crystal | Standard | Peak (sec) | Backgr. (sec) |
|---|---|---|---|---|---|
| Si | 1 | TAP | Plagioclase (NMNH 115900) | 40 | 20 |
| Ti | 2 | PETJ | Hornblende (Kakanui) (NMNH 143965) | 40 | 40 |
| Al | 1 | TAP | Anorthite (NMNH 137041) | 40 | 20 |
| Fe | 3 | LIFH | Hornblende (Kakanui) (NMNH 143965) | 40 | 20 |
| Mn | 3 | LIFH | Bustamite (Astimex Standards Ltd.) | 40 | 40 |
| Mg | 5 | TAP | Hornblende (Kakanui) (NMNH 143965) | 40 | 40 |
| Ca | 2 | PETJ | Anorthite (NMNH 137041) | 40 | 20 |
| Na | 5 | TAP | Anorthoclase (NMNH 133868) | 30 | 15 |
| K | 4 | PETL | Microcline (NMNH 143966) | 40 | 20 |
| Ba | 4 | PETL | Corning Glass C (NMNH 117218-2) | 40 | 40 |

TABLE 19f: Standards, spectrometers and analytical crystals used, counting times on peak and background on each side of peak for pyroxene analyses

| Element | Spec. | Crystal | Standard | Peak (sec) | Backgr. (sec) |
|---|---|---|---|---|---|
| Si | 1 | TAP | Augite (NMNH 122142) | 30 | 15 |
| Ti | 2 | PETJ | Hornblende (Kakanui) (NMNH 143965) | 30 | 30 |
| Al | 1 | TAP | Pyrope (NMNH 143968) | 30 | 15 |
| Fe | 3 | LIFH | Hornblende (Kakanui) (NMNH 143965) | 30 | 15 |
| Mn | 4 | LIFL | Bustamite (Astimex Standards Ltd.) | 30 | 30 |
| Mg | 5 | TAP | Hypersthene (USNM 746) | 30 | 15 |
| Ca | 2 | PETJ | Diopside (NMNH 117733) | 30 | 15 |
| Na | 5 | TAP | Omphacite (NMNH 110607) | 30 | 15 |
| Cr | 4 | LIFL | Chromite (NMNH 117075) | 30 | 15 |
| Ni | 3 | LIFH | Pentlandite (Astimex Standards Ltd.) | 30 | 30 |

TABLE 19g: Standards, spectrometers and analytical crystals used, counting times on peak and background on each side of peak for titanite analyses

| Element | Spec | Crystal | Standard | Peak (sec) | Backgr. (sec) |
|---|---|---|---|---|---|
| Si | 1 | TAP | Augite (NMNH 122142) | 20 | 10 |
| Ti | 2 | PETJ | Rutile (Astimex Standards Ltd.) | 30 | 15 |
| Al | 1 | TAP | Pyrope (NMNH 143968) | 30 | 15 |
| Fe | 3 | LIFH | Hornblende (Kakanui) (NMNH 143965) | 30 | 15 |
| Mn | 3 | LIFH | Bustamite (Astimex Standard Ltd.) | 30 | 30 |
| Mg | 5 | TAP | Hypersthene (USNM 746) | 30 | 30 |
| Ca | 2 | PETJ | Anorthite (NMNH 137041) | 30 | 15 |
| Na | 5 | TAP | Omphacite (NMNH 110607) | 30 | 30 |
| K | 4 | PETL | Corning Glass D (NMNH 117218-3) | 30 | 15 |
| F | 1 | LDE1 | Topaz (Astimex Standards Ltd.) | 45 | 45 |
| Cl | 4 | PETL | Scapolite (Meionite) (NMNH R6600) | 45 | 45 |
| Cr | 4 | LIFL | Chromite (NMNH 117075) | 30 | 3 |
| Ni | 3 | LIFH | Pentlandite (Astimex Standards Ltd.) | 30 | 30 |

## APPENDIX VII: Description table and analyses for the hornfels samples around Hrossatungur gabbro

Table 20.Description of hornfles samples and analysis

| No. | Sample (thinsection) No. | Fieldbook description | Thin section | ICP | LOI | SEM | EMP |
|---|---|---|---|---|---|---|---|
| 1 | 247A | On the western side of Hálsgil we have dominant dolerite-micrograbbro in scree probably ll to the slope as it does not extend into the eatern gully slope. Sample taken to see alteration difference cf to main gabbro. | | | | | |
| 2 | 247B | 10 cm vienfilling of llcc and Quartz. Taken in scree on eastern side of Halsgil derived from above there. | | | | | |
| 3 | 248A (101) | Hornfels taken 10-40 cm form the lower contact of the porph cone sheet. Sample shows 2 kinds of crystallnity that should be takien into consideration when analysis is done. much more slica and plagioclase then all the other samples and felsic veins as well | x | x | x | x | |
| 4 | 248B (104) | Sample taken from the porph cs in order to check the alteration to assess the alteration succeeding the intrusion. | x | | | | |
| 5 | 250 (103) | 5 m up gully sample of hornfels of vesicular basalt ve. Fine grained | x | x | x | | |
| 6 | 251 (102) | Contact of hornfels and fine grained intrusive contact of the gabbro. Picture taken. Dark grained sample taken about 0.5 m from contact. | x | x | x | x | |
| 7 | 251 (107) | Fine grained intrusive taken about 1.5 m from the contact, apparently relatively fresh, rare pyrite in rock. It is interesting to see the same kind of cooling jointing going from the intrusion into the hornfels. Interpretee as showing similar cooling features i.e the hornfels is at least in a plastic state | x | | | | |
| 8 | 252 (106) | Three sulfide chimneys seen, some 4x4, 2x2 and 2x2 cutting through the fine grained "gabbro", ca. 15- 20 m from the gabbro contact. These agrees with the degasing chimneys venting off the volatiles from the magma. | x | x | x | | |
| 9 | 271 (105) | A two sample profile. This sample is about 30 cm form contact of finegrained chilled gabbro contact. | x | x | x | x | |
| 10 | 272A | Sample taken about 70 cm from contact | | x | x | | |
| 11 | 272B | Profile taken from outer rim of hornfels up to the chilled margin of the gabbro. Small gairns build along the sample trail | | x | | | |
| 12 | 272C | Crumbly hornfels, no vesicle seen. As in other places the jointing in the hornfels extends into the doelrite-gabbro indicating common solidification. | | | x | | |

| No. | Sample (Thinsection) No. | Fieldbook description | Thin section | ICP | LOI | SEM | EMP |
|---|---|---|---|---|---|---|---|
| 13 | 272D (108) | 3 m from first sample | x | x | x | | |
| 14 | 272E (109) | 6 m from second sample. Fine grain and few phenocrysts plago that forms from old phenocysts lava after the hornfelsed processes | x | x | x | | |
| 15 | 273 (112) | Hornfels rock with white to yellow color minerals assimbledge | x | x | x | | |
| 16 | 274 (111) | Dolerite about 6 from the contact to check on the alteration | x | x | x | x | |
| 17 | 274 (122) | Small dioritic vein at the gabbro contact. | x | | | | |
| 18 | 290 (117) | Small exposure of hornfelsed heterogeneous grain size probably due to recrystallization of vesicle fillings. Sample for petrography and chemistry analysis | x | | | x | x |
| 19 | 291 (115) | Exposure ca. 8-10 m from point 290. Probbly relics of ves fillings. | x | | | x | x |
| 20 | 292 (114) | Small hornfels sample about 1 m from chilled margin of gabbro. Porphertic texture of phenocrystis of plagio with vary compositions, some magnitite is found in the plagio crystals which caused by the processes of hornfeling. | x | x | x | | |
| 21 | 293 (116) | Small patch of hornfels | x | x | x | | |
| 22 | 294 (113) | Crumbly hornfels ca 1.5 m above the fine grained gabbro cntact. | x | | | | |
| 23 | 20592 | „Contact“ to the intrusion hornfels. Very strong jointing, which probably is due to the later faulting in the pass. Sample light coloured and difficult to identify. Veins filled with Quartz and ore laumontite in vesicle | x | x | x | | |
| 24 | 20603 | Doelrite veinig in basalt breccia near to gabbro/dolerite exposure. Hornfels with py in groundmass and common pyrite veins. Dark veins that may be older than pyrite. | x | x | x | | |
| 25 | 20604 | Hornfels at gabbro margin. Probable granophyric veins and vesicle filling. Granophyric veins cutting through hornfels. Volatile pores in granopyre and magmatic Quartiz crystallizing from the margin. And fine nedles that may be amphiole. Large sample vesicular basalt hornfels, vesicles mostly filled with Quartz and minor garnet | x | x | x | | |
| 26 | 20605 | Fine light gray grain size (granophyric = felsic colors intrusion in the hornfels which come from the felsic magam remains after the partial melting of the mafic menrals ), the granophyric veins characterized by vescaular texture with empty porous that may taken for daitals fluid inclusion, lining viens along all the rock, big viens of white colors wich filled, some vesicals are empty, some others filled with vesicals like epidote qz. Veins are cut crossing? | x | X | X | | |

| No. | Sample (Thinsection) No. | Fieldbook description | Thin section | ICP | LOI | SEM | EMP |
|---|---|---|---|---|---|---|---|
| 27 | 20606 | Sample from hornfels, numerous felsic vesicle fillings. vesicular hornfelsed basalt. Vesicle-massive Quartz+occational ore, especially near margin but also within the Quartz. These are cut through by softer veins with darker minerals and threads of actinolite | x | x | x | | |
| 28 | 26 (26) | Sulphide vein in hornfels cuts through the hornfels. Very dark and fine grained hornfels charged with opaques, crosscut by sulfide veining i.e. hornfels>sulfide. Sulfide contaminating the boundary of the hornfels. looking on top of the vein it looks like the sulfides are spherial pitting into the rock? | x | x | x | | |
| 29 | 20608 | Vesicular hornfels with vesicle fillings mostly quartz. Dark band (possibly chlorite altered to opaque)>gt (faintgreen)>Q, gt+ore>Q, dark opaque ring around the vesicles, former chlorite or just opaque deposition during hornfels stage? | | x | x | | |
| 30 | 20622 | Hornfels, rare vesicles filled with dark material, seems fine grained, dark and hard. Standared charctersitcs of hornfels rocks. | x | x | x | | |
| 31 | 25 | Hornfels contains pyrite, plag and Quartz | x | x | x | | |
| 32 | 225 (121) | Two profiles of hornfels samples in Koppakofugil | x | x | x | | |
| 33 | 226 (118) | Hornfels profile with some pyroxene and maybe hornblende | x | x | x | x | x |
| 34 | 227 (124) | Hornfels with qz veinfilling | x | x | x | | |
| 35 | 228 (120) | Fine gran texture of hornfels | x | x | x | | |
| 36 | 229 (119) | Very recrystalized type of hornfels | x | x | x | | |
| 37 | 230 (123) | Fine grain texture of hornfels | x | x | x | x | x |
| 38 | 231 (125) | Very fine grain with white and gray color and vesicals fills with green may be chlorite. | x | x | x | | |
| 39 | HT Gabbro | This sample is taken as a gabro rock from Hrossatungur gabbro | | x | x | | |
| 40 | HE-42 (1500m) | This sample collceted from the cutting samples of well HE-42 in Hellisheidi geothermal field | x | | | x | x |
| | Total | | 33 | 30 | 30 | 9 | 5 |